ETHzürich

Model predictive building climate control
Steps towards practice

Doctoral Thesis

Author(s):
Sturzenegger, David

Publication date:
2014

Permanent link:
https://doi.org/10.3929/ethz-a-010379191

Rights / license:
In Copyright - Non-Commercial Use Permitted

DISS. ETH NO. 22422

Model Predictive Building Climate Control - Steps Towards Practice

A thesis submitted to attain the degree of

DOCTOR OF SCIENCES of ETH ZURICH

(Dr. sc. ETH Zurich)

presented by

DAVID CLAUDIO TOA STURZENEGGER

MSc in Mechanical Engineering, ETH Zürich, Switzerland

born on 21.04.1986

citizen of Zürich, Switzerland

accepted on the recommendation of

Prof. Dr. Manfred Morari (examiner)
Prof. Dr. Roy Smith (co-examiner)
Dr. Conrad Gähler (co-examiner)

2014

Automatic Control Laboratory
ETH Zurich
Switzerland

To

Heidi and Migg, Babička and Děda, Rolf and Eva

Acknowledgment

First and foremost, I want to thank Professor Manfred Morari for giving me the great opportunity of doing my PhD at the Automatic Control Laboratory (IfA). Professor Morari provided me with the freedom to discover my own research direction and always gave me the opportunities to learn, be it in- or outside of Switzerland. I was always impressed by his ability to almost instantaneously identify weak points of concepts and presentations; his high standards help others to improve. Thank you for your guidance and support.

I am also grateful to Professor Roy Smith for his constant supervision, not only teaching me research related matters but also style of writing and presentation. Several times, his advice gave me the right direction. Thank you for the many interesting discussions and for readily giving my presentation when Emirates refused to carry me to a conference.

My thanks go also to Conrad Gähler for being a co-referee in my PhD committee, for sharing his knowledge about state-of-the-art building control, and for enjoyable discussions whenever we met.

I also want to thank all my other colleagues from the OptiControl-II project. My thanks go to Markus Gwerder for patiently answering my many questions on building climate control and to Dimitrios Gyalistras for sharing his experience in software development. My thanks also go to Carina Sagerschnig who always willingly supported my simulations with EnergyPlus, even if they sometimes differed from the program's intended purpose. Much of my research would not have been possible without their help.

Special thanks go to Frauke Oldewurtel. As my building climate control predecessor, Frauke introduced me to our common research topic, resulting in many nice collaborations. Her positive attitude was always inspiring. Thank you for the great time sharing one of the best offices at ETH.

I also want to thank Dominik Keusch, Leonardo Muffato, and Dominique Kunz for their collaboration in the context of the presented identification experiments and Vito Semeraro for his support with developing the BRCM toolbox. My gratitude goes also to Professor Francesco Borrelli and his PhD students for giving me such a great time at UC Berkeley.

I also want to thank all my colleagues at IfA who make it the great place it is. Thanks to Giampaolo Torrisi for winning the NLB indoor volleyball championship with me and to Claudia Fischer for teaching me how to fold bills into butterflies. Thanks to Georg Schildbach for the many hours of enjoyable discussions, be it while supervising master students or sharing a room at a workshop in France. Thanks to Aldo Zgraggen for many "early lunches" (thus saving me from starvation) and to Joe Warrington for occasionally teaching me some English. Thanks to Xiaojing Zhang for the time-intensive but pleasant collaboration in the context of the MPC course and to Robert Nguyen and Robin Vujanic for the enjoyable lunches and sharing their knowledge of investing. Thanks to Tobias Baltensberger and again to Robert for the fun time sharing an office and to Christian Conte for describing the spirit of IfA to me before I started my PhD. Thanks to Marko Tanaskovic for the enjoyable co-supervision of a

iv

Contents

Abstract

This thesis investigates the application of Model Predictive Control (MPC) to climate control of buildings with the goal of improving its energy efficiency. Current practice in the control of Heating, Ventilation, and Air Conditioning (HVAC) systems is the use of Rule-Based Control (RBC). RBC control strategies are well-established but limited by the difficulty of consistently integrating weather predictions and systematically coordinating all actuators – both commonly regarded as ways to improve energy efficiency. The research interest into alternative, more energy efficient control strategies in buildings is mainly driven by three factors: i) a large fraction of the world's energy consumption occurs in buildings; ii) the majority of the building stock is already in place and refurbishments are expensive while control systems can be upgraded at comparatively low costs; iii) computational power is becoming ever cheaper, enabling the cost-effective use of advanced control techniques.

MPC presents a particularly attractive alternative in building climate control. The methodology has been successfully applied in many areas, in particular due to its capability of handling constraints on state and input variables. Applied to building climate control, MPC uses a mathematical model of the building and predictions of disturbances (e.g. ambient temperature) over a given prediction horizon (e.g. two days) to formulate an optimization problem. This is solved to find the control input trajectory that maintains comfort for the occupants over the whole horizon while minimizing some objective (e.g. total energy use or monetary costs). The first step of the control input trajectory is implemented on the building and the process is repeated at the next time step. MPC makes it possible to systematically integrate all available actuators and their interactions as well as predictions of the weather, internal gains, and electricity prices into a control framework that can handle constraints on the room temperatures (states) and on the use of HVAC systems (inputs). In recent years, many studies have analyzed the energy savings potential of MPC in simulations. However, while these studies have demonstrated the potential benefits of MPC, many problems still remain to be solved that relate to the appropriate modeling of real buildings and the practical feasibility of MPC, as for instance its compatibility with pre-installed control systems. This thesis is mainly concerned with addressing these issues.

This document is structured in four parts. Part I gives background information on MPC for building climate control and introduces the MPC formulation considered in this work.

Part II is concerned with the modeling of buildings for MPC. Creating an accurate building model that is simple enough to allow the resulting MPC problem to be tractable is a challenging but crucial task in the control design. In a first chapter, we present the Building Resistance-Capacitance Modeling (BRCM) Matlab toolbox that facilitates the physical modeling of buildings for MPC. The toolbox provides a means for the fast generation of bilinear resistance-capacitance (RC) type models from building geometry, building construction, and building systems data. We describe how the models are constructed and present a case study in which the toolbox was used to create a model that was then compared to the established building simulation software EnergyPlus. In a second chapter, an alternative method for ob-

taining a building model is investigated. We report a study in which we used identification techniques to model a ventilated room. Three models were derived: i) an empirical transfer function estimate (ETFE) derived from a pseudo-random binary sequence input signal; ii) an ETFE derived from a relay feedback closed-loop identification approach; iii) an RC model constructed using the BRCM toolbox. Using additional validation data, the models were compared in terms of accuracy. All models showed a reasonably good predictive performance. The effect of air mixing dynamics was demonstrated in a further experiment to be one of the main differences between the experimentally identified and the RC model. The study shows that an additional pole can be added to the RC model in order to compensate for the differences related to the air mixing dynamics.

Part III reports the results of the predictive building control project OptiControl-II that encompassed seven months of MPC of a fully-occupied Swiss office building. We describe the chosen control set-up, the modeling, the main experimental results, as well as simulation-based comparisons of MPC to the previously installed RBC strategy using the EnergyPlus simulation software. Based on these results, we analyze the costs and benefits of MPC for cases similar to the investigated building. In the experiments, MPC controlled the building reliably and achieved a good comfort level. The simulation results showed a significantly improved control performance in terms of energy and comfort. However, for similar buildings and with the tools currently available, the required initial investment appears to be too high to justify the deployment of MPC in everyday building projects on the basis of operating cost savings alone. Nevertheless, development investments in an MPC building automation framework and a tool for modeling building dynamics together with the increasing importance of demand response and rising energy prices may push the technology into the net benefit range.

Part IV investigates the energy savings potential of improved occupancy information by means of a simulation-based study. To evaluate the potential savings, different types of occupancy information were used in an MPC: i) a standard occupancy schedule (presence during office hours, vacancy otherwise) used to predict internal gains and comfort constraints; ii) the standard schedule used for prediction and additionally instantaneous occupancy measurements used to adjust lighting; iii) the standard schedule used for prediction and additionally instantaneous occupancy measurements used to adjust lighting and ventilation; iv) perfectly predicted occupancy information. Simulations were performed for every controller and over a set of building, HVAC system, internal gains level, and weather combinations. By comparing the energy usage of the individual controllers, we show that taking into account occupancy information in building climate control has a significant energy savings potential. However, a large part of this potential can already be captured by considering instantaneous occupancy measurements.

Zusammenfassung

Diese Arbeit untersucht die Anwendung von modellprädiktiver Regelung (Model Predictive Control, MPC) für die energieeffiziente Klimaregelung von Gebäuden. Die gängige Praxis in der Regelung der Heizungs-, Kühlungs- und Ventilationssysteme (Heating, Ventilation, and Air Conditioning, HVAC), ist die Verwendung von regelbasierter Regelung (Rule-Based Control, RBC). RBC Regelstrategien sind weit verbreitet; allerdings werden sie durch die Schwierigkeit konsistent Wettervorhersagen zu berücksichtigen und systematisch alle HVAC Aktuatoren zu koordinieren limitiert. Das Interesse der Forschung an alternativen, energieeffizienteren Regelungsstrategien in Geschäftsgebäuden basiert hauptsächlich auf drei Faktoren: i) Ein Grossteil des weltweiten Energieverbrauchs findet in Gebäuden statt; ii) ein Grossteil des Gebäudeparks ist bereits gebaut und Renovationen sind im Vergleich zu einer Verbesserung der Regelsysteme teuer; iii) Rechenleistung wird immer günstiger und ermöglicht die kosteneffiziente Verwendung von fortgeschrittenen Regelstrategien.

MPC ist eine besonders attraktive Alternative für die Klimaregelung von Gebäuden. Die Methode wurde insbesondere aufgrund ihrer Möglichkeit Beschränkungen auf die Regelgrössen und Prozessvariablen zu berücksichtigen in vielen Bereichen erfolgreich angewandt. Für die Klimaregelung von Gebäuden verwendet MPC ein mathematisches Gebäudemodell sowie Vorhersagen von Störungen (z.B. Umgebungstemperatur) über einen Vorhersagehorizont (z.B. zwei Tage), um ein Optimierungsproblem aufzustellen. Dieses wird gelöst, um diejenige Trajektorie von Regelgrössen zu finden, welche den Komfort der Personen im Gebäude garantiert und gleichzeitig eine Zielfunktion minimiert (z.B. totaler Energieverbrauch oder monetäre Kosten). Der erste Schritt der Regeltrajektorie wird dann auf dem Gebäude umgesetzt und der ganze Ablauf im nächsten Zeitschritt wiederholt. MPC ermöglicht es, sowohl alle verfügbaren Aktuatoren und deren Interaktionen als auch Vorhersagen des Wetters, der Wärmegewinne und Elektrizitätspreise in ein kohärentes mathematisches Regelungskonzept zu integrieren. In den letzten Jahren haben viele Studien das Energieeinsparpotential von MPC im Vergleich zu RBC in Simulationen analysiert. Zwar haben diese Studien die potentiellen Vorteile von MPC demonstriert, aber es gibt noch viele ungelöste Probleme im Zusammenhang mit der Modellierung von echten Gebäuden, dem Umgang mit Diskrepanzen zwischen Gebäude und Gebäudemodell sowie mit der praktischen Umsetzung von MPC wie beispielsweise dessen Kompatibilität mit den bereits installierten Regelsystemen. Im Zentrum dieser Arbeit steht hauptsächlich die Behandlung dieser Probleme.

Dieses Dokument ist in vier Teile gegliedert. Teil I umfasst Hintergrundinformationen zu MPC für Gebäuderegelung und führt die in dieser Arbeit verwendete MPC Formulierung ein.

Teil II handelt von der Modellierung von Gebäuden für MPC. Das Erstellen eines genauen Gebäudemodells, welches zu einem lösbaren MPC Problem führt, ist eine herausfordernde aber zentrale Aufgabe in der Entwicklung der Regelung. In einem ersten Kapitel führen wir die Building Resistance-Capacitance Modeling (BRCM) Matlab Toolbox ein, welche die physikalische Gebäudemodellierung für MPC vereinfacht. Die Toolbox erlaubt es aufgrund von Gebäudegeometrie-, Gebäudekonstruktions- und Gebäudesystemsdaten schnell bilinea-

re Widerstand-Kapazität (Resistance-Capacitance, RC) Modelle zu erstellen. Wir beschreiben wie die Modelle erstellt werden und präsentieren eine Fallstudie, in welcher die Toolbox verwendet wurde, um ein Modell eines Raumes zu generieren. Die Prädiktionsqualität des Modells wurde dann mit der verbreiteten Gebäudesimulationssoftware EnergyPlus verglichen. In einem zweiten Kapitel haben wir eine alternative Methode untersucht, um ein Gebäudemodell zu erstellen. Wir haben Frequenz-Bereich Identifikationsmethoden verwendet, um einen belüfteten Raum zu modellieren. Drei Modelle wurden entwickelt: i) eine empirische Schätzung der Übertragungsfunktion (Empirical Transfer-Function Estimate, ETFE) mittels eines pseudo-zufälligen binären Eingangssignals; ii) eine ETFE, welche aus einem mit einem Relay-Regler geschlossenen Regelkreis identifiziert wurde; iii) ein RC-Modell, welches mit der BRCM Toolbox erstellt wurde. In einem Validierungsexperiment haben wir die verschiedenen Modelle in Bezug auf Genauigkeit und Effizienz verglichen. Alle Modelle wiesen eine ziemlich gute Vorhersagequalität auf. In einem weiteren Experiment zeigten wir, dass die Dynamik der Luftmischung einer der Hauptunterschiede zwischen dem experimentell ermittelten und dem RC-Modell ist. Die Studie zeigt ausserdem, dass ein zusätzlicher Pol zum RC-Modell hinzugefügt werden kann, um die Unterschiede auszugleichen.

In Teil III präsentieren wir die Ergebnisse des OptiControl-II Projekts, welches prädiktive Gebäuderegelungsstrategien untersuchte und in welchem ein voll besetztes Schweizer Bürogebäude über sieben Monate hinweg mit MPC geregelt wurde. Wir beschreiben den Aufbau der Regelung, die Modellierung, die experimentellen Resultate sowie simulationsbasierte Vergleiche von MPC und der zuvor installierten RBC Strategie mit der EnergyPlus Simulationssoftware. Weiter analysieren wir basierend auf diesen Ergebnissen die Kosten und den Nutzen von MPC für ähnliche Gebäude. Die experimentellen Resultate zeigten, dass MPC das Gebäude zuverlässig steuerte und ein gutes Komfortniveau erreichte. Die Simulationen wiesen zusätzlich eine wesentlich verbesserte Regelgüte in Bezug auf Energie und Komfort im Vergleich zu RBC auf. Es zeigte sich allerdings, dass für ähnliche Gebäude und mit den derzeit verfügbaren Methoden, die erforderlichen Investitionen zu hoch sind, um den standardmässigen Einsatz von MPC alleine aufgrund von Betriebskosteneinsparungen zu rechtfertigen. Dennoch könnten Entwicklungsinvestitionen in ein MPC Gebäuderegelungssystem und eine automatisierte Modellierung, zusammen mit der zunehmenden Bedeutung von elektrischer Laststeuerung und steigenden Energiepreisen, die Technologie in einen Nettonutzen-Bereich bringen.

Teil IV untersucht mittels einer simulationsbasierten Studie das Potenzial von verbesserter Belegungsinformation für eine energieeffizientere Gebäuderegelung. Um das Einsparpotential abzuschätzen, werden verschiedene Arten von Belegungsinformationen in einem MPC Regler verwendet: i) ein Standardbelegungsplan als Vorhersage (Anwesenheit während der Bürozeiten, sonst Abwesenheit); ii) der Standardbelegungsplan als Vorhersage und zusätzliche instantane Anwesenheitsmessungen, welche verwendet werden, um bei Abwesenheit die Beleuchtung auszuschalten; iii) der Standardbelegungsplan als Vorhersage und zusätzliche instantane Anwesenheitsmessungen, welche verwendet werden, um Belichtung und Belüftung bei Abwesenheit abzuschalten; iv) perfekt vorhergesagte Belegungsinformationen. Die Simulationen wurden für eine Reihe von Kombinationen von Baustandards, HVAC Systemen, Wärmegewinne, und Wetterbedingungen durchgeführt. Wir zeigen, dass die Berücksichtigung von Belegungsinformationen in der Gebäudeklimaregelung ein erhebliches Energieeinsparpotenzial birgt, welches allerdings zu einem grossen Teil bereits durch die Berücksichtigung von instantanen Belegungsmessungen abgeschöpft werden kann.

List of Acronyms

AHU	Air Handling Unit
ANN	Artificial Neural Network
BACnet	Building Automation and Control Networks
BAS	Building Automation System
BRCM	Building Resistance-Capacitance Modeling
CHF	Swiss Francs
CSV	Comma-Separated Values
EHF	External Heat Flux
EN	European Norm
EP	EnergyPlus
ERC	Energy Recovery
ETFE	Empirical Transfer Function Estimate
HL	High-Level
HVAC	Heating, Ventilation, Air Conditioning
LL	Low-Level
MPC	Model Predictive Control(ler)
NRPE	Non-Renewable Primary Energy
OPC	Object Linking and Embedding for Process Control
PID	Proportional-Integral-Derivative (Controller)
PRBS	Pseudo-Random Binary Sequence
RBC	Rule-Based Control
RC	Resistance-Capacitance
SS	State-Space
TABS	Thermally Activated Building System

Notation

$:=$	assignment (in the computer science sense)
...	and so forth
$\in$	element of
$\forall$	for all
$<, \leq, =, \geq, >$	element-wise comparison of vectors
$\mathbb{R}$	real numbers
$\mathbb{R}^n$	the space of n-dimensional (column) vectors with real entries
$\mathbb{R}^{n \times m}$	the space of $n \times m$ matrices with real entries
$\mathbb{N}_a^b$	set of consecutive non-negative integers $\{a, ..., b\}$ ($0 \leq a \leq b$)
I	identity matrix (of appropriate size)
0	zero matrix (of appropriate size)
a^T	transpose of a vector
$||a||_1$	vector 1-norm (sum of absolute values)
$||a||_2$	vector 2-norm (euclidian distance)
M^T	transpose of a matrix
M^{-1}	inverse of a (square) matrix
$\mathbf{P}$	probability function ($\mathbf{P}(X = x)$ is the probability that the discrete random variable X takes on the value x)
$\mathbf{E}$	expected value
n_x	number of states
n_u	number of control inputs
n_v	number of disturbances
n_c	number of constraints
x	states ($x \in \mathbb{R}^{n_x}$)
u	control inputs ($u \in \mathbb{R}^{n_u}$)
v	disturbances ($v \in \mathbb{R}^{n_v}$)

Internet Links

Here we summarize links to companies, organizations, and softwares referred to in this thesis. The links were last accessed in November 2014.

Companies and Organizations

Actelion Pharmaceuticals Ltd.	`http://www.actelion.ch`
Federal Office of Meteorology and Climatology MeteoSwiss	`http://www.meteoswiss.admin.ch`
Gruner-Roschi Ltd.	`http://www.gruner.ch`
SAUTER Ltd.	`http://www.sauter-controls.com`
Siemens Switzerland Ltd.	`http://www.siemens.ch`
swiss*electric* research	`http://www.swisselectric.ch`

Projects and Institutes

OptiControl	`http://www.opticontrol.ethz.ch`
Automatic Control Laboratory	`http://control.ee.ethz.ch`

Softwares

BCVTB	`http://simulationresearch.lbl.gov/bcvtb`
BRCM toolbox	`http://www.brcm.ethz.ch`
CPLEX	`http://www-01.ibm.com/software/commerce/optimization/cplex-optimizer`
EnergyPlus	`http://apps1.eere.energy.gov/buildings/energyplus`
ESP-r	`http://www.esru.strath.ac.uk/Programs/ESP-r`
Excel	`http://www.office.microsoft.com/`
HAMBase	`http://archbps1.campus.tue.nl/bpswiki/index.php/Hamlab`
Matlab	`http://www.mathworks.com`
Radiance	`http://www.radiance-online.org`
Toolbox Manager	`http://www.tbxmanager.com`
TRNSYS	`http://www.trnsys.com`

Part I
Introduction and Background

Chapter 1

Introduction

Approximately 40 % of the global energy consumption occurs in buildings [1], of which, in industrialized countries, roughly half is used for Heating, Ventilation, and Air Conditioning (HVAC) [2]. This level of consumption makes measures aiming at HVAC energy reduction very attractive. Energy reductions can be realized by improving a building's HVAC systems and construction, its operation, or preferably some combination of both. However, the majority of the building stock is already in place and refurbishments of buildings are expensive. By contrast, control systems can be upgraded and their operation optimized at comparatively low costs. This is particularly attractive in commercial buildings which mostly already employ some level of automated control that may be improved without significant hardware installations. Improving the control of commercial buildings is the focus of this thesis. However, the interaction with building users and the complexity of many modern buildings make the design of energy-efficient, economic, robust, and easy to implement building control systems far from trivial.

In this thesis, we consider building climate control[1] to comprise the control of the HVAC system, the blinds, and the lighting. The relevant actuators[2] are components such as boilers, chillers, fans, pumps, mixing valves, heat exchangers, blinds and window motors, and lighting power switches. These systems need to be controlled such that the occupants' comfort (e.g. in terms of temperature, humidity, and CO_2 levels) is satisfied while using as little energy as possible.

Current practice in building climate control is the use of Rule-Based Control (RBC). In this approach, the setpoints of the individual components are determined by "if *condition* then *action*" rules and heating / cooling curves. These rules contain a potentially large number of parameters that need to be set in order to adapt the control strategy to a particular building. The setpoints determined by the RBC are typically tracked by Proportional-Integral-Derivative (PID) controllers (e.g. PID control of a mixing valve to track a desired supply water temperature). The *tuning* of the RBC parameters is critical for the performance of this strategy but is becoming increasingly more difficult due to the growing complexity of HVAC systems such as active thermal storage systems or intermittently available renewable energy sources. Nowadays, RBC strategies typically are not *integrated*, i.e. there is little to no coordination between the control of the heating, cooling, air conditioning, and blind systems. Moreover, systematically including weather forecasts – commonly regarded as a way to improve energy efficiency – is difficult in these strategies. Hence, even though RBC is a well-established technology, computationally inexpensive, and is able to satisfy comfort in most cases, its capability for further improving energy efficiency are likely rather limited.

Summarizing, the need to minimize energy consumption drives the research towards more energy efficient building automation but the energy savings potential of current building au-

---

[1]In the following, also referred to as *building control* or *building automation*.

[2]In the following, also referred to as *building systems*.

tomation strategies may already have been exploited. Hence, together with continuously decreasing computation costs, advanced building control solutions become ever more interesting alternatives.

Model Predictive Control (MPC[3]) presents one such alternative. The methodology has been successfully applied in many areas, in particular due to its capability of handling constraints on state and input variables. Applied to building climate control[4], MPC uses a mathematical model of the building and predictions of disturbances (e.g. ambient temperature) over a given prediction horizon (e.g. two days) to formulate an optimization problem. This is solved to find the control input trajectory that maintains comfort for the occupants over the whole horizon while minimizing some objective (e.g. total energy use or monetary costs). The first step of this control input trajectory is then implemented on the building. One time step later, this process is repeated, initializing the optimization problem with a current measurement (or estimate) of the building's state and optimizing over a shifted horizon which is why MPC is also known as *receding horizon control*. The aforementioned features make it possible to systematically integrate all available actuators and their interactions as well as predictions of the weather, internal gains, and electricity prices into a control framework that can handle constraints on the room temperatures (states) and on the use of HVAC systems (inputs). A further potential benefit of MPC lies in the area of electrical *demand response* which can be defined as "Changes in electric usage by end-use customers from their normal consumption patterns in response to changes in the price of electricity over time, or to incentive payments designed to induce lower electricity use at times of high wholesale market prices or when system reliability is jeopardized." [3]. In contrast to RBC, such time-varying electricity prices can straightforwardly be included in the cost function of an MPC. It can be shown that assuming a perfect model, ideal disturbance predictions, and a sufficiently long prediction horizon, an MPC's operation is very close to optimal in the sense of a minimum overall objective value and constraint satisfaction. Naturally, these assumptions are not satisfied in practice. In particular, finding a building model that is sufficiently accurate but simple enough to be used in an MPC is a challenging but crucial task in the controller design. In fact, as we will argue in this thesis, the difficulty and costs involved with the construction of such a model is the paramount reason why MPC is up until today only very rarely used in building automation. However, with the use of simulation models in the planning stage of buildings becoming standard and the development of building modeling frameworks for MPC, the application of building MPC is becoming more attractive.

In recent years, many studies have analyzed the energy savings potential of MPC in simulations, often in a best-case scenario where the simulation and the control model were identical. However, while these studies have demonstrated the potential benefits of MPC when compared to industry-standard RBC control, many problems still remain to be solved that relate to the appropriate modeling of real buildings, plant-model mismatch, and the practical feasibility of MPC, as for instance its compatibility with pre-installed control systems. Moreover, the usefulness of any proposed controller must be measured not only by its benefits but also by its incurred costs, such as the necessary hard- and software and the system's design, implementation and maintenance effort. These considerations are at the core of this thesis.

---

[3]Depending on the context, we use MPC also as an abbreviation for Model Predictive Controller.
[4]In the following, we will refer to model predictive building climate control, building MPC, and MPC for buildings interchangeably.

This PhD thesis was carried out in the context of the OptiControl-II project which involved and was co-sponsored by the following parties: swiss*electric* research; Siemens Switzerland Ltd., Building Technologies Division, Zug; Gruner-Roschi AG, Basel; and Actelion Pharmaceuticals Ltd., Allschwil (see the Internet Links section at the beginning of the document for links to the project's and the companies' websites).

1.1 Outline and Contributions

This thesis contains four parts. Part I is concerned with giving background information and contains no novel contributions. In Chapter 2, we formulate the building climate control task as an intractable optimal control problem over a very long horizon with the goal of ensuring comfort constraint satisfaction for the occupants at all times while minimizing total operating costs. MPC for buildings is then motivated as a tractable approximation of the optimal control problem and its literature is reviewed. Finally, we introduce the MPC formulation considered in this thesis which is based on linear costs and constraints and a bilinear building model and describe our approach to solve the resulting nonlinear optimization problem.

Part II is concerned with modeling of buildings for MPC. Chapter 3 gives an overview of and discusses the various approaches that are used to construct building models. The contribution of Chapter 4 is a Matlab toolbox that we developed to enable the fast modeling of bilinear building models as well as of linear costs and constraints from building geometry, building construction, and building systems data. First, we describe how the models are constructed. Then, we present a case study in which the toolbox was applied to create a model that was subsequently compared to the building simulation software EnergyPlus. In Chapter 5, an alternative method for obtaining a building model is investigated. It describes a study in which we used identification techniques to model a ventilated room. Three models for the room were derived: i) an empirical transfer function estimate (ETFE) derived from a pseudo-random binary sequence input signal; ii) an ETFE derived from a relay feedback closed-loop identification approach; iii) a model constructed using the BRCM toolbox. The main contributions are: a) the assessment of the different models in terms of accuracy; b) the demonstration that air mixing dynamics is one of the main differences between the experimentally identified and the BRCM model; c) we show that an additional pole can be added to the BRCM model in order to compensate for the differences.

Part III reports the results of the predictive building control project OptiControl-II that encompassed seven months of MPC of a fully-occupied Swiss office building. The main contributions are: i) the demonstration of the feasibility of MPC applied to the climate control of a fully-occupied office building under realistic conditions; ii) a detailed description of the modeling and of the integration of MPC into the existing building automation system; iii) a cost / benefit analysis of MPC for similar buildings.

Part IV investigates the energy savings potential of improved occupancy information by means of a simulation-based study. To evaluate the potential savings, different types of occupancy information were used in an MPC: i) a standard occupancy schedule (presence during office hours, vacancy otherwise) used to predict internal gains and comfort constraints; ii) the standard schedule used for prediction and additionally instantaneous occupancy measurements used to adjust lighting; iii) the standard schedule used for prediction and additionally

instantaneous occupancy measurements used to adjust lighting and ventilation; iv) perfectly predicted occupancy information. Simulations were performed for every controller and over a set of building, HVAC system, internal gains level, and weather combinations. The main contribution is the finding that taking into account occupancy information in building climate control has a significant energy savings potential but a large part of this potential can already be captured by considering instantaneous occupancy measurements. Hence, the effort of collecting improved occupancy predictions may not be worthwhile.

1.2 Publications

The presented results were obtained together with numerous colleagues. This dissertation is largely based on the following publications, all of which are available upon request from `http://control.ee.ethz.ch`.

Part II is based on the following publications:

- [4]: D. Sturzenegger, D. Gyalistras, M. Morari and R. S. Smith
  Semi-Automated Modular Modeling of Buildings for Model Predictive Control
  BuildSys 2012 - Workshop of ACM SenSys Conference, Toronto, Canada, 2012.
- [5]: D. Sturzenegger, D. Gyalistras, V. Semeraro, M. Morari and R. S. Smith
  BRCM Matlab Toolbox: Model Generation for Model Predictive Building Control
  American Control Conference, Portland, USA, 2014.
- [6]: D. Sturzenegger, D. Keusch, L. Muffato, D. Kunz and R. S. Smith
  Frequency-Domain Identification of a Ventilated Room for MPC
  IFAC World Congress on Automatic Control, Cape Town, South Africa, 2014.

Part III is mainly based on the following publications:

- [7]: D. Sturzenegger, D. Gyalistras, M. Morari and R. S. Smith
  Model Predictive Control of a Swiss Office Building: Implementation, Results and Cost-Benefit Analysis
  IEEE Transactions on Control Systems Technology, (conditionally accepted).
- [8]: D. Sturzenegger, D. Gyalistras, M. Gwerder, C. Sagerschnig, M. Morari and R. S. Smith
  Model Predictive Control of a Swiss Office Building
  Clima - RHEVA World Congress, Prague, Czech Republic, 2013.
- [9]: M. Gwerder, D. Gyalistras, C. Sagerschnig, R. S. Smith and D. Sturzenegger
  Final Report: Use of Weather and Occupancy Forecasts for Optimal Building Climate Control - Part II: Demonstration (OptiControl-II)
  Technical Report, 2013
  `http://www.opticontrol.ethz.ch/Lit/Gwer_13_Rep-OptiCtrl2FinalRep.pdf`.

Part IV is based on the following publications:

- [10]: F. Oldewurtel, D. Sturzenegger and M. Morari
  Importance of Occupancy Information for Building Climate Control
  Applied Energy, vol. 101, 2013.

- [11]: D. Sturzenegger, F. Oldewurtel and M. Morari
  Importance of Long-Term Occupancy Information - A Validation with Real Occupancy Data
  Clima - RHEVA World Congress, Prague, Czech Republic, 2013.

The following publications have been prepared during my doctorate, but are not part of this dissertation:

- [12]: F. Oldewurtel, D. Sturzenegger, G. Andersson, M. Morari and R. S. Smith
  Towards a Standardized Building Assessment for Demand Response
  Conference on Decision and Control, Florence, Italy, 2013.

- [13]: X. Zhang, G. Schildbach, D. Sturzenegger and M. Morari
  Scenario-Based MPC for Energy-Efficient Building Climate Control under Weather and Occupancy Uncertainty
  European Control Conference, Zurich, Switzerland, 2013.

- [14]: F. Oldewurtel, D. Sturzenegger, P. Mohajerin Esfahani, G. Andersson, M. Morari and J. Lygeros
  Adaptively Constrained Stochastic Model Predictive Control for Closed-Loop Constraint Satisfaction
  American Control Conference, Washington, DC, USA, 2013.

- [15]: M. Gwerder, S. Boetschi, D. Gyalistras, C. Sagerschnig, D. Sturzenegger, R. S. Smith and B. Illi
  Integrated Predictive Rule-Based Control of a Swiss Office Building
  Clima - RHEVA World Congress, Prague, Czech Republic, 2013.

Chapter 2

Model Predictive Control for Buildings

In this chapter, we introduce the idea of MPC for building climate control. It is not meant to be a comprehensive summary of the theory (see [16] for a standard book on MPC) but aims at illustrating the concepts relevant for the rest of this thesis. First, in Section 2.1, we introduce a very natural way of defining the control task in the form of a – typically not solvable – optimal control problem. In Section 2.2, we then introduce MPC as a tractable approximation of this problem. Section 2.3 provides a literature review of MPC for building climate control and finally, in Section 2.4, we describe the form and solution of the MPC optimization problem considered in this thesis.

2.1 Optimal Building Control Problem

Consider the control of a building described by the discrete-time system

$$x_{t+1} = g(x_t, u_t, v_t), \tag{2.1}$$

with a sampling time T_s, e.g. $0.25\,\text{h}$. In building models, the *states* $x_t \in \mathbb{R}^{n_x}$ most commonly describe temperatures of parts of the building, the *control inputs* $u_t \in \mathbb{R}^{n_u}$ describe the effect of the building systems and reflect for instance an applied heating power or a ventilation air mass flow, and the *disturbances* $v_t \in \mathbb{R}^{n_v}$ are exogenous influences such as the ambient temperature, solar gains, or internal gains from people and equipment. At time 0, the building is considered to be in the state x_0. We consider the system to be subject to *actuation constraints* (e.g. minimum and maximum heating power) written as

$$h_a(x_t, u_t, v_t) \leq 0. \tag{2.2}$$

We make the reasonable assumption that for every x_t and v_t there exists a u_t that satisfies (2.2). A very natural way of defining the control task is to formulate a *cost function* that is to be minimized while satisfying *comfort constraints* at every time step from 0 to a *horizon* N_f, i.e. for all $t \in \mathbb{N}_0^{N_f-1}$. The horizon N_f is considered to be very long, for instance the whole remaining lifetime of the building. We consider the following (scalar) cost function

$$\sum_{t=0}^{N_f-1} q_t(x_t, u_t, v_t), \tag{2.3}$$

where $q_t(x_t, u_t, v_t)$ are the *stage costs* at time t, usually denoting consumed energy or monetary costs incurred from the usage of the building system and sometimes also deviations of

x_t from reference values. The comfort constraints,

$$h_{c,t}(x_t, u_t, v_t) \leq 0, \tag{2.4}$$

most often encode bounds on room temperatures or on other measures of occupant comfort. Denote by

$$X_{0 \to N_f} = \begin{pmatrix} x_0 \\ x_1 \\ \vdots \\ x_{N_f-1} \end{pmatrix}, \qquad U_{0 \to N_f} = \begin{pmatrix} u_0 \\ u_1 \\ \vdots \\ u_{N_f-1} \end{pmatrix}, \qquad V_{0 \to N_f} = \begin{pmatrix} v_0 \\ v_1 \\ \vdots \\ v_{N_f-1} \end{pmatrix}, \tag{2.5}$$

the *state*, *control input*, and *disturbance trajectory*, respectively. We can now formulate the control task described above as the *optimal building control problem*,

$$U^*_{0 \to N_f}(x_0, V_{0 \to N_f}) = \arg \min_{U_{0 \to N_f}} \sum_{t=0}^{N_f-1} q_t(x_t, u_t, v_t) \tag{2.6a}$$

$$\text{subject to} \quad x_{t+1} = g(x_t, u_t, v_t) \qquad \forall t \in \mathbb{N}_0^{N_f-1} \tag{2.6b}$$

$$h_a(x_t, u_t, v_t) \leq 0 \qquad \forall t \in \mathbb{N}_0^{N_f-1} \tag{2.6c}$$

$$h_{c,t}(x_t, u_t, v_t) \leq 0. \qquad \forall t \in \mathbb{N}_0^{N_f-1} \tag{2.6d}$$

We make the following assumption:

Assumption 1 *For all x_0 and $V_{0 \to N_f}$, problem (2.6) has a solution.*

Note that Assumption 1 is not unrealistic. In fact, the building systems (reflected in g and h_a) are designed during the planning stage of the building to be able to satisfy comfort for all realistic disturbances. Additionally, we avoid technicalities by making Assumption 2:

Assumption 2 *The solution to (2.6) is unique.*

The minimizer of (2.6) is the *optimal control input trajectory*, $U^*_{0 \to N_f}(x_0, V_{0 \to N_f})$, as a function of x_0 and $V_{0 \to N_f}$. We denote by $J^*_{0 \to N_f}(x_0, V_{0 \to N_f})$ the attained minimum.

Note that the optimal building control problem is a very intuitive and general way of specifying the control task and that it would be desirable to solve (2.6) at time 0 and subsequently apply $U^*_{0 \to N_f}$ (which obviously would require knowledge of $V_{0 \to N_f}$ at time 0). Unfortunately, (2.6) is a nonlinear mathematical optimization problem with $N_f \cdot n_u$ decision variables and even under the assumption that we know $V_{0 \to N_f}$ at time 0, the problem is generally intractable[1]. Building MPC is motivated as a tractable approximation of the optimal building control problem. Its concept is described in the following section.

---

[1] In practice, also the model (2.6b) is not known well enough to make accurate predictions over such a long horizon. Hence, we cannot solve the optimal building control problem for the following reasons: i) intractability of the nonlinear optimization problem with $N_f \cdot n_u$ decision variables; ii) lack of knowledge about the future disturbances $V_{0 \to N_f}$; iii) insufficiently accurate model (2.6b).

Algorithm 2.1: Model Predictive Building Control

repeat

Measure the current state x_t

Obtain disturbance predictions $V_{t \rightarrow t+N|t}$

Solve (2.11) to obtain $U^*_{t \rightarrow t+N|t}$

Apply first step $u^*_{t|t}$ to the building

$t := t + 1$

2.2 Model Predictive Building Control

An MPC solves at every time step t a smaller, tractable version of (2.6) over a horizon of $N \ll N_f$ steps based on a measurement of the current state x_t and the *disturbance predictions*

$$V_{t \rightarrow t+N|t} = \begin{pmatrix} v_{t|t} \\ v_{t+1|t} \\ \vdots \\ v_{t+N-1|t} \end{pmatrix}. \tag{2.7}$$

We use the common notation that variables with subscript "$t+k|t$" are to be read as variable "at time $t+k$ predicted at time t"[2]. MPC then applies the first step $u^*_{t|t}(x_t, V_{t \rightarrow t+N|t})$ of the optimal (with respect to the approximated problem) input trajectory,

$$U^*_{t \rightarrow t+N|t}(x_t, V_{t \rightarrow t+N|t}) = \begin{pmatrix} u^*_{t|t}(x_t, V_{t \rightarrow t+N|t}) \\ u^*_{t+1|t}(x_t, V_{t \rightarrow t+N|t}) \\ \vdots \\ u^*_{t+N-1|t}(x_t, V_{t \rightarrow t+N|t}) \end{pmatrix}, \tag{2.8}$$

to the building. At the next time step, the procedure is repeated. The building MPC procedure is summarized in Algorithm 2.1. The resulting closed-loop behavior of system (2.1) is given by

$$x_{t+1} = g(x_t, u^*_{t|t}(x_t, V_{t \rightarrow t+N|t}), v_t) \tag{2.9}$$

The hope is that this closed-loop behavior resulting from applying the "short-sighted" MPC strategy is similar in terms of costs and comfort constraint satisfaction to the one of the optimal control problem, i.e.

$$\sum_{t=0}^{N_f-1} q_t(x_t, u^*_{t|t}, v_t) \approx J^*_{0 \rightarrow N_f}(x_0, V_{t \rightarrow N_f}) \tag{2.10a}$$

$$h_{c,t}(x_t, u^*_{t|t}, v_t) \leq 0 \quad \forall t \in \mathbb{N}_0^{N_f-1} \tag{2.10b}$$

---

[2]In the case of control inputs "computed at time t".

where $x_0, x_1, ..., x_{N_f-1}$ are understood to be the state trajectory of the closed-loop system (2.9) starting from x_0. The *MPC optimization problem* solved at time step t is

$$U^*_{t \to t+N|t}(x_t, V_{t \to t+N|t}) = \arg\min_{U_{t \to t+N|t}} \sum_{k=0}^{N-1} q_{t+k}(x_{t+k|t}, u_{t+k|t}, v_{t+k|t}) \qquad (2.11a)$$

$$\text{subject to} \quad x_{t+k+1|t} = g(x_{t+k|t}, u_{t+k|t}, v_{t+k|t}) \quad \forall k \in \mathbb{N}_0^{N-1} \quad (2.11b)$$

$$h_a(x_{t+k|t}, u_{t+k|t}, v_{t+k|t}) \leq 0 \qquad \forall k \in \mathbb{N}_0^{N-1} \quad (2.11c)$$

$$h_{c,t+k}(x_{t+k|t}, u_{t+k|t}, v_{t+k|t}) \leq 0 \qquad \forall k \in \mathbb{N}_0^{N-1} \quad (2.11d)$$

$$x_{t|t} = x_t. \qquad (2.11e)$$

Intuitively, it is clear that if we were able to solve (2.11) for a horizon of $N = N_f$ and if we had access to perfect disturbance predictions, i.e. $V_{t \to t+N|t} = V_{t \to t+N}$, then the input trajectory $\{u^*_{0|0}, u^*_{1|1}, ..., u^*_{N_f-1|N_f-1}\}$ resulting from applying Algorithm 2.1 (assuming no costs and constraints in the MPC problem after $N_f - 1$) would be identical to the solution $U^*_{0 \to N_f}$ of the optimal control problem. Moreover, the corresponding state trajectories would coincide and (2.10a) would hold with equality.

However, since in general we cannot solve (2.11) for $N = N_f$ and because the predictions are imperfect, the input trajectory and the state trajectory resulting from repeatedly applying Algorithm 2.1 are generally different from the input and state trajectory resulting from the optimal building control problem. Moreover, even with Assumption 1, there is in general no guarantee that the MPC problem (2.11) is feasible for all t. In theory, the MPC problem can (under some assumptions) be manipulated by adding additional cost and constraint terms to ensure *recursive feasibility*. However, this may lead to conservative behavior. In practice, often *soft constraints* are used, i.e. (2.11d) is replaced with $h_{c,t+k}(x_{t+k|t}, u_{t+k|t}, v_{t+k|t}) \leq z$ and a penalization term, for instance $\gamma||z||_1$, is added to the cost function with γ "sufficiently" large to enforce $z = 0$ if possible. This ensures feasibility of the resulting MPC problem (recall that we assumed that there always exists a u_t that can satisfy the actuation constraints).

Summarizing, the hope is that when applying the MPC Algorithm 2.1, the resulting closed-loop behavior satisfies the comfort constraints (see (2.10b)) and that its total cost is similar to the optimal cost, $J^*_{0 \to N_f}(x_0, V_{t \to N_f})$, of the optimal building control problem (see (2.10a)), but no guarantees can be given. Intuitively, the longer the prediction horizon and the better the disturbance predictions, the closer the MPC's closed-loop behavior's cost should be to $J^*_{0 \to N_f}(x_0, V_{t \to N_f})$ and the more likely it should be able to to satisfy comfort at every time step.

2.2.1 Practical Considerations

So far we assumed that the MPC had access to the exact model of the building's dynamics, its actuation constraints, the costs, and the comfort constraints. In practice, this is unrealistic. Much research effort has gone into the modeling of buildings but their behavior can still only be approximately predicted. This *model-mismatch* deteriorates the performance of the MPC. Additionally, recall that MPC was motivated by the need for a *tractable* approximation of the optimal building control problem. However, even though the number of decision variables has

been reduced to $N \cdot n_{\mathrm{u}}$, the MPC problem (2.11) is in general not easily solved if no special structure on q_t, g, h_{a}, and $h_{\mathrm{c},t}$ is imposed. In many cases, much effort goes into formulating the MPC problem to be *convex* which can be considered equivalent to "easy to solve". We refer for a general treatment of convex optimization to a standard textbook [17] but introduce in Section 2.4 a particularly desirable convex form of (2.11) relevant for this thesis.

Adding to this the fact that generally the building's state x_t is not perfectly known, we can list the reasons for sub-optimality of the MPC scheme with respect to the original optimal building control problem roughly in order of importance[3]:

1) Imperfect model (due to general incapability of exactly modeling building behavior and due to modeling simplifications necessary to ensure tractability of the optimization problem).
2) Imperfect disturbance predictions.
3) It may not be possible to solve (2.11) to optimality within reasonable time (usually the case if it is not convex).
4) Imperfect state information.
5) "Short" prediction horizon.

Even though it is interesting to know how MPC relates to the solution of the optimal building control problem, the more important question is how much it can improve on current standard control strategies (if at all). This has been investigated in many studies, some of which are reviewed in the following.

2.3 Literature Review

The studies on building MPC can be categorized in *simulation-based* (the plant is a simulation model) and *experimental*[4] (the plant is a part of or an entire building) investigations. In the following, we first consider the (substantially larger) simulation-based literature and outline the current directions of this research. Naturally, since conducting experimental MPC studies requires a significant effort, simulation-based studies were historically predominant and their results motivated the recent shift towards experimental works. Second and more importantly in the context of this thesis, we provide a comprehensive review of the experimental building MPC literature. This allows this thesis to be put into context, as it is mainly about the transition of building MPC from theory to practice.

2.3.1 Simulation-Based MPC Studies

In simulation-based studies, typically, two simulations with identical models, initial conditions, and disturbances are performed; in one, the simulation model is controlled by the proposed MPC scheme and in the other by some baseline controller. Then, the performances in terms of costs and constraint satisfaction are compared, usually resulting in MPC being superior. Such results have to be seen with a grain of salt for two reasons: i) obviously (but often not discussed), this outcome depends as much on the baseline controller's quality as on the MPC's; ii) most often, a perfect (with respect to the simulation model) model, perfect state

---

[3]This ordering is based on our experience and not on a systematic investigation. Moreover, it depends on the case at hand.

[4]We also use the expressions *practical* or *implementation* studies.

information, and frequently also perfect disturbance predictions are assumed, negating the reasons 1, 2, and 4 for MPC sub-optimality defined in the previous section. Nevertheless, these studies are important to indicate the maximum (due to the idealized setup) potential savings of MPC. If they were small, there would be no point in going through the effort of experimental studies.

Due to the body of literature being so vast, a comprehensive literature review of simulation-based MPC is beyond the scope of this section. On the other hand, selecting a subset of publications would be unsystematic, since none of the simulation-based studies can be said to relate more than others to this thesis. Hence, we refer to the extensive building MPC review paper [18] and provide in the following an overview of the research directions without mentioning individual publications. The connection to implementation studies is obvious: since simulations usually precede experiments, an overview of the simulation-based research directions can give an idea of what future experimental MPC studies might take place.

While the use of weather predictions has already been investigated earlier outside of an optimal control setting, the first publications on building MPC appeared around 1990. They used a standard simulation setting in which the model and the disturbances were perfectly known to the MPC. At first, only few researchers investigated building MPC strategies, but from around 2005 to 2010 the annual number of publications rapidly increased. Afterwards however, the literature moved away from this standard setting and considered either more realistic ones or different use cases.

Around 2010, studies began to appear in which building simulation softwares such as TRNSYS, EnergyPlus, or ESP-r (see the Internet Links section at the beginning of the document for links to the softwares' websites) were used as simulation models in order to obtain more realistic results.

Starting around 2009, the interest in *stochastic MPC* began to grow. These MPC formulations consider the fact that the disturbances acting on the building are usually not known exactly. Based on probabilistic models of the prediction errors, such an MPC controls the building so that comfort is guaranteed with a given (high) probability.

Another recent research direction that appeared around 2011 is the extraction of decision rules based on an analysis of the MPC operation. This is achieved by means of machine learning techniques using disturbance predictions, current measurements, and simulated MPC control decisions as training data. The hope is to be able to use the currently implemented RBC control systems but improve their configuration based on the extracted rules.

Around 2010, research into *distributed* building MPC formulations gained traction. In such methods, the MPC optimization problem is not solved centrally. Instead, smaller sub-problems are solved on distributed control devices with only limited communication, often sacrificing optimality with respect to the original centralized MPC problem, again in the hope of being able to use the existing control architecture.

Around 2011, studies into *adaptive* building MPC began appearing. These approaches try to cope with the difficulty of building modeling by adapting parameters of the MPC formulation, in particular of the model, based on measurements during the control. The hope is that this reduces the required accuracy of the initial model while still achieving a good closed-loop performance due to the "on-line" adaptation.

Finally, since around 2010, one of the most active branches is investigating the use of MPC

for demand response purposes. With the increasing integration of renewable energy sources into the grid, the power supply is fluctuating significantly more. A cost-effective method to cope with this fact is so called *demand side participation* where consumers lower or increase their electricity consumption based on requests of the grid operator. These requests often are formulated in terms of time-varying electricity prices. MPC has the unique ability make close-to-optimal decisions based on these prices and can be formulated to be able to almost instantaneously increase / decrease electricity consumption by a given amount for a given time and still guarantee comfort.

Almost all of the simulation-based studies that compared MPC to a baseline controller reported an improved performance of the former. Even with the initially mentioned caveat, this makes a strong case for further investigating these concepts in experimental studies.

2.3.2 Experimental Building MPC Studies

This section together with Table 2.1 summarizes all published experimental studies known to us in which buildings have been controlled by MPC. While the costs and comfort constraints are mostly similarly defined across the studies, the choice of the model arguably is the most distinctive feature in a building MPC. In the reviewed studies, the used models ranged from building simulation software models (e.g. EnergyPlus or ESP-r) and artificial neural networks (ANN) to the more commonly known linear and nonlinear state-space descriptions. In this review, we classify the studies according to the system that was controlled (whole building, test cells, etc.), the actuators, the total experiment time and the MPC model.

The earliest work on experimental building MPC used building simulation software models. A practical proof of this concept was first reported in 2002 [19]. The authors used an ESP-r model to optimize the starting time of a radiator in an unoccupied test cell in a three-hour-long experiment. In 2005, the authors of [20] extended the idea to a more complex HVAC setup in a four-days experiment using a TRNSYS model. The primary system consisted of two chillers and an active thermal energy storage while the secondary system comprised a ventilation unit serving two unoccupied test rooms. In 2011, the authors of [21] reported MPC experiments conducted over two months in two occupied Austrian office buildings mainly equipped with window shading and opening devices. In both cases, HAMBase and Radiance models were used.

The only experimental application known to us of an MPC using an ANN model was reported in 2012 [22]. Several experiments were conducted in four occupied rooms of a university building equipped with independent Air Handling Units (AHU) over a total experiment time of around three days.

To our knowledge, the experimental application of an MPC using a state-space model has first been published in 2010 [23]. The authors report the control of a boiler supplying two commercial buildings equipped with radiators over a period of 40 days. MPC was based on a low-order linear state-space model predicting a building-wide average room temperature. In [24], the authors report the control of a Thermally Activated Building System[5] (TABS) of an eight-floor building block of a university building over three months. Their setup provided the unique opportunity to systematically compare the MPC's performance to a baseline controller running in an identical nearby building block. The authors used a low-order linear state-

---

[5]Pipes buried in the concrete floor slabs through which heated / cooled water is pumped.

Table 2.1: Summary of experimental MPC studies. SS: state-space.

Study	System	Actuators	Exp. Time	MPC Model
[19]	One unoccupied test room	Radiator	3 hours	ESP-r
[20]	Two unoccupied test rooms	AHU, ice storage, chillers	4 days	TRNSYS
[21]	Two experiments with three and two occupied office rooms	Shading and window opening devices	60 days	HAMBase and Radiance
[22]	Four occupied rooms	AHU	3 days	Artificial neural network
[23]	Occupied commercial office building	Boiler supplying passive radiators	40 days	Linear SS model
[24]	Eight floors of an occupied university building	TABS heating	90 days	Linear SS model
[25]	Occupied student computer room	AHU	2 days	Linear SS model
[26]	Campus-wide cold water storage	Chillers and cooling tower	10 days	Nonlinear SS model
[27]	Occupied office room	Fan-coil unit	6 hours	Linear SS model
[28]	$650\,\mathrm{m}^2$ space of a research facility	AHU	21 days	Nonlinear SS model

space model. In [25], the authors report an experimental proof of concept of an adaptive MPC approach where in each step, additionally to the actual control, the internal model was improved. The scheme used a scalar linear state-space model and was applied to an air conditioning unit of a student computer room. In another study [26], a nonlinear state-space model was used in an MPC controlling the chillers supplying a large campus-wide cold water storage tank over two five day periods. The buildings' actuators were not controlled, instead the total campus cooling demand was estimated as a function of the weather forecast and then considered as a predictable disturbance. In [27], the authors report experimental results obtained over six hours in a single test room actuating the mass flow and cooling of a fan-coil unit using a linear state-space model. In [28], the authors report MPC experiments over three weeks in which a centralized AHU supplying a $650\,\mathrm{m}^2$ space of a research facility was controlled using a nonlinear model.

All the above studies report a successful operation of MPC and efficiency improvements when compared to baseline control. The experiment durations and the numbers of controlled zones varied significantly across the studies. However, all focused on the control of a single HVAC actuator. Generally, all of the studies aimed at demonstrating MPC's benefits but lacked a discussion of the development and implementation costs.

2.4 Building MPC Considered in this Work

Here we describe the form and solution of the MPC optimization problem considered in this thesis. For simplicity, we replace in the following the subscript notation $t + k|t$ with k and

likewise subscript t with subscript k. A (convex) form that is particularly desirable for the solution of the MPC problem (2.11) is a *linear program*

$$\underset{U_{0 \to N}}{\text{minimize}} \quad b_{\text{cost}}^T U_{0 \to N} \tag{2.12a}$$

$$\text{subject to} \quad A_{\text{ineq}} U_{0 \to N} \leq b_{\text{ineq}}. \tag{2.12b}$$

There exists software (*solvers*) that can solve linear programs very efficiently also for large numbers of decision variables and constraints. It can easily be shown that problem (2.11) can be cast in this way if for a fixed v the functions q_t, g, h_a, and $h_{c,t}$ are linear in x and u. Unfortunately, in particular the physics of the HVAC systems are often nonlinear.

2.4.1 Formulation

The motivation for the following MPC formulation, which is the one considered in the rest of this thesis, was to be "as close as possible" to a linear program while still allowing bilinear air flow effects to be modeled. Hence, we decided to use a linear cost function, linear actuation and comfort constraints, and a bilinear building model. It turned out that due to the "mild" nonlinearity this approach resulted in an MPC problem that could be reasonably well solved by a sequence of linear programs. The linear cost function,

$$\sum_{k=0}^{N-1} c_k^T u_k, \tag{2.13}$$

is usually only a small restriction in terms of modeling power since in most HVAC actuator models the energy consumption is linearly proportional to the corresponding control input's magnitude. Also the (aggregated) linear actuation and comfort constraints,

$$F_{x,k} x_k + F_{u,k} u_k + F_{v,k} v_k \leq f_k, \tag{2.14}$$

still allow a good representation of the comfort in terms of upper / lower bounds on room temperatures and minimum / maximum air flow rates. Moreover, also many actuators constraints can be expressed as lower and upper bounds on their corresponding control inputs. The bilinear dynamics model that allows the modeling of the product of room air temperatures (states) and air mass flow rates (inputs) as they appear for instance in ventilation models is given by

$$x_{k+1} = Ax_k + B_u u_k + B_v v_k + \sum_{i=1}^{n_u} (B_{vu,i} v_k + B_{xu,i} x_k) u_{k,i}. \tag{2.15}$$

We use the notation $u_{k,i}$ to denote the i-th element of u_k. In the following, whenever bilinearity is mentioned, we specifically mean it to be of the form (2.15), i.e. in x and u or in v and u. Using $\hat{x}$ to denote the estimated state of the system at the current time step, the resulting

MPC problem looks as follows

$$\underset{U_{0 \to N}}{\text{minimize}} \quad \sum_{k=0}^{N-1} c_k^T u_k \tag{2.16a}$$

$$\text{subject to} \quad x_{k+1} = A x_k + B_u u_k + B_v v_k + \sum_{i=1}^{n_u} (B_{vu,i} v_k + B_{xu,i} x_k) u_{k,i} \quad \forall k \in \mathbb{N}_0^{N-1} \tag{2.16b}$$

$$F_{x,k} x_k + F_{u,k} u_k + F_{v,k} v_k \leq f_k \qquad\qquad\qquad \forall k \in \mathbb{N}_0^{N-1} \tag{2.16c}$$

$$x_0 = \hat{x}. \tag{2.16d}$$

Denoting by n_c the number of constraints, the sizes of the matrices are given by

$$c_k \in \mathbb{R}^{n_u}, \quad F_{x,k} \in \mathbb{R}^{n_c \times n_x}, \quad F_{u,k} \in \mathbb{R}^{n_c \times n_u}, \quad F_{v,k} \in \mathbb{R}^{n_c \times n_v}, f_k \in \mathbb{R}^{n_c} \qquad \forall k \in \mathbb{N}_0^{N-1}$$

$$B_{vu,i} \in \mathbb{R}^{n_x \times n_v}, \quad B_{xu,i} \in \mathbb{R}^{n_x \times n_x} \qquad\qquad\qquad\qquad\qquad \forall i \in \mathbb{N}_1^{n_u}$$

$$A \in \mathbb{R}^{n_x \times n_x}, \quad B_u \in \mathbb{R}^{n_x \times n_u}, \quad B_v \in \mathbb{R}^{n_x \times n_v}.$$

2.4.2 Solution via Sequential Linear Programming

The convexity of the MPC problem is usually not guaranteed for nonlinear system dynamics such as the bilinear model in (2.16b). Many possibilities exist to solve the resulting nonlinear optimization problem. We use the common *sequential linear programming* approach which solves problem (2.16) at every time step iteratively. In iteration j, given $\hat{x}$ and $V_{0 \to N}$, the bilinear x terms are substituted with an assumed *linearization state trajectory*

$$\bar{X}_{0 \to N}^{(j)} = \begin{pmatrix} \hat{x} \\ \bar{x}_1^{(j)} \\ \vdots \\ \bar{x}_{N-1}^{(j)} \end{pmatrix}. \tag{2.17}$$

Then, the resulting linear program (see Section 2.4.2.1)

$$U_{0 \to N}^{*,(j)} = \underset{U_{0 \to N}}{\arg \min} \quad b_{\text{cost}}^T U_{0 \to N} \tag{2.18a}$$

$$\text{subject to} \quad A_{\text{ineq}}(\hat{x}, V_{0 \to N}, \bar{X}_{0 \to N}^{(j)}) U_{0 \to N} \leq b_{\text{ineq}}(\hat{x}, V_{0 \to N}, \bar{X}_{0 \to N}^{(j)}) \tag{2.18b}$$

is solved, returning the j-th iteration's optimal control input trajectory, $U_{0 \to N}^{*,(j)}$. By starting from $\hat{x}$ and applying $U_{0 \to N}^{*,(j)}$, $V_{0 \to N}$, and $\bar{X}_{0 \to N}^{(j)}$ to (2.15), the new linearization state trajectory $\bar{X}_{0 \to N}^{(j+1)}$ is computed (see Section 2.4.2.1). This is repeated until convergence is achieved (defined as an upper bound on the relative change of the input trajectory between two iterations) or a maximum iteration number is reached. The procedure is described in Algorithm 2.2. The trajectory $\bar{X}_{0 \to N}^{(0)}$ is often initialized using the (correspondingly shifted) trajectory from the last time step. Such a sequential linear programming approach has been successfully applied in

---

Algorithm 2.2: Sequential linear programming.

Obtain $\hat{x}$, $V_{0\to N}$. Initialize $\bar{X}_{0\to N}^{(0)}$ and $j = 0$. Compute b_{cost} as in (2.27a).
repeat

    Compute $A_{\text{ineq}}(\hat{x}, V_{0\to N}, \bar{X}_{0\to N}^{(j)})$ and $b_{\text{ineq}}(\hat{x}, V_{0\to N})$ as in (2.27b)-(2.27c)
    Solve (2.12) and obtain $U_{0\to N}^{*,(j)}$
    Calculate $\bar{X}_{0\to N}^{(j+1)}$ from $\hat{x}$, $U_{0\to N}^{*,(j)}$, $\bar{X}_{0\to N}^{(j)}$, and $V_{0\to N}$ as in (2.28)
    if $j > 1$ **then**

        Compute $\delta U := \left\| U_{0\to N}^{*,(j)} - U_{0\to N}^{*,(j-1)} \right\| \big/ \left\| U_{0\to N}^{*,(j)} \right\|$
        if $j > maxIt$ **or** $\delta U \le relTol$ **then**

            $U_{0\to N}^{*} := U_{0\to N}^{*,(j)}$
            return

        end

    end
    $j := j + 1$

---

many cases, also because the system typically is only very mildly nonlinear (i.e. the bilinear x terms usually are controlled room temperatures that do not significantly vary from iteration to iteration) but obviously the optimality of the solution is not guaranteed.

2.4.2.1 Construction of the Linear Program

In this section, we describe the construction of b_{cost}, A_{ineq}, and b_{ineq} from the matrices and vectors in (2.16), $\hat{x}$, $V_{0\to N}$, and $\bar{X}_{0\to N}^{(j)}$. We begin by linearizing the equality constraints (2.16b) around $\bar{X}_{0\to N}^{(j)}$ and writing them in a stacked form

$$X_{0\to N} = \begin{pmatrix} x_0 \\ x_1 \\ \vdots \\ x_{N-1} \end{pmatrix} = \mathbf{A}\hat{x} + \mathbf{B}_{\text{u}}(\bar{X}_{0\to N}^{(j)}, V_{0\to N})U_{0\to N} + \mathbf{B}_{\text{v}}V_{0\to N}. \tag{2.19}$$

The matrix $\mathbf{A}$ is given by (to more easily guess the sequence, we write A^0 instead of I)

$$\mathbf{A} = \begin{pmatrix} A^0 \\ A^1 \\ A^2 \\ \vdots \\ A^{N-1} \end{pmatrix}, \tag{2.20}$$

the matrix $\mathbf{B}_{\mathrm{u}}(\bar{X}^{(j)}_{0 \to N}, V_{0 \to N})$ is given by,

$$
\mathbf{B}_{\mathrm{u}}(\bar{X}^{(j)}_{0 \to N}, V_{0 \to N}) =
\begin{pmatrix}
0 & \cdots & \cdots & \cdots & \cdots & 0 \\
A^0 B_{\mathrm{u},0} & \ddots & & & & \vdots \\
A^1 B_{\mathrm{u},0} & A^0 B_{\mathrm{u},1} & \ddots & & & \vdots \\
A^2 B_{\mathrm{u},0} & A^1 B_{\mathrm{u},1} & A^0 B_{\mathrm{u},2} & \ddots & & \vdots \\
\vdots & \vdots & \vdots & \ddots & \ddots & \vdots \\
A^{N-2} B_{\mathrm{u},0} & A^{N-3} B_{\mathrm{u},1} & A^{N-4} B_{\mathrm{u},2} & \cdots & A^0 B_{\mathrm{u},N-2} & 0
\end{pmatrix}
\tag{2.21}
$$

$$
B_{\mathrm{u},k} = B_{\mathrm{u}} + \left(B_{\mathrm{xu},1}\bar{x}^{(j)}_k, \ B_{\mathrm{xu},2}\bar{x}^{(j)}_k, \ \cdots, B_{\mathrm{xu},n_u}\bar{x}^{(j)}_k \right) + \left(B_{\mathrm{vu},1}v_k, \ B_{\mathrm{vu},2}v_k, \ \cdots, B_{\mathrm{vu},n_u}v_k \right)
\tag{2.22}
$$

and the matrix $\mathbf{B}_{\mathrm{v}}$ is given by

$$
\mathbf{B}_{\mathrm{v}} =
\begin{pmatrix}
0 & \cdots & \cdots & \cdots & \cdots & 0 \\
A^0 B_{\mathrm{v}} & \ddots & & & & \vdots \\
A^1 B_{\mathrm{v}} & A^0 B_{\mathrm{v}} & \ddots & & & \vdots \\
A^2 B_{\mathrm{v}} & A^1 B_{\mathrm{v}} & A^0 B_{\mathrm{v}} & \ddots & & \vdots \\
\vdots & \vdots & \vdots & \ddots & \ddots & \vdots \\
A^{N-2} B_{\mathrm{v}} & A^{N-3} B_{\mathrm{v}} & A^{N-4} B_{\mathrm{v}} & \cdots & A^0 B_{\mathrm{v}} & 0
\end{pmatrix}.
\tag{2.23}
$$

We can also write the inequality constraints (2.16c) in stacked form

$$
\mathbf{F}_{\mathrm{x}} X_{0 \to N} + \mathbf{F}_{\mathrm{u}} U_{0 \to N} + \mathbf{F}_{\mathrm{v}} V_{0 \to N} \leq \mathbf{f}
\tag{2.24}
$$

where

$$
\mathbf{F}_{\mathrm{x}} =
\begin{pmatrix}
F_{\mathrm{x},0} & 0 & \cdots & 0 \\
0 & F_{\mathrm{x},1} & \ddots & \vdots \\
\vdots & \ddots & \ddots & 0 \\
0 & \cdots & 0 & F_{\mathrm{x},N-1}
\end{pmatrix}, \quad
\mathbf{F}_{\mathrm{u}} =
\begin{pmatrix}
F_{\mathrm{u},0} & 0 & \cdots & 0 \\
0 & F_{\mathrm{u},1} & \ddots & \vdots \\
\vdots & \ddots & \ddots & 0 \\
0 & \cdots & 0 & F_{\mathrm{u},N-1}
\end{pmatrix},
\tag{2.25}
$$

$$\mathbf{F}_v = \begin{pmatrix} F_{v,0} & 0 & \cdots & 0 \\ 0 & F_{v,1} & \ddots & \vdots \\ \vdots & \ddots & \ddots & 0 \\ 0 & \cdots & 0 & F_{v,N-1} \end{pmatrix}, \quad \mathbf{f} = \begin{pmatrix} f_0 \\ f_1 \\ \vdots \\ f_{N-1} \end{pmatrix}. \tag{2.26}$$

Finally, substituting (2.19) in (2.24), we can write the matrices of the linear program as

$$b_{\text{cost}} = \begin{pmatrix} c_0 \\ c_1 \\ \vdots \\ c_{N-1} \end{pmatrix} \tag{2.27a}$$

$$A_{\text{ineq}}(\bar{X}^{(j)}_{0 \to N}, V_{0 \to N}) = \mathbf{F}_u + \mathbf{F}_x \mathbf{B}_u(\bar{X}^{(j)}_{0 \to N}, V_{0 \to N}) \tag{2.27b}$$

$$b_{\text{ineq}}(\hat{x}, V_{0 \to N}) = \mathbf{f} - \mathbf{F}_x(\mathbf{A}\hat{x} + \mathbf{B}_v V_{0 \to N}) - \mathbf{F}_v V_{0 \to N}. \tag{2.27c}$$

Computing the next linearization state trajectory from $\hat{x}$, $\bar{X}^{(j)}_{0 \to N}$, $V_{0 \to N}$, and $U^{*,(j)}_{0 \to N}$ is analogous to (2.19), i.e.

$$\bar{X}^{(j+1)}_{0 \to N} = \mathbf{A}\hat{x} + \mathbf{B}_u(\bar{X}^{(j)}_{0 \to N}, V_{0 \to N})U^{*,(j)}_{0 \to N} + \mathbf{B}_v V_{0 \to N}. \tag{2.28}$$

Part II

Modeling for Building MPC

Chapter 3

Introduction

All models are wrong, but some are useful.
George E. P. Box

In building MPC, a model is used to predict the building's behavior as a function of control inputs (e.g. the applied heating power) and disturbances (e.g. the ambient temperature). The predicted quantities of interest are typically room air temperatures but can also include illumination, CO_2 levels, or more sophisticated measures of human comfort such as the predicted mean vote comfort model (see [29]). The predicted quantities can then be constrained to enforce a desired control behavior. Additionally for MPC, formulations of the actuation costs (often representing energy use or monetary costs) and the actuation constraints are required.

One possible way to categorize building modeling approaches is by the type of data they require to construct the model. In *physics-based* modeling, the model is derived based on physical first-principles from building geometry (room sizes, wall / floor / ceiling thicknesses, etc.), building construction (materials of the wall / floor / ceiling layers), and building systems data[1] (e.g. type, location, efficiency, and distribution of HVAC systems). On the other hand, in *identification-based* approaches, a model is constructed on the basis of measured input (control inputs and disturbances) and output (predicted quantities) data. Of course, the boundary between these categories is blurred. For instance, measured data are sometimes used to identify selected parameters of a mainly physics-based model or a physics-inspired model structure is used in an identification approach. For the following discussion, we consider a model to be physics-based (and identification-based otherwise) if all its parameters can either be derived from geometry, construction, and building systems data or at least can be reasonably estimated based on physical arguments.

The main difficulty of the physics-based method is that for most buildings, the geometry data can be obtained but construction and systems data are only partially available. Moreover, to limit model complexity, often simplifications are made (e.g. air mixing dynamics within a room are not considered), possibly neglecting phenomena that might otherwise be captured using an identification approach (see Section 5). The main problem with the latter method is the fact that it is due to time and building usage constraints often highly impractical or even impossible to excite buildings sufficiently for the identification of multi-input multi-output building models. Moreover, the effort required for the preparation and conduction of the identification experiments may well be prohibitive (see the discussion in Section 6.9).

Naturally, it depends on the case at hand which method is better suited and both approaches have been successfully applied to model buildings for MPC. Nevertheless, in particular for buildings exhibiting slow dynamics such as the TABS system in the OptiControl-II building (see Section 6.2), we suggest the use of physics-based models, possibly together with an online adaptation of a few parameters related to the faster dynamics of the model.

---

[1]In the following, also referred to as *geometry, construction, and systems data*.

Additionally, by varying parameters in physics-based models, large sets of different building models can be constructed. This allows investigations into the effect of particular parameters on for instance the control performance (see e.g. [30]).

Physics-based building modeling has a long history and many modeling frameworks of varying complexity and purposes have been developed. The most sophisticated are building simulation softwares such as EnergyPlus, TRNSYS, and ESP-r. These programs allow the detailed simulation of most relevant physical phenomena in buildings. However, they were developed to enable energy and temperature simulations for planning studies but unfortunately exhibit several severe drawbacks when they are to be used as a control model in an MPC. First, the highly nonlinear models result in general in non-convex optimization problems that have to be solved without access to an explicit gradient or to other problem structure. Second, the solution of the optimization problems requires the simulation of many different candidate control trajectories from the same initial state which most of these programs are not designed to do. Third, their scope, complexity, and hence the required input data are beyond what is necessary for MPC. Finally, learning how to use such software requires a significant amount of training and using them to model a building is a time-consuming task even for experts.

Therefore, even though building simulation software has been used by some as control model in an MPC (see Section 2.3), most use simpler descriptions of the building's thermal dynamics. In simplified building modeling, the main approach is the so-called thermal *resistance-capacitance* (RC) modeling, sometimes also referred to as lumped-capacitance modeling, see for instance [31, 32, 33, 34].

In this approach that is named after its analogy to electrical circuit modeling[2], the building is partitioned into several regions, each of which is assumed to have a uniform temperature described by a state x_i in the model. Typical choices of such lumped-capacitance regions are the air volume of a room or zone[3] or of building element[4] layers. For each region i, its *heat capacitance*, C_i, is calculated as the product of its specific heat capacity and mass. The heat flux between *adjacent* regions i and j is assumed to be linearly proportional to the difference between the regions' temperatures with proportionality constant $1/R_{i,j}$. The value $R_{i,j}$ is called the *thermal resistance* and includes effects of thermal conduction and convection (if at least one of the regions is air) as well as possibly linearized radiation effects (e.g. between two walls separated by room air). Using the law of energy conservation, this results in a system of linear ordinary differential equations describing the evolution of the regions' temperatures in the absence of external influences. As an example, for two adjacent regions 1 and 2, the system is given by

$$C_1 \dot{x}_1(t) = (x_2(t) - x_1(t))/R_{1,2} \tag{3.1a}$$
$$C_2 \dot{x}_2(t) = (x_1(t) - x_2(t))/R_{1,2} . \tag{3.1b}$$

The model's accuracy but obviously also its size are increased if the regions are made smaller. Influences such as ambient air, solar irradiation, and building systems are considered as heat fluxes acting on the states. Modeling the heat exchange between the lumped-capacitance

---

[2]Temperature corresponding to voltage, heat flux to current, thermal capacitance to electrical capacitance, and thermal resistance to electrical resistance.

[3]A thermal *zone* can be one or multiple rooms considered to have the same thermal dynamics. We use *room* and *zone* interchangeably.

[4]We use *building element* to denote walls, floors, ceilings, and internal masses.

regions, also referred to as *nodes*, can be rather well generalized to arbitrary buildings (see Section 4.3). Modeling the external influences, however, is more difficult and finding a balance between accuracy and model complexity is not a trivial task since their physics often are nonlinear. Moreover, these influences and in particular the building systems vary significantly from building to building. For these reasons, it is unsurprising that the way the external influences are modeled is the most distinguishing factor between different RC models and that many such variants exist of which not all are suited for MPC.

The rest of this part is organized as follows. Given this short introduction into RC modeling, the following Chapter 4 introduces a variant of this method that was particularly designed for MPC. It describes the Building Resistance-Capacitance Modeling (BRCM) Matlab toolbox that we developed to enable the automatic generation of bilinear RC models from geometry, construction, and systems data. Moreover, it supports the generation of the corresponding potentially time-varying costs and constraints necessary to set up the MPC problem (2.16).

Subsequently, Chapter 5 describes a study in which we used identification techniques to model a ventilated room. Three models were derived: i) an empirical transfer function estimate (ETFE) derived from a pseudo-random binary sequence input signal; ii) an ETFE derived from a relay feedback closed-loop identification approach; iii) an RC model constructed using the BRCM toolbox. Using additional validation data, the models were compared in terms of accuracy. The effect of air mixing dynamics was demonstrated in a further experiment to be one of the main differences between the experimentally identified and the RC model. The study shows that an additional pole can be added to the RC model in order to compensate for the differences related to the air mixing dynamics.

Chapter 4

BRCM Matlab Toolbox: Model Generation for Model Predictive Building Control

4.1 Introduction

Creating an accurate building model that is simple enough to allow the resulting MPC problem to be tractable arguably is the most crucial task in the development of a building MPC. A key result of the OptiControl-II project described in Chapter 6 was that the generation of a suitable model is also the most challenging and time-consuming part of the control design. This was also the finding of other implementations of MPC on real buildings (e.g. see [35]). However, for MPC to become an interesting alternative for wide-spread commercial use, the modeling effort must be small (see the discussion in Section 6.9). Hence, there is great need for reliable and efficient methods for generating MPC suitable models of buildings.

In this chapter, we describe the Building Resistance-Capacitance Modeling (BRCM) Matlab toolbox that aims at providing such a method. Because of the inherent connection between the actuator models, constraints, and operating costs, we consider the modeling to include the derivation of all these components. Based on geometry, construction, and systems data, the BRCM toolbox generates the model, costs, and constraints of the MPC problem (2.16) which is repeated here for convenience

$$\underset{U_{0 \to N}}{\text{minimize}} \quad \sum_{k=0}^{N-1} c_k^T u_k \tag{4.1a}$$

$$\text{subject to} \quad x_{k+1} = Ax_k + B_u u_k + B_v v_k + \sum_{i=1}^{n_u}(B_{\text{vu},i}v_k + B_{\text{xu},i}x_k)u_{k,i} \quad \forall k \in \mathbb{N}_0^{N-1} \tag{4.1b}$$

$$F_{\text{x},k}x_k + F_{\text{u},k}u_k + F_{\text{v},k}v_k \leq f_k \quad \forall k \in \mathbb{N}_0^{N-1} \tag{4.1c}$$

$$x_0 = \hat{x}. \tag{4.1d}$$

In particular, the toolbox generates the matrices A, B_u, B_v, $B_{\text{vu},i}$, $B_{\text{xu},i} \; \forall i \in \mathbb{N}_1^{n_u}$ and provides parameterized functions for generating the costs and constraints matrices c_k, $F_{\text{x},k}$, $F_{\text{u},k}$, $F_{\text{v},k}$, f_k as a function of potentially time-varying parameters (e.g. electricity prices, time-varying comfort constraints, etc.). The geometry, construction, and systems data – in the following also referred to as *input data* – have to be specified in a set of files having a well defined structure, see Sections 4.3 and 4.4. The geometry and construction data files can be either entered by hand or extracted from an EnergyPlus model, enabling the use of graphical editors
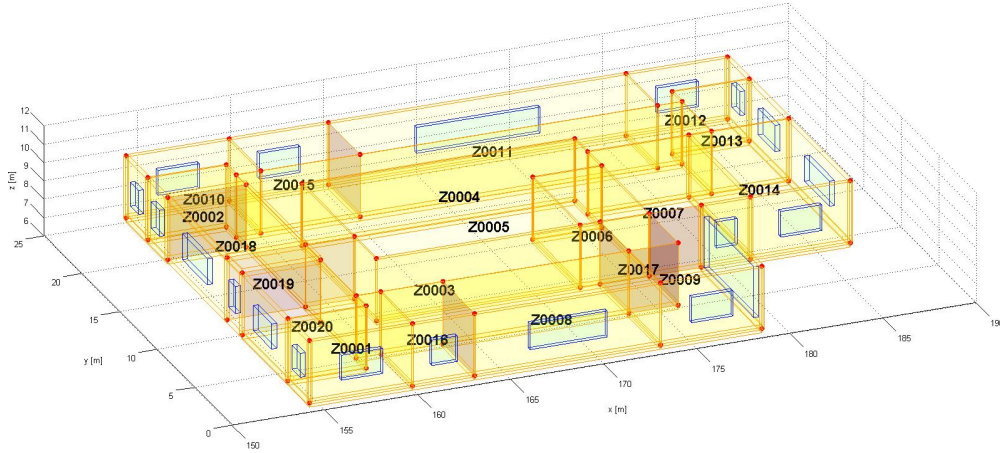
Figure 4.1: Visualization produced by the BRCM toolbox showing the second floor of the building controlled in the OptiControl-II project (see Chapter 6).

developed for EnergyPlus to generate the building geometry. The toolbox has been written exclusively in Matlab, not employing any other toolboxes. It is open source and can be used under the GPLv3 license. The detailed documentation and installation instructions can be found on the BRCM website (see the Internet Links section).

The rest of the chapter is organized as follows. In Section 4.2, we introduce the modeling concept. Sections 4.3 and 4.4 describe the required input data and the detailed models. A case study presented in Section 4.5 demonstrates the toolbox' functionality by showing the steps involved in generating a simple one-zone model. Additionally, the resulting model is compared to an EnergyPlus model. In Section 4.6, the application of the toolbox for experimental and simulation-based building MPC as well as its modeling accuracy are discussed. In Section 4.7, finally, conclusions are drawn.

4.2 Modeling Concept

The generation of the dynamic *thermal model* (describing the heat transfer between rooms, walls, floors, and ceilings) is separated from deriving static *external heat flux* (EHF) models describing external influences (e.g. solar gains, ambient air, building systems, internal gains, etc.). Table 4.1 gives an overview of the heat fluxes that are considered in the toolbox and the model part they belong to. This procedure allows the separation of the rather generic modeling of the building's thermal dynamics, which can be automated for most relevant geometries, from the much more case specific modeling of building systems and other external influences. This case-to-case variability is handled by modularly parameterizing and adding only those of the EHF models in Table 4.1 which are present in the building to be modeled. The costs and constraints generating functions are set up during the generation of the EHF models. Figure 4.2 depicts this workflow schematically. The thermal model is derived from geometry and construction data, while the EHF models additionally require building systems data.

---

[1]We use *building element* to denote walls, floors, ceilings, and roofs. To facilitate the modeling, we assume a building element to be planar and to be in contact with at most two zones. In the case of, for instance, a wall being in contact with multiple zones, it is simply considered as multiple building elements. In the case of, for instance, a round wall or a wall with varying thickness we approximate it using multiple building elements.

Table 4.1: Heat fluxes that can be modeled using the BRCM toolbox and the model they belong to.

Heat flux	Model
Heat exchange between room air and building elements[1]	Thermal model
Heat exchange within building elements (conduction)	Thermal model
Heat exchange among building elements (radiation)	Thermal model
Heat exchange of building elements with ambient air	EHF model: Building hull
Heat exchange of room air with ambient air (windows)	EHF model: Building hull
Air infiltration	EHF model: Building hull
Solar radiation absorbed by the facade	EHF model: Building hull
Solar radiation transmitted by windows and blinds	EHF model: Building hull
Thermal reradiation of the facade	EHF model: Building hull
Internal heat gains (people, lighting, equipment)	EHF model: Internal gains
Ventilation: Air flow / heater / energy recovery / cooling	EHF model: Air handling unit
Radiators	EHF model: Radiators
TABS / floor heating / chilled ceiling	EHF model: Building element heat flux
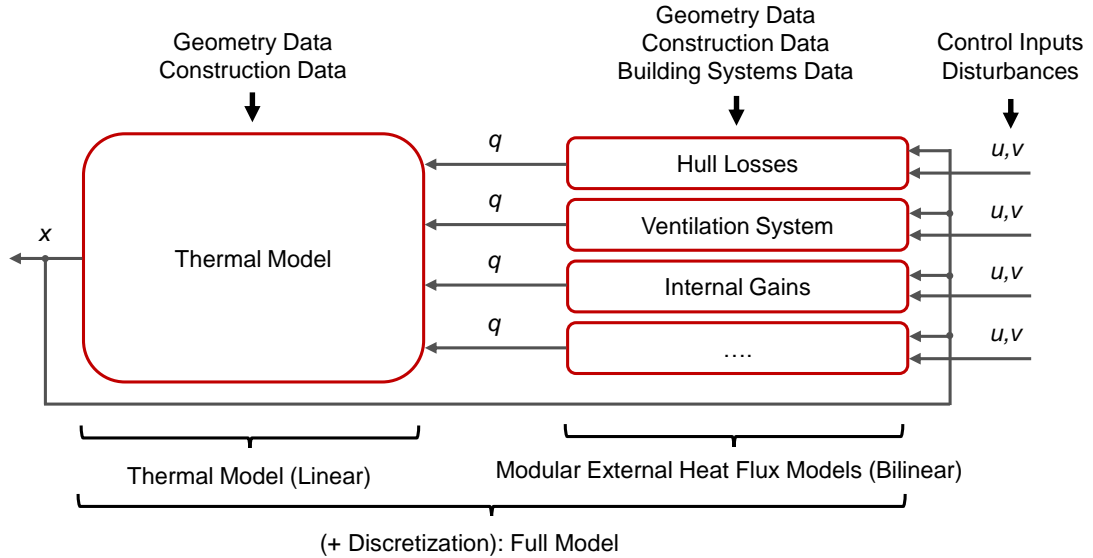
Figure 4.2: Schematic description of the modular modeling approach. A linear thermal model is generated from construction and geometry data. To this a set (depending on the case at hand) of modular EHF models is added. The EHF models are parameterized with geometry, construction, and building systems data. A discretization of the combined model yields the full model.

The building's thermal model[2] as a function of the *aggregated external heat fluxes* (EHFs), $q \in \mathbb{R}^{n_x}$, is given by

$$\dot{x}(t) = A_\text{t}x(t) + B_\text{t}q(x(t), u(t), v(t)). \tag{4.2}$$

The construction of (4.2) is described in Section 4.3. The *aggregated EHF model* as a function

---

[2]We use the subscript "t" to denote matrices of the thermal model (e.g. A_t) and subscript "q" for matrices of the EHF models.

of the states, control inputs, and disturbances,

$$q(x(t), u(t), v(t)) = A_{\mathsf{q}}x(t) + B_{\mathsf{q,u}}u(t) + B_{\mathsf{q,v}}v(t) + \sum_{i=1}^{n_{\mathsf{u}}}(B_{\mathsf{q,vu},i}v(t) + B_{\mathsf{q,xu},i}x(t))u_i(t), \quad (4.3)$$

is modeled bilinearly. Model (4.2) is then combined with (4.3) and subsequently discretized (see Section 4.2.1) to obtain (4.1b), which we refer to as the *full model*. Section 4.4 describes how the aggregated EHF model is constructed. When constructing the EHF models, also functions taking time-varying parameters as input and returning the discrete-time costs and constraints matrices in (4.1a) and (4.1c) are created.

4.2.1 Discretization

Consider the linear system

$$\dot{x}(t) = A_{\mathsf{lin,c}}x(t) + B_{\mathsf{lin,c}}u(t) \tag{4.4}$$

and assume that the control input is constant during every sampling interval[3] of length T_s (also known as the *zero-order hold* assumption). The state of the discrete-time system

$$x_{k+1} = A_{\mathsf{lin}}x_k + B_{\mathsf{lin}}u_k \tag{4.5}$$

where

$$A_{\mathsf{lin}} = e^{A_{\mathsf{lin,c}}T_s}, \qquad B_{\mathsf{lin}} = \int_0^{T_s} e^{A_{\mathsf{lin,c}}\tau}d\tau \; B_{\mathsf{lin,c}} \tag{4.6}$$

is identical to the continuous-time system's state at the sampling times, i.e. $x_k = x(kT_s)$ (e.g. see [36]).

   To apply this method to the bilinear system resulting from the combination of (4.2) and (4.3), it must additionally be assumed that: i) the disturbances are constant during every sampling interval; and ii) the state in the bilinear input-state term, i.e. $\sum_{i=1}^{n_{\mathsf{u}}} B_{\mathsf{q,xu},i}x(t)u_i(t)$, is constant during every sampling interval. While i) is analogous to the zero-order hold assumption for the control input, ii) clearly is not exact and will lead in general to a different evolution of the discrete-time system's state compared to the continuous-time system's. However, our experience showed that with a sufficiently small T_s (e.g. 0.25 h), the differences are negligible.

   Hence, defining the continuous-time system matrix $A_{\mathsf{c}} = A_{\mathsf{t}} + B_{\mathsf{t}}A_{\mathsf{q}}$, the matrices of (4.1b) are then computed as

$$A = e^{A_{\mathsf{c}}T_s}, \qquad B_{\mathsf{u}} = \int_0^{T_s} e^{A_{\mathsf{c}}\tau}d\tau B_{\mathsf{t}}B_{\mathsf{q,u}}, \qquad B_{\mathsf{v}} = \int_0^{T_s} e^{A_{\mathsf{c}}\tau}d\tau B_{\mathsf{t}}B_{\mathsf{q,v}}$$

$$B_{\mathsf{vu},i} = \int_0^{T_s} e^{A_{\mathsf{c}}\tau}d\tau B_{\mathsf{t}}B_{\mathsf{q,vu},i}, \qquad B_{\mathsf{xu},i} = \int_0^{T_s} e^{A_{\mathsf{c}}\tau}d\tau B_{\mathsf{t}}B_{\mathsf{q,xu},i} \qquad \forall i \in \mathbb{N}_1^{n_{\mathsf{u}}}$$

---

[3]That is, $u(t) = u_k$, $\forall t \in [kT_s, (k+1)T_s)$.

Note that if A_c is invertible, it can be shown that $\int_0^{T_s} e^{A_c \tau} d\tau = A_c^{-1}(e^{A_c T_s} - I)$. Since all realistic building models are asymptotically stable (consider the total thermal energy above $0\,°C$ stored in the building as a Lyapunov function), A_c has only eigenvalues with strictly negative real part and can always be inverted. Hence, for building models the solution to the integral is explicitly available.

4.3 Thermal Model

The following assumptions are made for the thermal model:

 i) The air volume of each zone has uniform temperature.
 ii) The temperature within a layer of a building element is uniform.
 iii) Temperatures within building elements (assumed to be planar, see Footnote 1) vary only along the direction of the surface normal.
 iv) There is no conductive heat transfer between different building elements.
 v) Long-wave (i.e. thermal) radiation is considered in a combined convective heat transfer coefficient.
 vi) All thermal model parameters are constant over time.

Assumption i) and ii) directly lead to modeling the temperature (or thermal energy) of every zone's air volume and every layer of every building element using one state. Assumption iii) leads to modeling the (conductive) heat transfer within a building element linearly proportional to the temperature difference between neighboring layers. Assumptions iv) and v) imply that direct heat transfer among different building elements is neglected. Finally, based on assumptions i) and iii), the heat transfer between surface layers of building elements and air is modeled to be proportional to the respective temperature difference.

Apart from the heat exchange with a zone, the following boundary conditions are supported for the building elements: *adiabatic*, *ambient* (convective heat transfer and solar radiation), and *ground*.

In the following, the thermal model input data and the algorithm that constructs the thermal model (4.2) are described.

4.3.1 Thermal Model Input Data

The thermal model input data were defined such that any number of thermal zones, building elements, and windows can be modeled. They consist of seven distinct input data files (Zones, Building Elements, Constructions, No-Mass Constructions, Materials, Windows, Parameters) either in Microsoft Excel or comma-separated values (CSV) format. Every file consists of one header row and an arbitrary number of data rows. Table 4.2 shows the first few lines of a Zones input data file example. All headers have a unique identifier field (fixed format) and a description field (arbitrary string) in common. For each of the input data files, the other header fields are described in the Tables 4.3-4.9. Wherever denoted in the tables, the toolbox supports the entering of an algebraic expression instead of simple numerical values. The expressions are evaluated at the time of model generation and may contain parameter identifiers defined in the Parameters input data file (Table 4.9).

Table 4.2: First lines of a Zones input data file example.

	Identifier	Description	Area	Volume	Group	
header row $\longrightarrow$	Identifier	Description	Area	Volume	Group	
data row 1 $\longrightarrow$	Z0001	Zone 1 West	10	3	WestGroup	
data row 2 $\longrightarrow$	Z0002	Zone 2 West	12.5	3	WestGroup	
	...	...	...	...	...	

Note that the Windows input data file (Table 4.8) is a special case in the sense that most of its data are used in the building hull EHF model which models the convective and radiation heat flux through windows (see Section 4.4). Nevertheless, since the window area is necessary to compute a building element's net area and because of the convenience of specifying the type of a window (if present) in the Building Element input data file, the Windows input data file is also considered a part of the thermal model.

All thermal model input data files can be either specified by hand or extracted from an EnergyPlus model, enabling the use of graphical editors designed for EnergyPlus to generate the thermal model input data.

Table 4.3: Fields of the Zones data file. The identifier and description fields are not shown.

Field	Description	Type
Area	Zone floor area in [m^2].	Numerical or algebraic expression
Volume	Zone volume in [m^3].	Numerical or algebraic expression
Group	Can be used to address groups of zones.	Zone group identifier string (optional)

Table 4.4: Fields of the Building Elements data file. The identifier and description fields are not shown.

Field	Description	Type
Construction	Defines the construction type of the building element.	Identifier of a construction or a no-mass construction
Adjacent A	Denotes the building element's boundary condition on side A.	Zone identifier or boundary condition identifier (adiabatic, ambient, ground)
Adjacent B	Denotes the building element's boundary condition on side B.	Zone identifier or boundary condition identifier (adiabatic, ambient, ground)
Window	Defines the building element's window type.	Window identifier (optional)
Area	Area of the building element in [m^2].	Numerical or algebraic expression (optional if vertices are specified)
Vertices	3-D numerical coordinates of the building element's corners in clock- or anticlockwise direction in [m]. Must lie in a plane.	List of the form $(x_1, y_1, z_1), ...$ (optional if area specified, but no visualization possible if lacking)

Table 4.5: Fields of the Constructions file. The identifier and description fields are not shown.

Field	Description	Type
Materials	Denotes the materials of the layers within the building element. By convention, the first entry corresponds to the layer on side A of the building element and the last entry to side B.	Ordered list of material identifiers
Thickness	List of thicknesses of the layers in the same order as the materials list in [m].	Ordered list of numerical or algebraic expressions
Convective Coefficient Adjacent A	Combined convective and radiation heat transfer coefficient on building element side A in $[W/(m^2 K)]$.	Numerical or algebraic expression
Convective Coefficient Adjacent B	Combined convective and radiation heat transfer coefficient on building element side B in $[W/(m^2 K)]$.	Numerical or algebraic expression

Table 4.6: Fields of the No-Mass Constructions file. The identifier and description fields are not shown. No-mass constructions are modeled as a stateless thermal resistance, e.g. to model openings.

Field	Description	Type
U-Value	Heat transfer coefficient in $[W/(m^2 K)]$ of a building element that is to be modeled statically, i.e. without states.	Numerical or algebraic expression

Table 4.7: Fields of the Materials file. The identifier and description fields are not shown.

Field	Description	Type
Specific Heat Capacity	In $[J/(kg\,K)]$.	Numerical or algebraic expression
Specific Thermal Resistance	In $[(m\,K)/W]$.	Numerical or algebraic expression
Density	In $[kg/m^3]$.	Numerical or algebraic expression

Table 4.8: Fields of the Windows file. The identifier and description fields are not shown.

Field	Description	Type
Glass Area	Area of the window glass. In $[m^2]$.	Numerical or algebraic expression
Frame Area	Area of the window frame. In $[m^2]$.	Numerical or algebraic expression
U-Value	Combined total heat transfer coefficient of frame and window including convective coefficients. In $[W/(m^2 K)]$.	Numerical or algebraic expression
Solar Heat Gain Coefficient	Coefficient scaling the global solar radiation perpendicularly incident on the window to obtain the resulting heat flux. Models primary (transmitted solar radiation) and secondary (radiation absorbed by the window and frame) solar heat gains. [-].	Numerical or algebraic expression

Table 4.9: Fields of the Parameters file. The identifier and description fields are not shown.

Field	Description	Type
Value	Value of the parameter	Numerical

Algorithm 4.1: Algorithm generating the thermal model[4,5]. The symbols c_{air} and ρ_{air} denote the specific heat capacity and density of air, respectively.

Data: Thermal model input data (see Section 4.3.1): `Zones`, `Building Elements`,
       `Constructions`, `No-Mass Constructions`, `Materials`, `Parameters`, `Windows`
Result: Thermal model of the form (4.2)
Initialize empty capacitance matrix Z, empty resistance matrix $\bar{A}$
for every zone in `Zones` **do**
    | $\bar{A} := \mathrm{bdg}(\bar{A}, 0)$
    | $Z := \mathrm{bdg}(Z, c_{air} \cdot \rho_{air} \cdot \texttt{zone.Volume})$;
end
for every BE in `Building Elements` **do**
    | $[\bar{A}_{BE}, Z_{BE}] := \texttt{getBEModel(BE, Constructions, Materials, Parameters, Windows)}$
    | $\bar{A} := \mathrm{bdg}(\bar{A}, \bar{A}_{BE})$
    | $Z := \mathrm{bdg}(Z, Z_{BE})$
    | $\bar{A} := \texttt{connectBEToAdjZones}(\bar{A}, \texttt{BE, Constructions, Materials, Parameters, ...}$
                                `No-Mass Constructions, Windows`$)$
end
$A_t := Z^{-1}\bar{A}$
$B_t := Z^{-1}I$

4.3.2 Model Generation Algorithm

Algorithm 4.1 constructs the building's thermal model (4.2). It first considers the model to be of the following form

$$Z\dot{x}(t) = \bar{A}x(t) + Iq(x(t), u(t), v(t)), \tag{4.7}$$

with I being the identity matrix and Z being the diagonal matrix of heat capacitances, both of the same size as $\bar{A}$. The matrices $\bar{A}$ and Z are constructed iteratively as follows. The algorithm first iterates over all zones in the `Zones` data, adding for each a state to $\bar{A}$ and its corresponding heat capacitance value to Z. Then it iterates over all building elements and calls `getBEModel` (see Section 4.3.2.1) to construct sub-models of the building elements, $\bar{A}_{BE}$ and Z_{BE}, which are subsequently also included in $\bar{A}$ and Z. The building element's boundary conditions (often heat exchange with its adjacent zones) are then modeled by the function `connectBEToAdjZones` (see Section 4.3.2.2). Finally, A_t and B_t are assigned[4] as

$$A_t := Z^{-1}\bar{A} \tag{4.8}$$

$$B_t := Z^{-1}I. \tag{4.9}$$

The algorithm uses the function $C := \mathrm{bdg}(A, B)$ that returns B, A, or an empty matrix if A,

---

[4]We use ":=" as the assignment operator.

B, or both are empty, respectively. If both are non-empty, it returns

$$C := \begin{pmatrix} A & 0 \\ 0 & B \end{pmatrix},$$ (4.10)

where 0 denotes zero matrices of appropriate sizes. The other functions are described in the following.

4.3.2.1 Function getBEModel

The function

$[\bar{A}_{BE}, Z_{BE}] := \texttt{getBEModel(BE, Constructions, Materials, Parameters, Windows)},$

generates the sub-model of the building element BE given by $\bar{A}_{BE}$ and Z_{BE} (analogous to (4.7)). If BE.Construction is a no-mass construction, empty $\bar{A}_{BE}$ and Z_{BE} are returned. Otherwise, let l denote the number of material layers (specified in the Constructions data) of BE.Construction[5]. Then

$$\bar{A}_{BE} := \begin{pmatrix} -\frac{1}{R_{1,2}} & \frac{1}{R_{1,2}} & 0 & \cdots & 0 \\ \frac{1}{R_{1,2}} & -\frac{1}{R_{1,2}} - \frac{1}{R_{2,3}} & \frac{1}{R_{2,3}} & \ddots & \vdots \\ 0 & \frac{1}{R_{2,3}} & -\frac{1}{R_{2,3}} - \frac{1}{R_{3,4}} & \ddots & 0 \\ \vdots & \ddots & \ddots & \ddots & \frac{1}{R_{l-1,l}} \\ 0 & \cdots & 0 & \frac{1}{R_{l-1,l}} & -\frac{1}{R_{l-1,l}} \end{pmatrix}$$ (4.11)

$$Z_{BE} := \begin{pmatrix} C_1 & 0 & \cdots & 0 \\ 0 & C_2 & 0 & 0 \\ \vdots & 0 & \ddots & 0 \\ 0 & 0 & 0 & C_l \end{pmatrix},$$ (4.12)

where $R_{i,i+1}$ is the thermal resistance between layer i and $i+1$ (calculated as the sum of the conductive resistances to the centers of the layers) and C_i is the i-th layer's thermal heat capacitance, i.e.

$$R_{i,i+1} = \frac{1}{a_{BE}} \left(\frac{d_i}{2} r_i + \frac{d_{i+1}}{2} r_{i+1} \right)$$ (4.13)

$$C_i = a_{BE} d_i \rho_i c_i.$$ (4.14)

---

[5]We use X.Y to denote property Y of object X.

The symbol a_{BE} denotes the building element's net area, i.e. without the window's area if one is present (specified in the `Building Elements` and `Windows` data). Furthermore, d_i denotes the i-th layer's thickness (specified in the `Constructions` data) and r_i, ρ_i, c_i the specific thermal resistance, density, and specific thermal heat capacity of the i-th layer's material (specified in the `Materials` data).

4.3.2.2 Function connectBEToAdjZones

The function,

$\bar{A} := \texttt{connectBEToAdjZones}(\bar{A},\ \texttt{BE},\ \texttt{Constructions},\ \texttt{Materials},\ ...$
$$\texttt{No-Mass Constructions},\ \texttt{Parameters},\ \texttt{Windows}),$$

manipulates $\bar{A}$ to model the heat exchange of the building element `BE` with its adjacent zones. For both of the building element's surfaces, a boundary condition is specified in `BE.AdjacentA` and `BE.AdjacentB` (a zone identifier, *adiabatic*, *ambient*, or *ground*). We consider the case of `BE.Construction` being: i) a no-mass construction (modeled as pure thermal resistance without a state added in `getBEModel`); or ii) a regular construction.

In case i), both boundary conditions must be zone identifiers. Then $\bar{A}$ is manipulated as follows. Let $i_{Z,A}$ and $i_{Z,B}$ be the indices of the state of the zone on side A and B, respectively. Moreover, let $\bar{A}(i,j)$ denote the element of $\bar{A}$ at row i and column j, then

$$\bar{A}(i_{Z,A}, i_{Z,B}) := \bar{A}(i_{Z,A}, i_{Z,B}) + a_{BE} U \tag{4.15}$$

$$\bar{A}(i_{Z,A}, i_{Z,A}) := \bar{A}(i_{Z,A}, i_{Z,A}) - a_{BE} U \tag{4.16}$$

$$\bar{A}(i_{Z,B}, i_{Z,A}) := \bar{A}(i_{Z,B}, i_{Z,A}) + a_{BE} U \tag{4.17}$$

$$\bar{A}(i_{Z,B}, i_{Z,B}) := \bar{A}(i_{Z,B}, i_{Z,B}) - a_{BE} U. \tag{4.18}$$

The symbol U denotes the U-Value of the no-mass construction (specified in the `No-Mass Constructions` data).

In case ii), `BE.Construction` is a regular construction. We show only the handling of the boundary condition of side A, all steps for side B are analogous. We consider the cases of different boundary conditions. Obviously, if it is *adiabatic*, $\bar{A}$ is left unchanged. If it is any other boundary condition, (i.e. *ambient* or *ground*), $\bar{A}$ is also left unchanged and the boundary condition is handled by the Building Hull EHF model (see Section 4.4). If it is a zone identifier, $\bar{A}$ is manipulated as follows. Let $i_{Z,A}$ and $i_{BE,A}$ be the index of the zone's state and of the building element's first layer's state (which by convention is on side A), respectively. Then,

$$\bar{A}(i_{Z,A}, i_{BE,A}) := \bar{A}(i_{Z,A}, i_{BE,A}) + \frac{a_{BE}}{d_1 r_1/2 + 1/\alpha_{BE,A}} \tag{4.19}$$

$$\bar{A}(i_{BE,A}, i_{BE,A}) := \bar{A}(i_{BE,A}, i_{BE,A}) - \frac{a_{BE}}{d_1 r_1/2 + 1/\alpha_{BE,A}} \tag{4.20}$$

$$\bar{A}(i_{BE,A}, i_{Z,A}) := \bar{A}(i_{BE,A}, i_{Z,A}) + \frac{a_{BE}}{d_1 r_1/2 + 1/\alpha_{BE,A}} \tag{4.21}$$

$$\bar{A}(i_{Z,A}, i_{Z,A}) := \bar{A}(i_{Z,A}, i_{Z,A}) - \frac{a_{BE}}{d_1 r_1/2 + 1/\alpha_{BE,A}}, \tag{4.22}$$

where $\alpha_{\text{BE,A}}$ denotes the convective heat transfer coefficient on side A (specified in the `Constructions` data).

4.4 External Heat Flux Models

For the sake of brevity, in this section only an overview of the supported EHF models is given. A detailed equation-based description of the EHF models including the required input data as well as of the costs and constraints generating functions is provided in the Appendix 9.1.

- *Building Hull.* This EHF model considers convective and radiation heat transfer to all opaque facade parts as well as convective and radiation heat transfer through windows to the zones. Additionally, this EHF model models air infiltration through the building hull and the conductive heat exchange of building elements with a *ground* boundary condition (see Section 4.3). Global solar radiation incident onto the facades is modeled as disturbance inputs[6] in [W/m^2]. Solar heat gains to the opaque facade parts are modeled by an absorption coefficient scaling the global solar radiation. Thermal radiation exchange of the opaque facade parts is considered in the convective coefficients. Solar heat gains through windows are considered by scaling the incident solar radiation with a constant Solar Heat Gain Coefficient (SHGC) and the current blinds position (if present, modeled as a controllable gain between 0 and 1). The primary solar heat gains (the transmitted radiation) are distributed among the innermost building element layers proportionally to their surface area while the secondary heat gains (due to radiation absorbed by the windows and frames) are added to the zone air. Infiltration is modeled as a fixed air change rate to the zones.

- *Internal Gains and Radiators.* Internal gains and radiators are modeled as simple heat gains to the zones with the difference that the former are modeled as a disturbance while the latter are modeled as a controlled heat flux.

- *Ventilation.* The supported ventilation model can include a controllable air mass flow, a controllable energy recovery system, a controllable supply air heater and/or cooler, and a controllable evaporative return air cooler[7]. Air flow paths, used to model situations where air supply and exhaust are not located in the same zone, can be specified. It is possible to constrain the supply air temperature.

- *Building Element Heat Flux.* This EHF model can be used to model building systems such as floor heating, chilled ceilings, or TABS. These systems are modeled as simple controllable heat gains to the respective building element layers.

4.5 Case Study

This section describes first how the toolbox can be used to generate a model and second, compares the resulting model to EnergyPlus. For simplicity, we chose a single south facade zone (Z0013) of the building shown in Figure 4.1. This allowed a comparison between the BRCM and the EnergyPlus model on a more detailed basis. First, the single zone was simu-

---

[6]Note that this implies that these disturbances have to be externally calculated from the solar radiation on a horizontal surface (which is typically what is forecasted). This is discussed in Section 4.6.

[7]An evaporative cooler cools the air flow through evaporation of water sprayed into the air. Due to the resulting undesired moisture in the air, it is placed in the return air duct and the cold is transferred to the supply air through the heat exchanger.

lated for five days in EnergyPlus using weather data from April 1, 2010 in Basel, Switzerland. The EnergyPlus and the BRCM model were initialized to 23 °C. From the EnergyPlus simulation outputs, the room and surface temperatures (for comparison) as well as the weather disturbances (used as inputs to the BRCM model) were obtained. In the following, we show how the BRCM model was generated, simulated, and compared to the resulting temperature trajectories. The following command installs the BRCM toolbox, assuming the Toolbox Manager software is installed.

```
tbxmanager install brcm;
```

First, the thermal model data were extracted from the EnergyPlus input data file (IDF). Naturally, they could also have been entered manually.

```
convertIDFToBRCM(idfFileName,pathToThermalModelData);
```

Then, a new building object was created, the thermal model data were loaded, and the EHF model to be included was declared. For simplicity, we only considered the Building Hull EHF model. Before this step, the Building Hull EHF model input data file (see Appendix 9.1) was specified manually.

```
B = Building;
B.loadThermalModelData(pathToThermalModelData);
B.declareEHFModel('EHFM_BuildingHull.m',pathToEHFMData);
```

The following commands programmatically change the field 'Density' of the material 'M0003' to 1000 and save the resulting thermal model back to disk in the input data format. The programmatical manipulation of parameters allows the fast generation of a set of models with varying parameters for example for sensitivity studies. The commands are shown just for illustration purposes; the changes have not been applied to the model that was compared to EnergyPlus.

```
B.thermal_model_data.setValue('M0003','Density',1000);
B.writeThermalModelData(pathToModifiedThermalModelData);
```

Based on the thermal model data, a visualization of the building can be generated, for instance for visual checking of the thermal model's geometrical correctness and completeness. In this example, the command generates a one-zone version of Figure 4.1.

```
B.drawBuilding();
```

We then generated the continuous-time building model and discretized it.

```
B.generateBuildingModel();
B.building_model.discretize(discretizationTimestep);
```

Assuming that the control input and disturbance data, U and V, respectively, have already been retrieved from EnergyPlus, we created a new simulation experiment object SimExp, set the initial condition and performed an open loop simulation with the control and disturbance input matrices.

```
SimExp = SimulationExperiment(B.building_model);
```
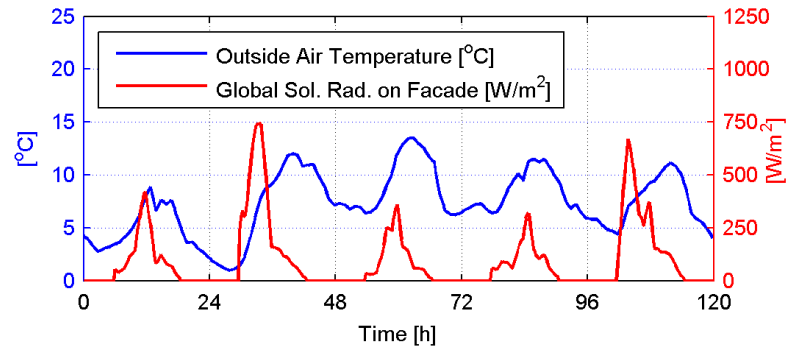
a): RC simulation inputs. Outside temperature and global solar radiation on the facade.
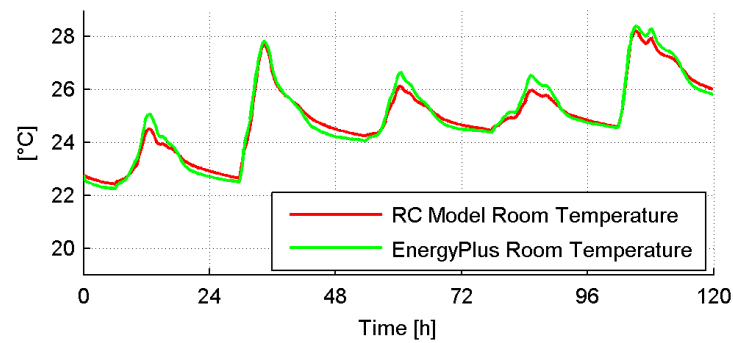
b): Room temperatures of RC and EnergyPlus model.
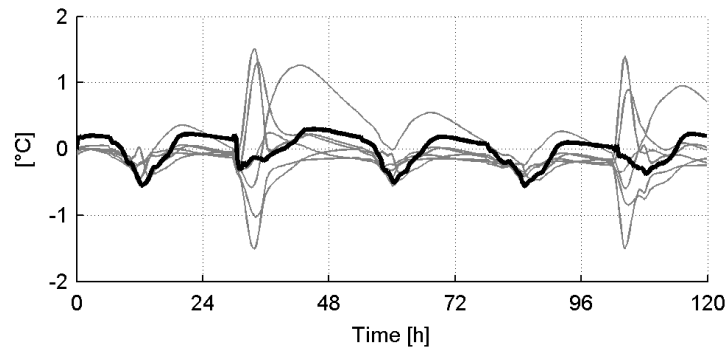
c): RC-EnergyPlus building element surface temperature differences in grey. RC-EnergyPlus room temperature difference in bold.

Figure 4.3: Comparison of a BRCM to a EnergyPlus model.

```
SimExp.setNumberOfSimulationTimeSteps(numberOfTimesteps);
SimExp.setInitialState(23*ones(numberOfStates,1))
SimExp.simulateBuildingModel('inputTrajectory',U,V);
```

In Figure 4.3a, we show the ambient air temperature and the solar global radiation on the facade. In Figure 4.3b, the room temperatures of both models are shown. Finally, Figure 4.3c shows the differences (BRCM-EnergyPlus) of the building element surface temperatures and the room temperature difference. The surface temperatures varied in a same range as the room temperature. Over the five-day period, the zone air temperature difference was within $0.5\,°C$ while the wall building element temperatures mostly also agreed well except for times with high solar radiation. A closer analysis showed that this was due modeling the thermal

radiation indirectly by a modified convective heat transfer coefficient.

Naturally, the model matrices can not only be used in simulation but also be directly accessed from the structures

```
B.building_model.discrete_time_model;
B.building model.continuous_time_model;
```

For a model with control inputs, the following commands would generate the costs and constraints matrices based on the costs and constraints parameters `costsParam` and `constrParam`, respectively. Which parameters are required naturally depends on the included EHF models (see Appendix 9.1). Again this command is just shown for illustration purposes.

```
[Fx_k,Fu_k,Fv_k,f_k] = B.building_model.getConstraintsMatrices(constrParam);
c_k = B.building_model.getCostVector(costsParam);
```

4.6 Discussion

4.6.1 Application of the Toolbox

This toolbox serves two purposes: i) facilitating the generation of models of real buildings that are to be controlled by MPC; and ii) supporting MPC related simulations by providing a method for generating individual or sets of building models (e.g. for parameter sensitivity studies).

Purpose i) is motivated by the finding that the construction of an MPC-suitable model of a real building is the most time-consuming task in the MPC control development (see Section 6.8). The toolbox aims at facilitating this by reducing it to the specification of the input data. The toolbox' algorithms have been successfully used for the generation of the model used in the MPC of the OptiControl-II project's demonstrator building (see Chapter 6). However, the application of the toolbox for Purpose i) is not trivial for several reasons.

First, for most buildings, geometry data can be obtained but construction and building systems data are only partially available. Missing values have to be estimated and it is not clear how much this deteriorates the performance of an MPC.

Second, many of the EHF models are formulated in terms of heat fluxes. However, most building systems such as TABS and radiators are operated by controlling their supply water temperature. Hence, applying an optimal control input obtained from solving (4.1) to a TABS or radiator system requires the conversion from a heat flux to a supply temperature. Even more difficult, the conversion of an optimal control input for the blinds (expressed in the toolbox as a gain in 0 to 1) has to be converted to a blinds setpoint (sometimes limited to discrete positions). The implementation of such post-processing steps is not straightforward.

Third, solving (4.1) requires predictions of the disturbances, in most cases including ambient temperature, solar radiation onto the facades, and internal gains. While the ambient temperature is readily forecasted by weather services, typically only global solar radiation on a horizontal (or perpendicular to the sun) surface is provided and the conversion to the facade

values is not trivial[8]. Internal gains are also difficult to predict due to the inherent uncertainty of occupancy and equipment usage.

Even though the problems described above have been overcome in the OptiControl-II project, they make clear that there is more to consider when modeling an actual building than just generating a model using the toolbox. Nevertheless, we believe that the toolbox significantly reduces the effort to build detailed, physics-based building models.

Given these difficulties, it is natural to ask whether alternative approaches such as identification-based methods might be better suited. As discussed initially, due to time and building usage constraints, they may be very difficult or even impossible to apply if the goal is a detailed multi-input multi-output building model. However, it still remains an open question how significantly the level of modeling detail influences the performance of a building MPC. If the building at hand was sufficiently fast-reacting, or if it turned out that simpler models neglecting the long time-constants are sufficient, identification approaches may be preferable.

Purpose ii) is more easily satisfied, since only a realistic building model but not an exact reproduction of the thermal behavior of a particular building is required. Indeed, the toolbox has been used to this end by researchers also from several other institutions such as the University of Cambridge (England), the University of California Berkeley (United States), the University of Applied Sciences Biberach (Germany), the Swiss Federal Laboratories for Materials Science and Technology (EMPA) (Switzerland), and the University of Pennsylvania (United States).

4.6.2 Model Validations

Naturally, it is of interest to assess the validity of the models generated by a modeling framework such as the BRCM toolbox. One such study was presented in Section 4.5 where we compared a small single-zone model to EnergyPlus. Several other analogous studies performed for larger models gave similar results, see for instance [4]. As mentioned before, a model generated using the toolbox' algorithms was successfully used in the MPC of a real building and was additionally validated by comparing predicted and measured temperatures in step experiments on the building. Also, in the study described in the following Chapter 5, a BRCM model of a ventilated room was derived and compared to measurements.

The experimental as well as the simulation-based comparisons showed that errors (i.e. the difference between the BRCM model's and the measured or the EnergyPlus model's predicted room temperatures, respectively) of around $0.5\,°\mathrm{C}$ with peaks of up to $1\,°\mathrm{C}$ have to be expected when predicting room temperatures over several days.

4.7 Conclusions

In this chapter, we presented a new Matlab toolbox facilitating the generation of bilinear building models as well as of linear costs and constraints for MPC. The models are constructed from building geometry, building construction, and building systems data specified in Excel or

---

[8]Within the OptiControl-II project, algorithms for this have been developed and validated using measured radiation data from the demonstrator building (see Section 3.4.1 of [9]). These algorithms have been preliminarily included in an unpublished version of the toolbox (see [37]) and will be incorporated in the next release.

CSV files. To our knowledge, this is the first modeling framework tailored for MPC. Several such models have been validated in simulation and experiments, showing that prediction errors of around $0.5\,^\circ$C with peaks of up to $1\,^\circ$C have to be expected. The toolbox was used in several institutions to generate models for MPC related simulations. Applying it in the implementation of an MPC on an actual building requires the estimation of missing model parameters (mostly related to construction types and materials), a post-processing of the optimal control input obtained in the optimization, and the generation of predictions of the disturbance inputs. Nevertheless, we believe that the toolbox significantly lowers the modeling effort which is the most time-consuming task in a practical MPC implementation.

Chapter 5

Frequency-Domain Identification of a Ventilated Room for Model Based Control

5.1 Introduction

In this chapter, we report the results of several identification experiments conducted in a well instrumented ventilated test room of the company SAUTER. The purpose of this study was: i) to investigate identification methods that can be used to model the effect of a pre-heating ventilation on the room temperature; ii) to compare physics-based models generated using the BRCM toolbox to the identified model and to assess both models' predictive capabilities in experiments; iii) to gain insight into the physical nature of ventilated rooms.

In the experiments, we fixed the air flow rate to the test room (see Section 5.2) and used a heating device to excite the thermal room dynamics. Section 5.3 shows the results of the identification experiments. We calculated empirical transfer function estimates (ETFE) on one hand from an experiment with a pseudo-random binary sequence (PRBS) signal as input and on the other hand in a closed-loop identification setup with a relay feedback controller. In Section 5.4, we show the results of a validation experiment conducted to compare several models: the model identified in Section 5.3, M_{ID}; the physics-based RC model, M_{RC}; and a modified version of the latter, $M_{RC,mod}$. The modification consisted of an additional pole and compensated for discrepancies found when comparing the identified and the physics-based model in the frequency-domain. In Section 5.5, the results are discussed and conclusions are drawn in Section 5.6.

5.2 Experimental Setup

A rectangular room located at SAUTER's headquarter and production site in Basel, Switzerland, was chosen as experimental facility. The system was defined to be the whole room, including the walls, ceiling, and floor. Figure 5.1 shows a map of the room's surroundings. The room comprised a ventilation unit having air inlet and outlet in the nearby control room, a heating device in the supply air duct, and ten temperature sensors. Active cooling of the supply air was not possible. All components are illustrated in Figure 5.2. To avoid overheating of the control room, the door from the control room towards the big storage hall was kept open.
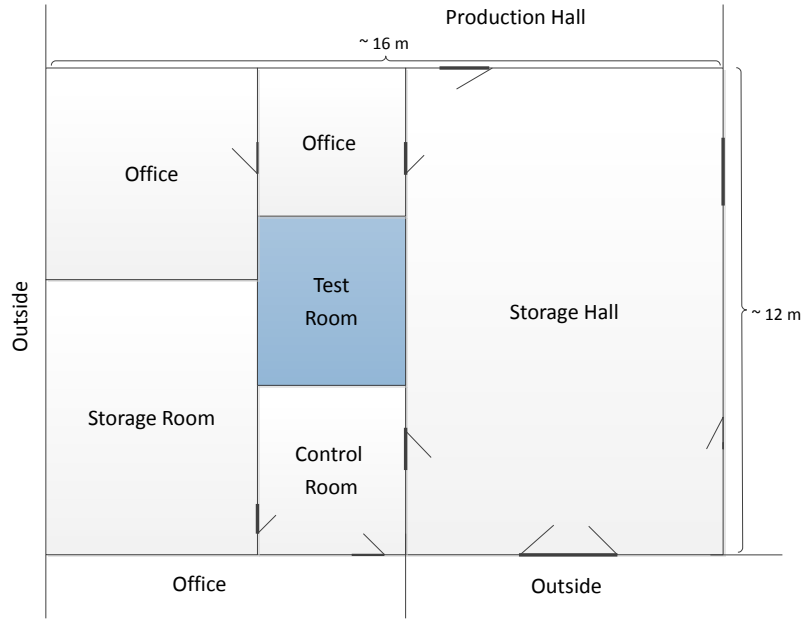
Figure 5.1: Room surroundings.

Table 5.1: Temperature sensor locations.

Sensor	Location	Sensor	Location
T_{amb}	In the control room	T_{floor}	Center of the floor underneath the table
T_{sup}	Supply air duct after the heater	$T_{wall,N}$	Center of the wall opposite of the door
T_{ret}	Return air duct	$T_{wall,W}$	Center of the wall left from the door
T_{table}	On the table in the center of the room	$T_{wall,E}$	Center of the wall right from the door
$T_{ceiling}$	Center of the ceiling	$T_{wall,S}$	Center of the wall next to the door

5.2.1 Temperature Sensors

Prior to the system identification, a test was conducted to compare the steady-state and dynamic behavior of the temperature sensors. The static differences of the sensors were measured to lie within $0.12\,°C$ and the temperature values after a temperature step (but before equilibrium was reached again) were found to differ at most by $0.25\,°C$. This was sufficiently accurate in the context of the planned experiments. Table 5.1 lists the location of the sensors. The sensors on the walls, ceiling and floor were attached at a distance of approximately $10\,cm$ off the wall to reduce direct influences from the wall temperature. For acquiring the sensor measurements, a data logger was used. The sampling time of the data acquisition was set to $t_{samp} = 10\,s$.

5.2.2 Actuators

A heating device was used for the excitation of the room dynamics. The device takes as input a 0-10 V signal and produces a pulse width modulated heating power signal with a maximum value of 1800 W. To be able to exactly predict switching times in the identification
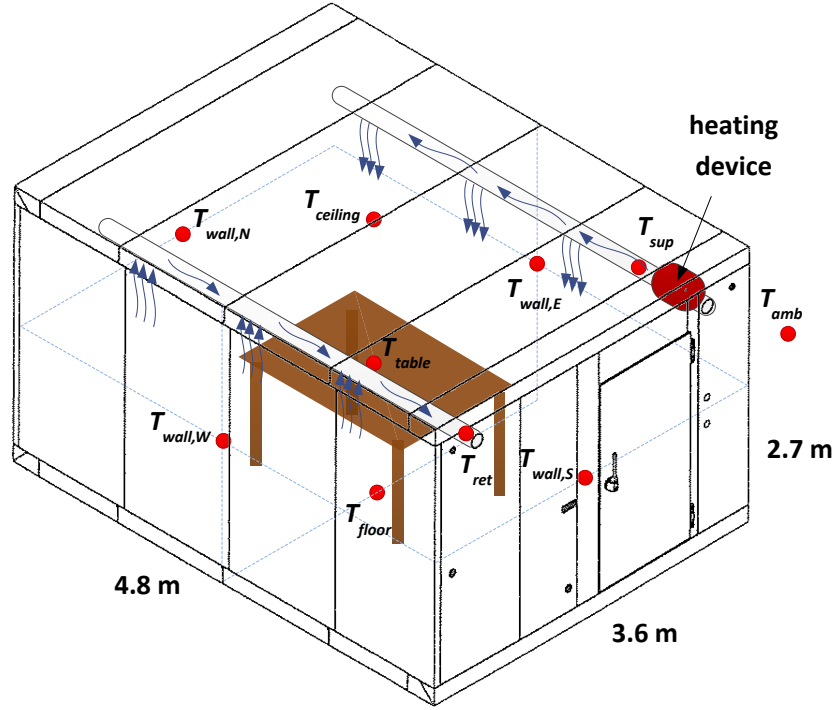
Figure 5.2: Experimental setup. Red dots denote temperature sensor locations.

experiments[1], we decided to modulate the signal ourselves by applying either $0\,\mathrm{V}$ or $10\,\mathrm{V}$. These input values resulted in instantaneous changes of the heating power to $0\,\mathrm{W}$ or $1800\,\mathrm{W}$, respectively. Our modulation period was chosen to be $20\,\mathrm{s}$. Since the minimum time between two switches of the heating device is $5\,\mathrm{s}$, this modulation was capable of producing $0\,\%$, $25\,\%$, $50\,\%$, $75\,\%$ and $100\,\%$ of the maximum heating power. Due to temperature limitations of the heater, it was not possible to use it for a longer period in $75\,\%$ or $100\,\%$ mode. Hence, it was subsequently never used more than in $50\,\%$ mode which was sufficient for all purposes of this study.

5.3 Identification Experiments

The system was mainly influenced by three variables: i) the surrounding air temperature, $T_{\mathrm{amb}}(t)$, influencing the supplied air temperature and the heat gain to the room's outer wall layers; ii) the (volumetric) ventilation air flow rate, $\dot{V}(t)$; and iii) the power of the heating device, $\dot{Q}_{\mathrm{heat}}(t)$. The net heat gain to the room air from the ventilation can be modeled as

$$c_{\mathrm{air}}\rho_{\mathrm{air}}\dot{V}(t)(T_{\mathrm{amb}}(t) - T_{\mathrm{ret}}(t)) + \dot{Q}_{\mathrm{heat}}(t) \tag{5.1}$$

with c_{air} and ρ_{air} being the heat capacity and density of air, respectively. In the present experiments, $\dot{V}(t)$ was set constant to $\dot{V}_0 = 180\,\mathrm{m^3/h}$, which corresponds to an air change rate of 5 per hour. This is a typical configuration for a heating case. In this study, we considered

---

[1]For the validation experiment, the original modulation was used.

the system to have just
$$\Delta\dot{Q}_{\text{heat}}(t) = \dot{Q}_{\text{heat}}(t) - \dot{Q}_{\text{heat,ss}}$$
as a single input and to treat $T_{\text{amb}}(t)$ as a disturbance ($\dot{Q}_{\text{heat,ss}}$ denotes the steady-state heating power value). However, the direct effect of $T_{\text{amb}}(t)$ on the room can be considered by using instead of $\Delta\dot{Q}_{\text{heat}}$

$$\Delta\dot{Q}_{\text{heat}}{}'(t) = \Delta\dot{Q}_{\text{heat}}(t) + c_{\text{air}}\rho_{\text{air}}\dot{V}_0(T_{\text{amb}}(t) - T_{\text{amb,ss}}), \tag{5.2}$$

where $T_{\text{amb,ss}}$ is the steady-state ambient air temperature. The sensor T_{table} was chosen as (main) output since it represents the best approximation to the temperature occupants feel. In Section 5.4.4 also the other sensors are considered. In the following, whenever not differently stated, the system is considered to be single-input single-output from $\Delta\dot{Q}_{\text{heat}}{}'(t)$ to $\Delta T_{\text{table}}(t) = T_{\text{table}}(t) - T_{\text{table,ss}}$, with $T_{\text{table,ss}}$ being the steady-state temperature corresponding to $T_{\text{amb,ss}}$, $\dot{Q}_{\text{heat,ss}}$, and V_0. In a preliminary step response experiment, the dominant time-constant (i.e. the time-constant of the best first-order approximation) was identified to be around 168 min.

5.3.1 Identification Using a PRBS Signal

As a first approach, we identified the ETFE using a PRBS signal. A PRBS signal is an n_{periods} times repeated periodic signal. Each period consists of n_{samples} intervals of length t_{switch}. The value of the signal during each interval is constant and determined by a pseudo-random binary number specifying whether the signal's maximum or minimum value is applied. As discussed in Section 5.2, there was no cooling device and the maximum heating power was restricted to 50 % peak output, i.e. to 900 W. Hence, the signal's minimum and maximum values were 0 W and 900 W, respectively. The interval length was fixed to $t_{\text{switch}} = 480$ s. Choosing $n_{\text{samples}} = 127$ resulted in a lowest achievable frequency point $\frac{2\pi}{t_{\text{switch}}\cdot n_{\text{samples}}} = 1.0307 \cdot 10^{-4}$ rad/s, which is lower than the cutoff frequency of the first-order approximation and results in a PRBS period of approximately 17 h.

The modulation of the heating device changes the frequency spectrum of the input signal. An analysis taking into account this effect, the maximum PRBS signal frequency, and the sampling led to disregarding all frequencies higher than 0.01 rad/s.

Two PRBS experiments were performed, each encompassing 8 periods of 17 h. For the first PRBS experiment, the temperature measured by T_{table} during the first five periods is shown in Figure 5.3. For sake of space, the other periods' and the second experiment's temperature trajectories are not shown. Clearly, period 1 contained most of the transients and was discarded in the further steps. The ETFE was calculated as

$$\hat{G}(j\omega_k) = \frac{\Delta T_{\text{table}}(k)}{\Delta\dot{Q}_{\text{heat}}{}'(k)}, \qquad k \in \mathbb{N}_1^{n_{\text{samples}}} \tag{5.3}$$

with $\omega_k = \frac{2\pi(k-1)}{n_{\text{samples}}\cdot t_{\text{switch}}}$. $\Delta T_{\text{table}}(k)$ and $\Delta\dot{Q}_{\text{heat}}{}'(k)$ are the discrete Fourier transforms of the $\Delta T_{\text{table}}(t)$ and $\Delta\dot{Q}_{\text{heat}}{}'(t)$ signals averaged over all considered PRBS periods (i.e. all periods' first measurements were averaged, all second measurements were averaged, etc.). The Fourier
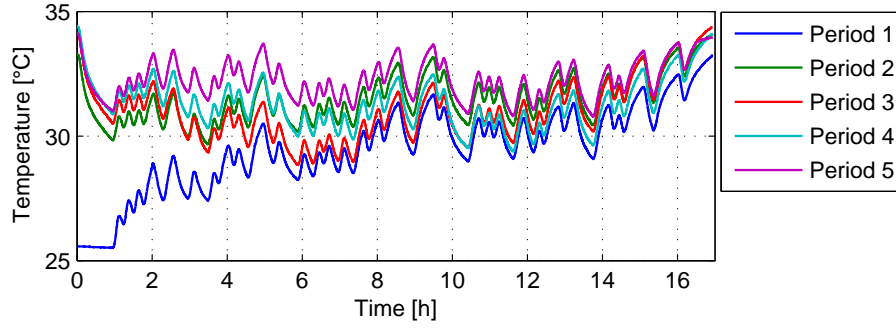
Figure 5.3: Measurements of sensor T_{table} during the first 5 periods of PRBS Experiment 1.

transforms were calculated as

$$X(k) = \sum_{n=1}^{n_{\text{samples}}} x(n) \cdot e^{-2\pi j \cdot \frac{(n-1)}{n_{\text{samples}}} \cdot (k-1)}, \qquad k \in \mathbb{N}_1^{n_{\text{samples}}}. \tag{5.4}$$

Figure 5.4 shows the ETFE calculated from periods 2-5 for both PRBS experiments. Moreover it shows a Bode plot of a fitted transfer function, see Section 5.3.1.1. It can be seen that both ETFE match very well. Naturally, they had been first calculated from periods 2-8. Since these did not differ from the shown ones, we concluded that 4 periods are sufficient for calculating the ETFE of this setup.
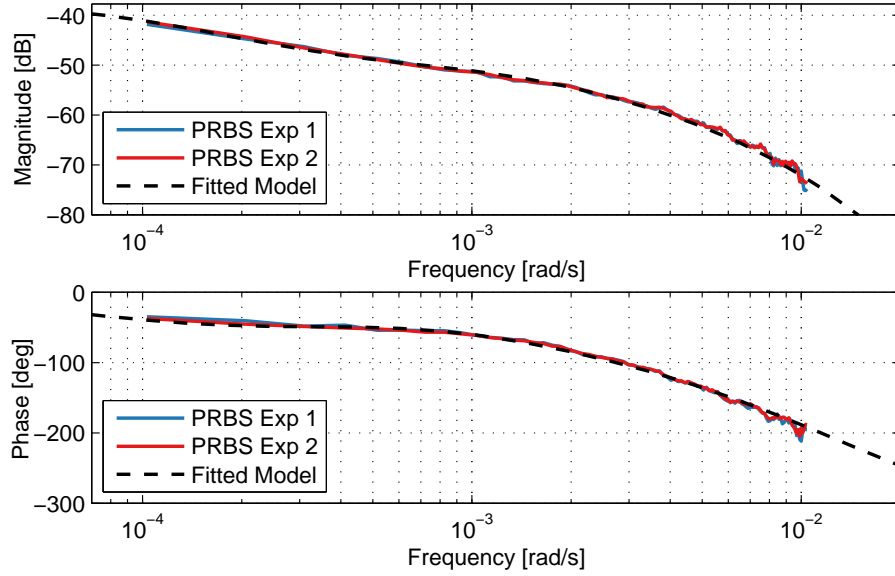
Figure 5.4: Magnitude and phase plots of the ETFEs from two PRBS experiments and of a transfer function (see Equation (5.5)) fitted to the ETFEs.

5.3.1.1 Parametric Model Representation

For simulation purposes a parametric representation of the identified model, M_{ID}, was required. The fitting of a transfer function $G_{\text{ID}}(s)$ to the ETFEs was done manually. The resulting

transfer function,

$$G_{ID}(s) = \frac{0.0132}{11800 \cdot s + 1} \cdot (2800 \cdot s + 1) \cdot \frac{1}{640 \cdot s + 1} \cdot \frac{1}{(90 \cdot s + 1)^2} \cdot \frac{1}{(40 \cdot s + 1)}, \quad (5.5)$$

is shown in Figure 5.4.

5.3.2 Identification Using a Relay Feedback

As an alternative identification approach, we used a relay feedback controller to determine the ETFE. A relay feedback controller always switches after passing the steady-state point resulting in a controlled oscillation that can be used to identify the frequency at which the plant has -180° phase and its magnitude at this frequency. In combination with a lead / lag controller, which effectively shifts the plant's -180° phase frequency, this enables the identification of any desirable point on the ETFE (up to measuring accuracy), see e.g. [38]. Since the relay's control signal as a function of the plant's output is piecewise constant with only one discontinuity, the input is almost uncorrelated to the plant's output noise. This justifies the calculation of the ETFE using the method described in Section 5.3.1. In the implementation, a relay with hysteresis was used to avoid potential instability at the switching point due to measurement noise.

For every lead / lag setting, the ETFE was calculated at the oscillation frequency, resulting in the data-points shown in Figure 5.5. It can be seen that they corresponded very well to the ETFEs estimated in the PRBS experiments.
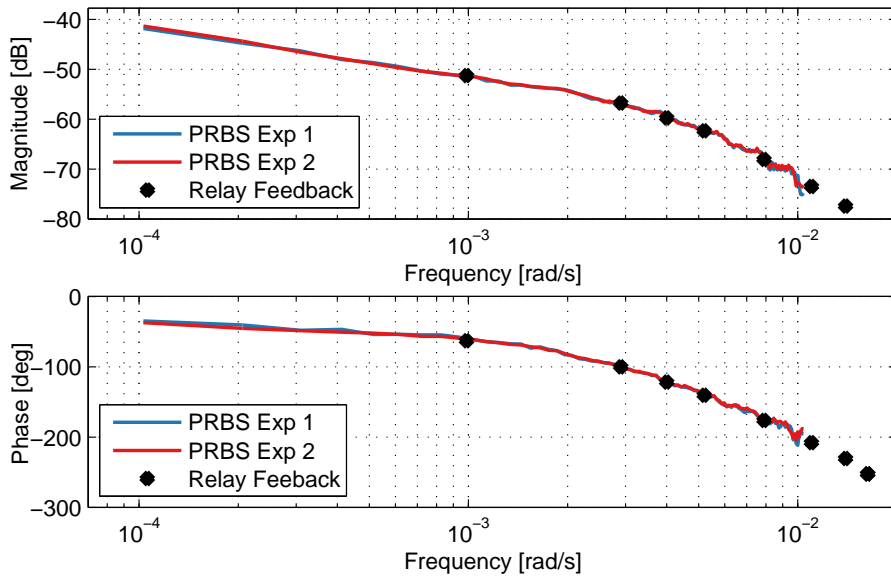
Figure 5.5: Magnitude and phase plots of the ETFEs estimated from the two PRBS experiments and from the relay feedback experiment.

5.4 Validation Experiment and Comparison to RC Model

In this section, we show the results of a 134 h validation experiment consisting of heating power steps, ramps, and PRBS-like fast signals. Using these data, we assessed the predictive capabilities of several models: i) the identified model (5.5), M_{ID}; ii) a physics-based resistance-capacitance (RC) model, M_{RC}; iii) a modified version, $M_{RC,mod}$, of M_{RC} having an additional pole. The modification was motivated by a comparison of the identified and the RC model in frequency-domain. Last, we show by another PRBS experiment with fans in the room that the main source of the found difference were neglected room air mixing dynamics.

5.4.1 RC Model

The RC model, M_{RC}, was generated with the BRCM toolbox described in Chapter 4. The resulting model had 13 states representing the average room air temperature (one state) and the four walls', the floor's and the ceiling's layer temperatures (two states each). The output of the model was the operative room temperature, i.e. the average of the room air temperature and the *mean radiant temperature* which is an area weighted average of the walls', floor's and ceiling's surface temperature. Note that due to the radiation exchange, the temperature measured by the sensors also is a combination of the room air and the wall surface temperatures. Hence, the operative temperature often is a better approximation of the measured temperatures. The inputs to the RC model were the ventilation air flow rate (fixed to $180 \, \text{m}^3/\text{h}$, see Section 5.2), the ambient temperature, $T_{amb}(t)$, and the heater's power, $\dot{Q}_{heat}(t)$. The floor and the ceiling as well as the west and east walls in direct contact with the heavy load-bearing walls (see Figure 5.1) were modeled to have a constant temperature boundary condition. The north and south walls were modeled to be in contact with air at $T_{amb}(t)$.

5.4.2 RC Model Modification

Figure 5.6 shows the Bode plot of M_{ID} as well as of M_{RC} (heater power to operative temperature) and $M_{RC,mod}$ (heater power to the modified operative temperature). Clearly, M_{ID} and M_{RC} differ significantly at higher frequencies. To compensate for this effect in $M_{RC,mod}$ (otherwise identical to M_{RC}), another pole at $4 \cdot 10^{-4}$ rad/s was added to the output. In the time-domain, this corresponded to adding a state which was solely driven by the original model's output, influenced none of the other states, and was considered as the modified model's output. The pole's frequency was fitted by hand. The modification is motivated on one hand by Figure 5.6 and on the other hand by the time-domain validation results of the following Section 5.4.3. Both show clearly that M_{RC} responds significantly faster to high-frequency inputs than the actual room. As we show in Section 5.4.4 this stems mostly from not modeling mixing dynamics of the room's air.

5.4.3 Validation Experiment

Figure 5.7 shows in the top plot the input signal, the temperature measured by T_{table} as well as the outputs of M_{ID}, M_{RC}, and $M_{RC,mod}$. In the bottom plot, the differences between the measured and the model output temperatures are plotted. In relation to the peak-to-peak
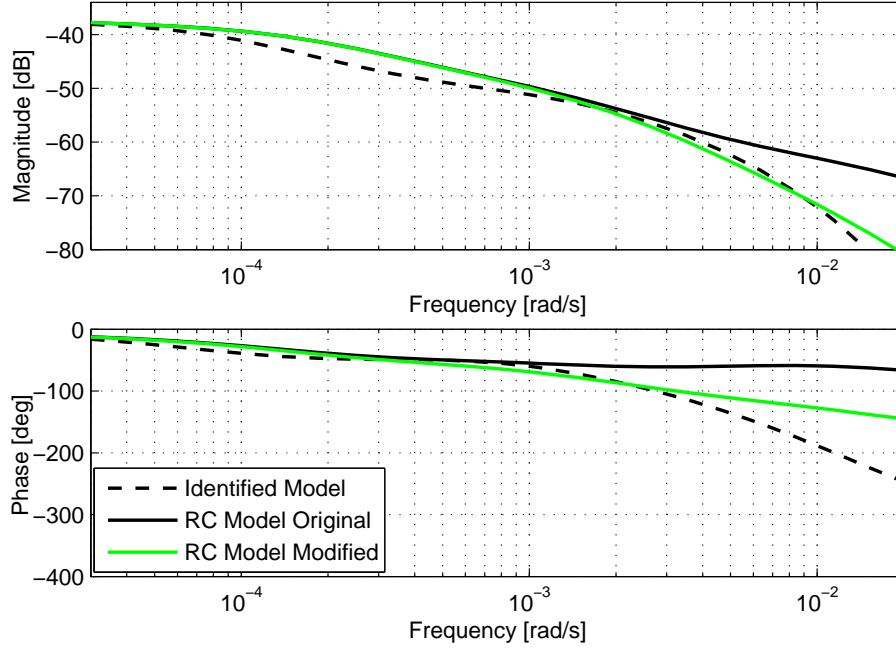
Figure 5.6: Frequency-domain comparison of the identified model, the original RC model, and the modified RC model.

temperature change of around $12\,°C$, it is apparent that all models predict the temperatures reasonably well with an average and maximum error of roughly $0.5\,°C$ ($5\,\%$ of peak-to-peak) and $1.2\,°C$ ($10\,\%$), respectively. Comparing M_{RC} and $M_{RC,mod}$, the temperature and error trajectories are almost identical except for the high-frequency part of the signal (around hour 120) where the error is significantly reduced in magnitude and fluctuation.

5.4.4 Mixing Dynamics

Considering the discrepancy at high frequencies between M_{RC} and $M_{RC,mod}$ shown in Figure 5.6, a likely cause seemed to be neglected air mixing dynamics. In building modeling, it is often assumed that the air of a zone has uniform temperature and hence that heating, for instance of the supply air, has an immediate effect at all points within the room air volume. Naturally, this is a simplification; in general, because the heat exchange within the air is not instantaneous and hot air tends to rise and in particular in ventilated rooms, air paths (inlet to outlet) may additionally shortcut much of the air volume. To investigate the magnitude of these effects and their influence on the identified transfer function, another PRBS experiment with the same heating power input as the first two was conducted. However, during this experiment, three standard office fans were stirring the air in the room. In Figure 5.8, we show a small part of the temperature trajectories of the first PRBS experiment from Section 5.3.1 and the same part of the experiment with the fans. Note the different temperature offsets. The mixing dynamics effect is apparent, seeing the temperature differences between the sensors of up to $2.5\,°C$ in the first experiment while in the second experiment the maximum discrepancy was just $0.4\,°C$. In Figures 5.9 and 5.10, we show the ETFEs of the fastest ($T_{wall,E}$) and the slowest (T_{floor}) sensor as well as of T_{table} of the PRBS experiment with and without fans, respectively. Also, the Bode plots of M_{ID} and M_{RC} are shown. Naturally, the Bode plot of M_{ID} corresponds well with T_{table} in Figure 5.9 since it was the basis for the model fitting.
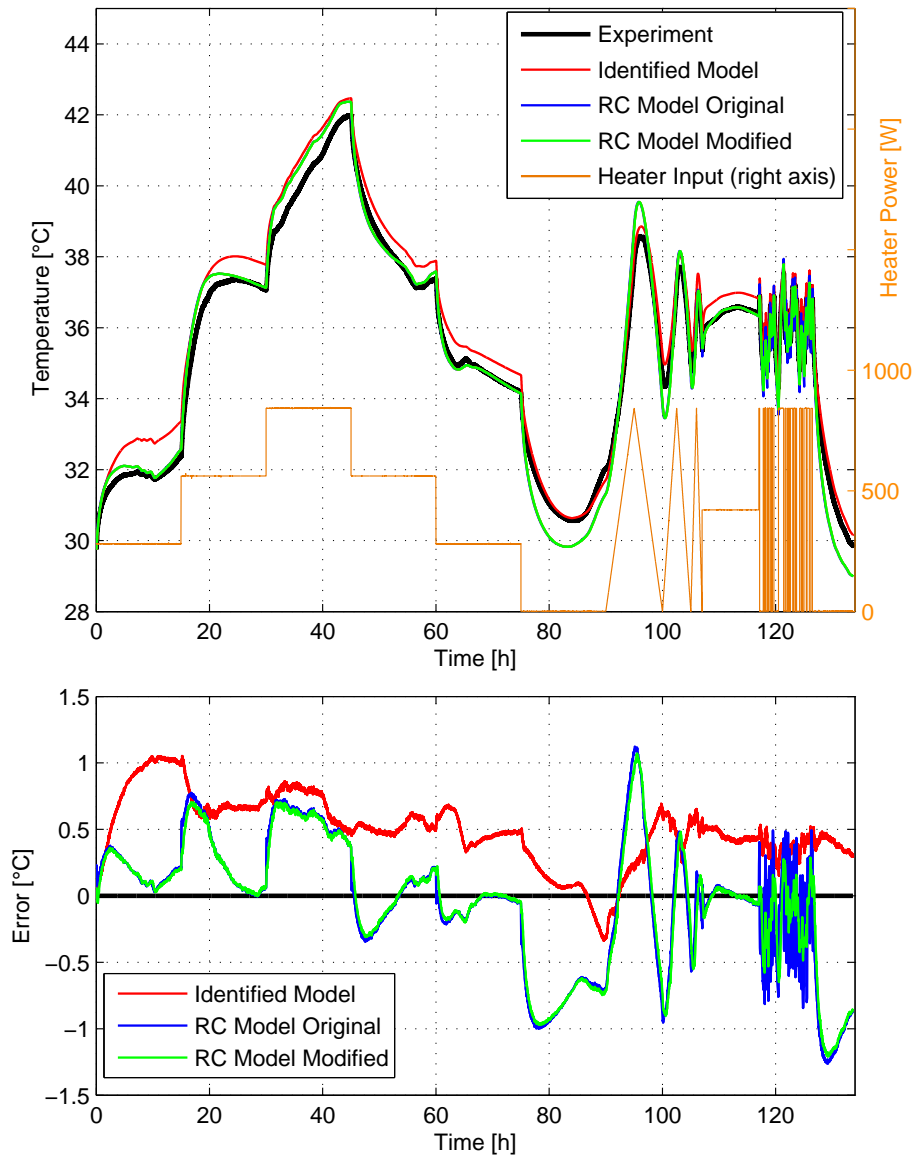
Figure 5.7: Validation experiment. Upper plot: Experimental data and temperature trajectories predicted by the identified model, the original and the modified RC model. Lower plot: Errors (measured - model output) of all models.

In the same figure, large discrepancies between the three sensors' ETFEs can be observed. In Figure 5.10, two particular observations can be made. First, all sensors now have almost identical ETFEs. Second, these ETFEs now correspond much better with the Bode plot of the original RC model. This indicates that the discrepancies between the sensors and the RC model actually were due to neglected air mixing dynamics.

5.5 Discussion

Both applied identification methods showed very reproducible and closely matching results. A critical issue in the practical application of an identification method is time efficiency. While the PRBS method identifies all points in one long experiment (in our case at least 3, ideally 5
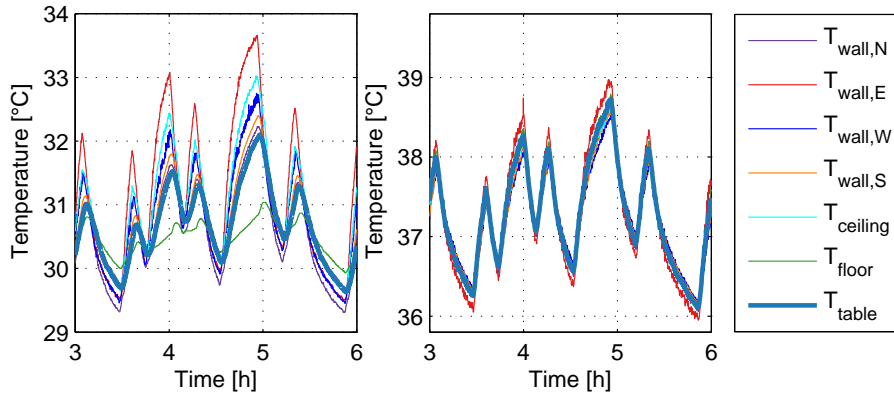
Figure 5.8: Measurements of all room temperature sensors during the PRBS experiments. Left: PRBS experiment 1 (without fans). Right: PRBS experiment with fans in the room.
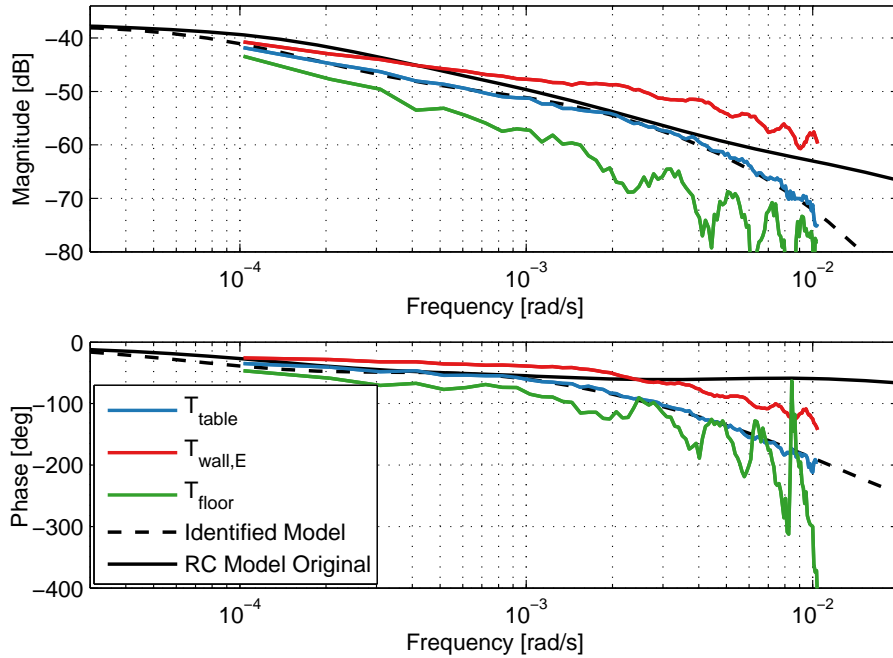
Figure 5.9: Results of the PRBS experiment 1 (without fans in the room). ETFEs of T_{table}, $T_{wall,E}$ and T_{floor} as well as Bode plots of the identified and the original RC model.

periods of 17 h), the relay method can be used to subsequently identify single points[2] in much shorter experiments (several cycles at the frequency at which the system is to be identified are sufficient). Unsurprisingly for such a thermal system, the ETFE turned out not to be very complex which suggests that only a few points may suffice for the identification of the whole system.

Both, M_{ID} and M_{RC}, showed a reasonable performance in predicting the room temperature measured by T_{table} during the 134 h validation experiment. However, in contrast to M_{ID}, M_{RC} predicted much faster responses of the room temperature to the fast switching input signals around hour 120 of the experiment. This discrepancy was significantly reduced by the additional pole in $M_{RC,mod}$. Moreover, the pole significantly reduced the gap between the Bode

---

[2]Having no cooling device diminishes this advantage since the system must be first brought to steady-state conditions.
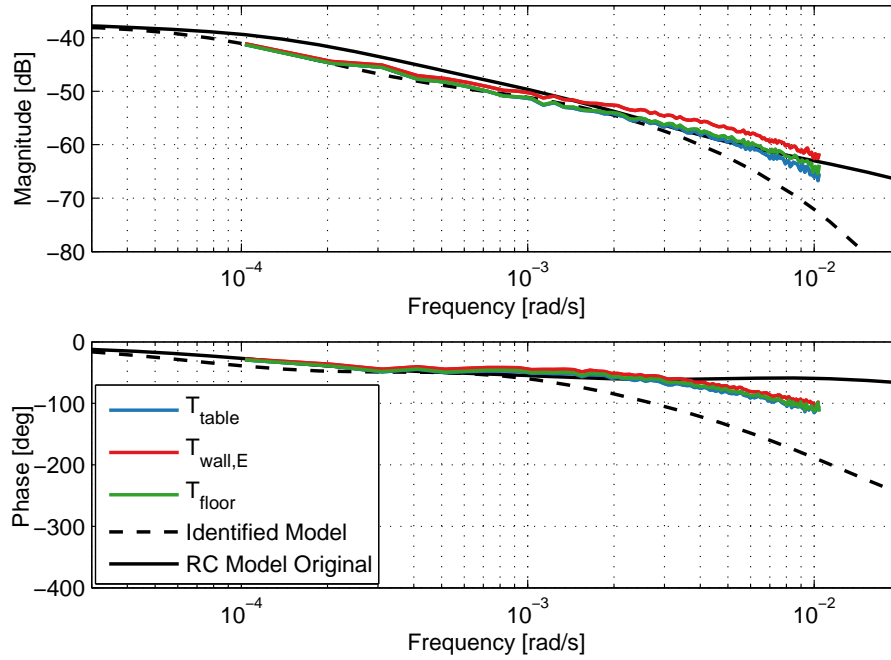
Figure 5.10: Results of the PRBS experiment with fans in the room. ETFEs of T_{table}, $T_{\text{wall,E}}$ and T_{floor} as well as Bode plots of the identified and the original RC model.

plots of the identified and the original RC model. The high-frequency part of the validation experiment had a minimum switching time of 480 s. Since this is in the order of building MPC sampling times, this finding may be meaningful in that context. The location of the pole was fitted to best reduce the frequency-domain discrepancy between M_{ID} and M_{RC}. Naturally, there is in general no identified model available and the best pole position may lie at a different frequency. Nevertheless, this is a one-parametric approach for improving an RC model's fast dynamics in a standard ventilation setup. Since most other building systems are slower, their responses likely are insignificantly affected.

Comparing the results of the PRBS experiment with and without fans showed that the discrepancy of the identified and the RC model stems from neglected mixing dynamics. The experiment with fans resulted in ETFEs which corresponded significantly better with the original RC model's Bode plot.

5.6 Conclusion

A well instrumented ventilated test room was used for identification experiments. Pseudo-random binary sequence (PRBS) and relay feedback based identification methods were applied to calculate empirical transfer function estimates (ETFE). The relay feedback method used a number of lead / lag controller settings to identify the system at various frequencies. The PRBS method resulted in very reproducible results which coincided also well with the relay feedback results. A parametric model was fitted to the identified ETFE and was shown in a validation experiment to have an average and maximum error of roughly 0.5 °C (5 % of peak-to-peak) and 1.2 °C (10 %), respectively. A physics-based RC model was generated and compared in frequency-domain to the identified model. At high frequencies, the original RC

model was found to have a much higher gain and less phase lag than the identified model. This was shown in a separate PRBS experiment including fans in the room to be mainly due to neglected air mixing dynamics. To compensate, an additional pole was added to the RC model's output. Both, the original and the modified RC model were found to produce errors in the same range as the identified model. Moreover, the modified RC model was found to have in the high-frequency part of the validation experiment a much reduced error compared to the original RC model (otherwise almost identical). The improvement of the RC model from the additional pole may be relevant in building MPC since it improves the model in a time range that is similar to typical control sampling times. However, it is unclear how heavily the compensating pole's location depends on the room configuration.

Part III

Model Predictive Control of a Swiss Office Building

Chapter 6

Model Predictive Climate Control of a Swiss Office Building: Implementation, Results, and Cost-Benefit Analysis

6.1 Introduction

In recent years, many studies have analyzed the energy savings potential of MPC in simulations, often in a best-case scenario where the simulation and the control model were identical (see Section 2.3). However, while these studies have demonstrated the potential benefits of MPC when compared to industry-standard RBC, many problems still remain to be solved that relate to the appropriate modeling of real buildings, plant-model mismatch, and the practical feasibility of MPC, as for instance its compatibility with pre-installed control systems. Moreover, the usefulness of any proposed controller must be measured not only by its benefits but also by its incurred costs, such as the necessary hardware and software and the system's design, implementation, and maintenance effort.

This chapter reports the results of the predictive building control project OptiControl-II[1] that aimed at answering these questions. The three-year project was done in close collaboration with a pre-development and research team from Siemens Building Technologies as well as with building simulation experts from Gruner-Roschi. The project included seven months of MPC of a thermally activated building system (TABS), an air handling unit (AHU) which was also used for heating and cooling, and a blinds system of a fully-occupied typical Swiss office building. In addition to the experiments, the MPC strategy was compared in terms of comfort compliance and energy use to the previously installed industry-standard RBC strategy using whole-year simulations with the EnergyPlus simulation software. Here, the MPC aspects of the detailed project report [9] are presented. Experiences with novel integrated predictive RBC strategies developed within the OptiControl-II project by the Siemens engineers are reported in [15].

The work presented here differs from the experimental building MPC studies reported in the literature (see Section 2.3.2 for a review) in several respects. First, we considered the integrated control of several actuators (TABS, ventilation, blinds). Second, unlike many of the reviewed studies, we did not consider only test cells or individual rooms, but an entire, fully operational building. Third, we did not manipulate or replace the existing control hierarchy, but rather we introduced an additional level of supervisory control. Finally, we performed long-term experiments in both, heating and cooling seasons.

The rest of the chapter is organized as follows. Section 6.2 describes the building and its

---

[1]http://www.opticontrol.ethz.ch

Figure 6.1: The building used for the experiments. Located in Allschwil, close to Basel, Switzerland.

HVAC system. In Section 6.3, the control task is defined. Section 6.4 describes how the MPC was connected to the existing building automation system. In Section 6.5, we detail how we modeled the building dynamics, the operating costs, and the constraints such that the resulting MPC problem represented the control task. In Section 6.6, we describe the control algorithm, i.e. the acquisition of the measurements and weather forecast, the preparation of the MPC problem, its solution, as well as the post-processing and communication of the optimal control inputs to the actuators. Section 6.7 then reports the experimental and simulation results. A cost-benefit analysis of building MPC for cases similar to the investigated target building, backed by the practical experience of the Siemens team, is provided in Section 6.8. Finally, in Sections 6.9 and 6.10, we discuss our results and present our conclusions.

6.2 The Building

Figure 6.1 shows the building used in the experiments. It is located in Allschwil, close to Basel, Switzerland and owned and operated by Actelion Pharmaceuticals Ltd. The building was constructed in 2007 and has a total floor area of ca. 6'000 m^2. The ground floor hosts a kitchen and a restaurant while the upper five floors are used as offices. The measured average heat and electricity consumption of the whole building are $46\,kWh/m^2$ and $83\,kWh/m^2$ per year, respectively. The building is of a heavy construction type with a glazing fraction of approximately 50 %. The overall heat transfer coefficients of the opaque parts and windows are $0.32\,W/(m^2K)$ and $1.34\,W/(m^2K)$, respectively. In terms of usage, HVAC systems, insulation level, window fraction, and building automation system, it is a typical modern Swiss office building. The MPC strategy was applied to the upper five floors, while the ground floor was separately actuated.

6.2.1 Actuation

A TABS is the main heating and cooling actuator, supplied by a gas boiler and a cooling tower, see Figures 6.2a and 6.2b. The entire building is served by a single TABS zone, i.e.

the circulating water's mass flow rate and supply water temperature are determined globally for the entire building. The water mass flow rate is fixed to 28.7 m^3/h in the cooling and 17.7 m^3/h in the heating case (or off).

A central AHU supplies the offices with fresh air, see Figure 6.3. It includes a heat exchanger for return air heat / cold recovery[2], a heating coil in the supply air, and an evaporative cooler[3] in the return air duct. The supply air temperature and mass flow rate are again determined globally for the entire building. On each floor, fixed fractions of the total air mass flow are supplied to the offices on the outer parts of the floors and returned from the rooms in the center of the building. Natural ventilation by manual opening of windows is possible in all office rooms.

Additionally, in the corner offices, radiators are available to cover the additional heat demand due to the increased facade area. However, the amount of heat provided by the radiators is significantly smaller than that provided by the TABS or AHU.

The gas boiler provides all heating energy for the TABS, the AHU heating coil, and the radiators. The cold water for the TABS is generated by a hybrid cooling tower[4]. However, to minimize maintenance effort, the tower was operated prior to and throughout the project in "dry mode" only, i.e. without water being sprayed on the tubes.

The Venetian blinds on a particular facade can only be set collectively and just to four distinct positions (open, low shading position, high shading position, closed). Their position can be overridden by the occupants. Lighting in the offices is switched on / off by the users and, if turned on, is controlled by a local controller to a luminance setpoint.

6.2.2 Sensing

Several wireless room temperature and window contact sensors, electric load meters, as well as TABS and AHU heating / cooling power meters were installed at the beginning of the project for the following purposes: i) to enable the thorough evaluation of the control experiments; ii) to facilitate the validation of building models; iii) to support the newly developed RBC and MPC control strategies. Moreover, the blinds control was integrated into the building's automation system. Already prior to the project, a weather station was in place on the building's roof. It was complemented by additional temperature and radiation sensors on all four facade orientations. Finally, an industry PC was set up for running the investigated control algorithms and an external database was established to monitor and analyze the building's operation.

6.3 Control Task

The main goal of the control system is to ensure the comfort of the occupants while minimizing operating costs. In this section, we define "comfort" and "operating costs" for our particular

---

[2]Also referred to as *ERC*.

[3]An evaporative cooler cools the air flow through evaporation of water sprayed into the air. Due to the resulting undesired moisture in the air, it is placed in the return air duct and the cold is transferred to the supply air through the heat exchanger.

[4]Hybrid cooling towers pass the fluid to be cooled through a tube bundle, upon which water is sprayed and a fan-induced draft applied.
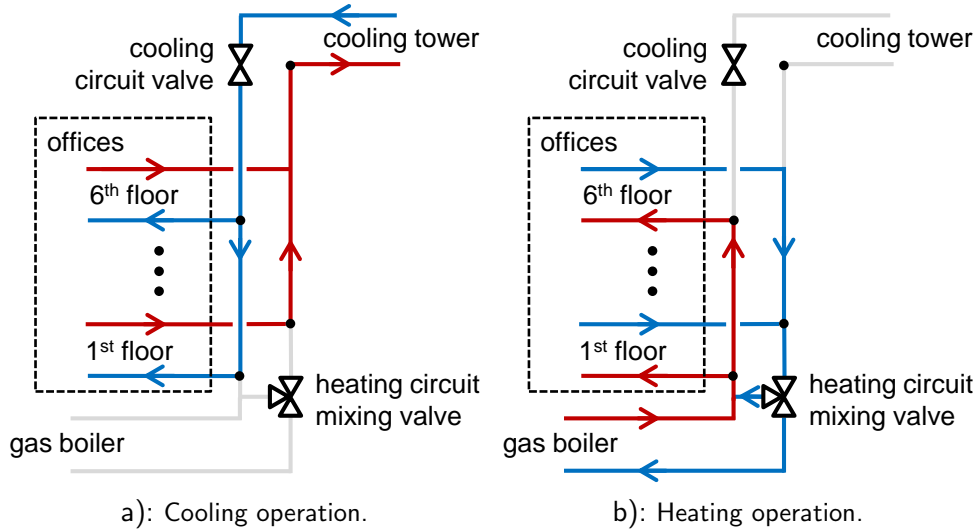
Figure 6.2: Schematic of the TABS in heating and cooling operation. Arrows indicate the directions of the water flow. Blue and red indicate, relative to each other, hot and cold water flow, respectively. Grey indicates no water flow. The pumps (not shown) and valves are operated such that at no time hot water from the boiler enters while the cooling tower is active and vice versa.
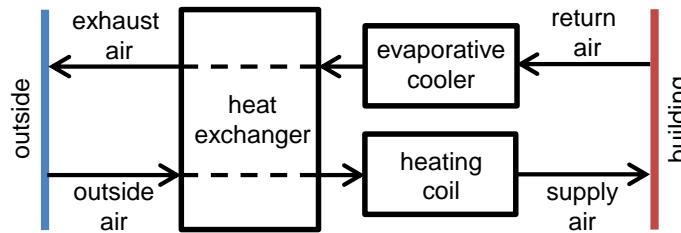
Figure 6.3: Schematic of the AHU. Arrows indicate the directions of the air flow. No air mixing takes place in the heat exchanger.

case.

6.3.1 Comfort Specification

In coordination with the facility management, four quantitative comfort criteria that had to be met during working hours (defined as 08:00-19:00 on Mondays–Fridays) were specified as follows.

Thermal comfort. Thermal comfort was defined to be satisfied if the room air temperatures lied within a comfort range. The lower end of the comfort range was 22 °C. The upper end varied between 25 °C-27 °C depending on the running mean of the outside air temperature calculated according to the European Norm (EN) 15251 [39] (see Section 6.6.2). To prevent air draught, the supply air temperature setpoint of the AHU was limited to 16 °C-28 °C in summer and 22 °C-28 °C in winter.

Blinds movements. To keep disturbance for the occupants at a minimum level, the controller was only allowed the execution of one blinds control action at 13:00. During nights and

Table 6.1: Operation costs coefficients. High-tariff period: Monday-Friday 06:00-21:00, Saturday 06:00-12:00. Low-tariff period: otherwise.

Objective	Costs type	Value	Unit
Money	Natural gas	0.075	CHF[5]/kWh
	Electricity (low tariff)	0.097	CHF/kWh
	Electricity (high tariff)	0.145	CHF/kWh
NRPE	Natural gas	1.2	kWh/kWh
	Electricity	3.32	kWh/kWh

weekends, no restrictions were applied.

Visual comfort. To avoid glare, the 13:00 blinds control action for facades with higher than $200\,\text{W/m}^2$ irradiation (indicating direct sunlight) was restricted to positions that ensured the complete blocking of direct sunlight. Moreover, completely closed blinds positions were not allowed during working hours.

Air quality. To satisfy air demand in the offices, a minimum ventilation rate was enforced.

6.3.2 Operating Costs

Operating costs arise from the usage of the boiler (gas) and the electricity costs of the cooling tower fans, the ventilation fans, the evaporative cooler, the lighting, and the pumps of the TABS system. No costs were associated with the use of the blinds system. The costs were considered either in terms of money or Non-Renewable Primary Energy (NRPE) via the coefficients shown in Table 6.1. We consider the NRPE costs to be that amount of an unprocessed fuel's energy (gas, coal, etc.) that is necessary to produce a particular amount of *final* (i.e. consumed) energy (including conversion and transport losses). Hence, one Joule of electricity results in significantly higher NRPE costs than one Joule of gas.
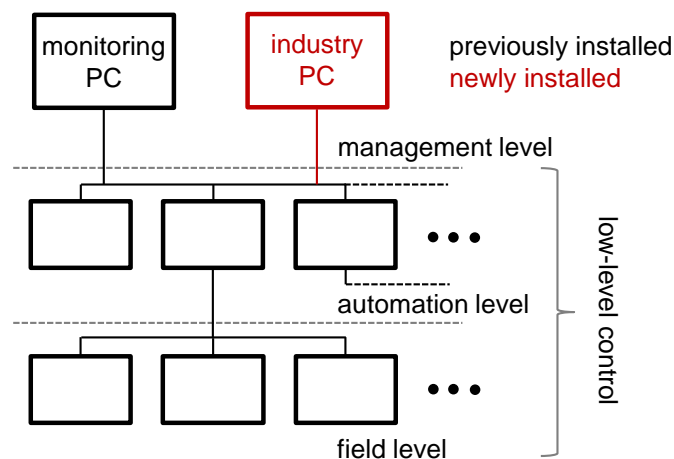
Figure 6.4: Schematic of the control topology.

---

[5]Swiss Francs.

Table 6.2: High-level control data acquisition interface. Only the subset of all available measurements relevant for the discussion in this study is shown.

System	Description	Unit	Sensors
Rooms	Temperature	°C	29
	Presence	{0,1}	19
	Window contact	{0,1}	31
	Electrical energy meters (illumination, appliances)	kWh	31
Weather	Ambient air temperature (N,E,S,W facades)	°C	4
	Global solar radiation (N,E,S,W,horizontal)	W/m^2	5
TABS heating	Water flow	m^3/h	1
	Supply / return water temperature	°C	1
	Heating energy	kWh	1
TABS cooling	Water flow	m^3/h	1
	Supply / return water temperature	°C	1
	Cooling energy	kWh	1
Radiators	Water flow	m^3/h	1
	Supply / return water temperature	°C	1
	Heating energy	kWh	1
AHU	Supply air flow	m^3/h	1
	Supply / return air temperature	°C	1
	Heating energy heating coil	kWh	1

6.4 Control System Topology

In this section, the control system topology of the building automation system (BAS) and the placement of the MPC supervisory control is described. The building is equipped with the Siemens building automation system DESIGO [40], which is partitioned hierarchically into field, automation and management level, see Figure 6.4. The field level includes all sensors, actuators, and their local controllers. The automation level executes primary plant control (e.g. control of air handling units, heat / cold generation, and distribution). The default rule-based control strategy RBC-0 that previously controlled the building had been implemented in the automation level. MPC on the other hand was implemented on a newly installed industry PC in the management level. Prior to the project, the management level was mainly used for monitoring and manual setpoint adjustments. In the following, we use the term high-level (HL) control for the MPC on the industry PC and low-level (LL) control for the automation and field-level controllers.

The HL control received measurements from and sent setpoints and operating modes to the LL control via the Building Automation and Control networks (BACnet) protocol using a BACnet Object Linking and Embedding for Process Control (OPC) server running on the industry PC. Moreover, it downloaded weather forecasts from the Swiss Federal Office of Meteorology and Climatology MeteoSwiss over an internet connection which was also used to remotely access the industry PC.

Table 6.3: High-level control write interface (to low-level control).

System	Description	Range / Unit
General	Enable high-level control	{0,1}
	Live check flag	{0,1}
TABS heating	Enable high-level control	{0,1}
	Operating Mode	{Off,On}
	Flow temperature setpoint	[10,35] °C
TABS cooling	Enable high-level control	{0,1}
	Operating Mode	{Off,On}
	Flow temperature setpoint	[10,35] °C
Radiators	Enable high-level control	{0,1}
	Operating Mode	{Off,On}
	Flow temperature setpoint	[10,35] °C
AHU	Enable high-level control	{0,1}
	Operating Mode	{Off,On}
	Supply air temperature setpoint heating	[10,35] °C
	Supply air temperature setpoint cooling	[10,35] °C
	Supply air temperature setpoint ERC	[10,35] °C
	Differential pressure setpoint supply	[0,300] Pa
	Differential pressure setpoint exhaust	[0,300] Pa
Blinds	Enable high-level control	{0,1}
	Open North/East/South/West	{0,1}
	Shading Position 1 North/East/South/West	{0,1}
	Shading Position 2 North/East/South/West	{0,1}
	Close North/East/South/West	{0,1}

The HL data acquisition interface used to gather measurements comprised only a small subset of the information available at the automation level (several thousand signals). Table 6.2 shows the subset of measurements relevant for the discussion in this study.

The complete HL write interface that was used to send setpoints and operating modes to the LL control is shown in Table 6.3. It was possible to enable / disable HL control for every subsystem (TABS, AHU, radiators, blinds) as well as for the overall HL control system. If HL control was disabled for a particular subsystem, the corresponding previously installed LL controller would take over. When high-level control was active, every subsystem could be turned on or off (operating mode). For a description of the low-level controllers that track the setpoints we refer to Section 4.1.4 of [9]. The HL control set the live check flag in every iteration to 1. If it failed to do so, control reverted to the default strategy RBC-0. The MPC control algorithm (see Section 6.6) was executed in Matlab using the OPC client toolbox to connect to the BACnet OPC server. The control had a sampling time of $T_s = 0.25$ h. The control algorithm took about 3 min to complete, of which the solution of the optimization problem used about 30 s. Matlab was restarted at the beginning of every control time step by

a periodic operating system task in order to be robust against previous execution errors and to avoid memory fragmentation.

6.5 Modeling

In this section, we describe how we modeled the building dynamics, the operating costs, and the constraints such that the resulting MPC problem represented the control task defined in Section 6.3. We used a bilinear building dynamics model as well as linear operating costs and constraints as in the MPC problem (2.16). Additionally, we explicitly defined model outputs, y, to facilitate a model order reduction. The modeling followed the BRCM toolbox' procedure introduced in Section 4.2. Including additionally the output definition and model reduction step, it is summarized in Figure 6.5 which also serves as this section's outline. The thermal model input data and the EHF parameters are described in Sections 6.5.1 and 6.5.2, respectively.

   Using a tilde to denote the reduced order model's variables and matrices, the resulting MPC optimization problem was given by

$$\underset{U_{0\to N}}{\text{minimize}} \quad \sum_{k=0}^{N-1} c_k^T u_k \tag{6.1a}$$

$$\text{subject to} \quad \tilde{x}_{k+1} = \tilde{A}\tilde{x}_k + \tilde{B}_u u_k + \tilde{B}_v v_k + \sum_{i=1}^{n_u}(\tilde{B}_{vu,i} v_k + \tilde{B}_{xu,i}\tilde{x}_k)u_{k,i} \quad \forall k \in \mathbb{N}_0^{N-1} \tag{6.1b}$$

$$y_k = \tilde{C}\tilde{x}_k \qquad\qquad\qquad\qquad\qquad\qquad \forall k \in \mathbb{N}_0^{N-1} \tag{6.1c}$$

$$y_{\text{min},k} \leq y_k \leq y_{\text{max},k} \qquad\qquad\qquad\qquad\quad \forall k \in \mathbb{N}_0^{N-1} \tag{6.1d}$$

$$\tilde{F}_{x,k}\tilde{x}_k + F_{u,k}u_k + F_{v,k}v_k \leq f_k \qquad\qquad\quad \forall k \in \mathbb{N}_0^{N-1} \tag{6.1e}$$

$$\tilde{x}_0 = \hat{\tilde{x}}. \tag{6.1f}$$

Note that this formulation including outputs (6.1c) and output constraints (6.1d) is just a notational convenience and is completely equivalent to the MPC problem (2.16). However, since $\tilde{x}$ are the reduced order model's states, they cannot be interpreted anymore as individual building elements' or rooms' temperatures and the quantities we want to predict must be represented in y. We used a prediction horizon of 58 h, limited by the length of the weather forecast's prediction horizon just before the next update. We discretized with a sampling time of $T_s = 0.25$ h which resulted in a horizon length of $N = 232$.

   We modeled the entire second floor which we, supported by measurements, assumed to be representative for the whole building. Recall that due to the building's HVAC system design, the identical control actions had to be applied to all of the office floors. The inputs and outputs of the model are listed in Table 6.4. Note that ideally one would want to formulate the optimization problem in terms of its setpoints and operating modes (see Table 6.3) that can be communicated directly to the LL control. However, by limiting the model to a bilinear form, this was not possible. Hence, the control inputs in Table 6.4 are intermediate quantities
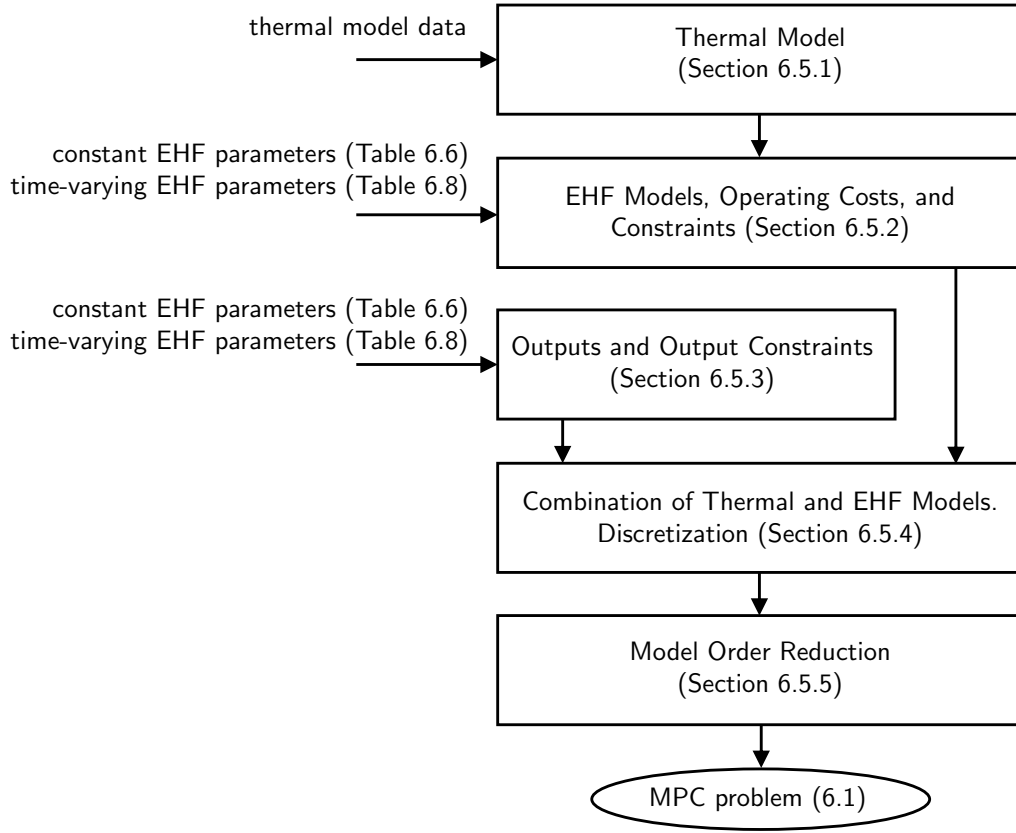
Figure 6.5: Modeling procedure.

that had to be post-processed after the optimization (see Section 6.6.4).

6.5.1 Thermal Model

Using the same algorithms as in the BRCM toolbox (see Section 4.2), the thermal model data were extracted from an EnergyPlus model that had been developed to enable the simulation-based controller comparisons (see Section 6.7.2). The EnergyPlus model was mostly built based on planning data[6]. For the parameters that were unavailable, standard Swiss office building data were used. For more information on how the EnergyPlus model was built, see [41]. Figure 6.6 shows the EnergyPlus model's and hence also the thermal model's zones, as well as the zone groups for which averaged operative room temperature outputs, $y_{\mathrm{AvgOpRoomT},\{N,E,W,S,C\}}$, were defined (see Section 6.5.3). The floors and ceilings were modeled to have adiabatic boundary conditions. Given the extracted thermal model data, the full-order thermal model,

$$\dot{x}(t) = A_t x(t) + B_t q(x(t), u(t), v(t)), \tag{6.2}$$

was constructed using the same algorithms as in the toolbox. Thus, with every zone in Figure 6.6 and all corresponding building element layers, a state describing its temperature and an EHF was associated. This resulted in $x, q \in \mathbb{R}^{n_x}$ with $n_x = 390$. The following Section 6.5.2 describes how the aggregated EHFs, $q(x(t), u(t), v(t))$, were modeled.

---

[6]The architectural data based on which the building was built.

Table 6.4: Model outputs y, control inputs u, and disturbances v. {N,E,W,S,(C)} or {NE,SE,SW,NW} in the subscript of a variable denotes that there are individual variables per zone location north/east/west/south/(core) or north-east/south-east/south-west/north-west, respectively.

Variable	Description	Unit
$y_{AvgOpRoomT,\{N,E,W,S,C\}}$	Averaged operative room temperatures	$^\circ$C
$y_{AHU,ReturnT}$	AHU return air temperature	$^\circ$C
$y_{TABS,Core}$	TABS core temperature	$^\circ$C
$u_{TABS,H}$	Total TABS heating heat flux	W
$u_{TABS,C}$	Total TABS cooling heat flux	W
$u_{Rad,\{NE,SE,SW,NW\}}$	Radiator heat flux in the corner offices	W
$u_{TransmSol,\{N,E,W,S\}}$	Transmitted solar heat flux into room	W/m^2
$u_{Light,\{N,E,W,S\}}$	Electrical lighting power in the offices	W/m^2
$u_{AHU,\dot{m},ERC}$	Air mass flow through ERC	kg/s
$u_{AHU,\dot{m},NoERC}$	Air mass flow bypassing ERC	kg/s
$u_{AHU,\dot{m},EvapC}$	Air mass flow through evaporative cooler	kg/s
$u_{AHU,H}$	AHU heater heat flux	W
$v_{IG,Off}$	Internal gains in the offices (does not include lighting)	W/m^2
$v_{IG,NonOff}$	Internal gains in non-office zones (includes lighting)	W/m^2
v_{AmbT}	Ambient air temperature	$^\circ$C
$v_{Sol,\{N,E,W,S\}}$	Solar radiation on facade	W/m^2

6.5.2 External Heat Flux Models

The modeling of the EHFs is first described by example of a generic zone i. Figure 6.7 shows this zone's RC network with indicated EHFs $q_{(.)}^i$ where "(.)" denotes the state the EHF applies to (states without indicated EHFs have no external influences acting on them). For simplicity, in Figure 6.7 only one interior (zone to zone) and one exterior (zone to environment) wall branch and a fixed number of three states per building element are shown (there may be more or fewer). Table 6.5 describes all indicated EHFs. In the following Sections 6.5.2.1-6.5.2.7, we describe their bilinear models as well as the linear operating costs and constraints. Not all EHF models are applicable to every zone (e.g. there are no solar gains in the core zones), hence we also indicate the set of zones $\mathcal{Z}^{(.)}$ for which EHF "(.)" was modeled. The aggregated EHF model for all zones,

$$q(x(t), u(t), v(t)) = A_q x(t) + B_{q,u} u(t) + B_{q,v} v(t) + \sum_{i=1}^{n_u} (B_{q,vu,i} v(t) + B_{q,xu,i} x(t)) u_i(t), \quad (6.3)$$

is then constructed by iterating over all zones in Figure 6.6 and parameterizing and aggregating for each zone those EHFs from Table 6.5 which are applicable (see Section 6.5.2.8).

Two types of parameters appear in the EHF models: i) constant parameters are listed and described in order of appearance in Table 6.6. Most were derived from planning data while some were calculated based on EnergyPlus simulations. This dependency on EnergyPlus is discussed in Section 6.9. Additionally, ii), time-varying operating costs and constraints
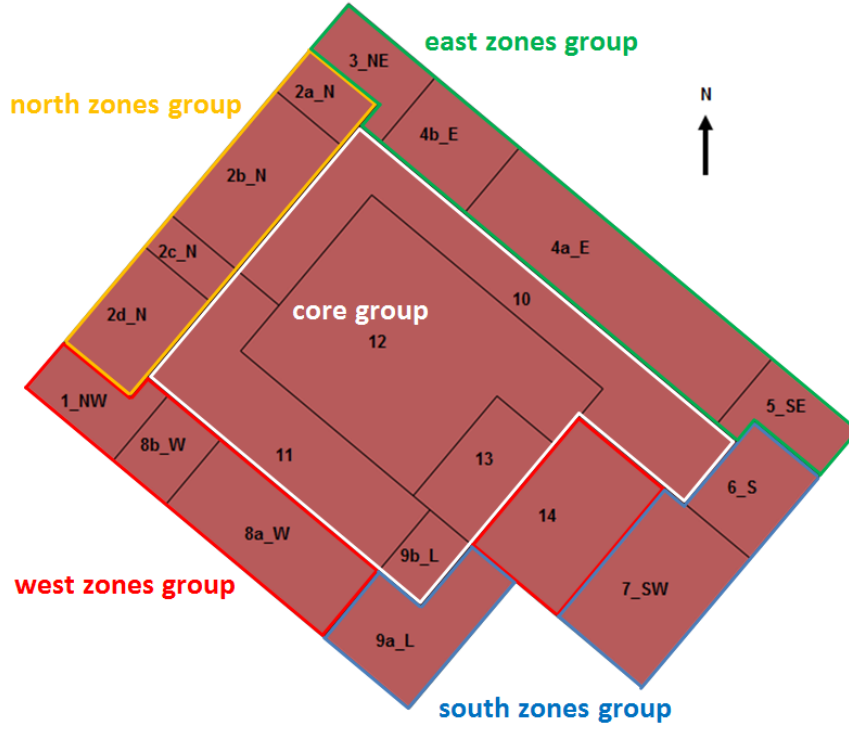
Figure 6.6: EnergyPlus model zones and output zone groups.
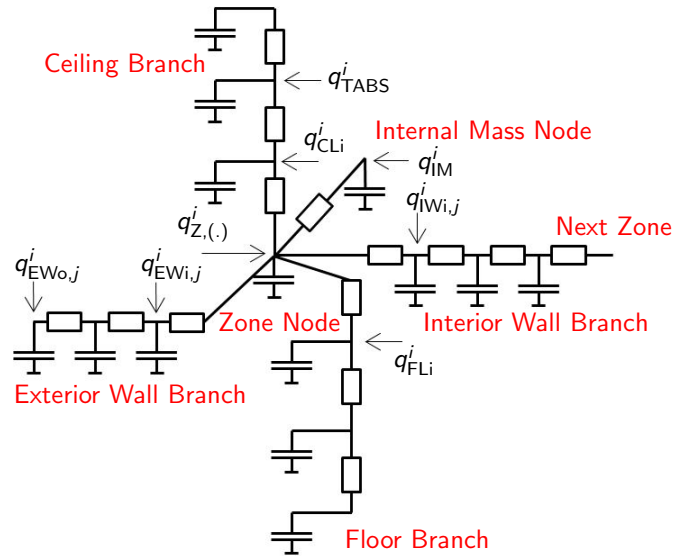
Figure 6.7: RC network for a generic zone i. The symbols $q^i_{(.)}$ represent EHFs where "(.)" denotes the state the EHF applies to (states without indicated EHFs have no external influences acting on them). See Table 6.5 for a description of the EHFs. $q^i_{Z,(.)}$ is a placeholder for several individual heat fluxes acting on the zone node.

parameters are listed and described in order of appearance in Table 6.8. To set up the costs and constraints, the time-varying parameters must be available over the whole MPC horizon. Their calculation is described in Section 6.6.2.

Table 6.5: This table lists for a generic zone i in Figure 6.7 the EHFs, the state they apply to, the state's location, a description, and the EHF models they are part of.

EHF	State	Location	Description	EHF model
$q_{Z,IG}^i$	x_Z^i	Zone i	Internal gains	Internal gains
$q_{Z,infilt}^i$	x_Z^i	Zone i	Air infiltration	Infiltration
$q_{Z,win}^i$	x_Z^i	Zone i	Solar radiation and conduction through windows	Windows
$q_{Z,Rad}^i$	x_Z^i	Zone i	Radiator heat gains	Radiators
$q_{Z,AHU,Dir}^i$	x_Z^i	Zone i	Direct air supply by AHU	AHU
$q_{Z,AHU,ZtoZ}^i$	x_Z^i	Zone i	Zone to zone air exchange induced by AHU	AHU
$q_{EWo,j}^i$	$x_{EWo,j}^i$	Outermost layer of external wall j of zone i	Solar radiation and convection	Opaque building hull
q_{TABS}^i	x_{TABS}^i	TABS layer in zone i	TABS	TABS
q_{FLi}^i	x_{FLi}^i	Innermost layer of the floor in zone i	Solar radiation	Windows
q_{CLi}^i	x_{CLi}^i	Innermost layer of ceiling in zone i	Solar radiation	Windows
$q_{EWi,j}^i$	$x_{EWi,j}^i$	Innermost layer of external wall j of zone i	Solar radiation	Windows
$q_{IWi,j}^i$	$x_{IWi,j}^i$	Innermost layer of internal wall j of zone i	Solar radiation	Windows
q_{IM}^i	x_{IM}^i	Internal mass of zone i	Solar radiation	Windows

Table 6.6: Constant parameters of the EHF models. EP: EnergyPlus.

Parameter	Description	Unit	Source
α_{EW}	Combined convective/radiative heat transfer coefficient between external wall and ambient air	$m^2 K/W$	EP simulations
$a_{EW,j}^i$	Area of external wall j of zone i	m^2	Planning data
$r_{EWo,j}^i$	Thermal resistance of the outermost layer of external wall j in zone i	$m\,K/W$	Planning data
$d_{EWo,j}^i$	Thickness of the outermost layer of external wall j in zone i	m	Planning data
γ_{absorp}	Solar absorption coefficient	-	Planning data
c_{air}	Specific heat capacity of air	$J/(kg\,K)$	Standard value
ρ_{air}	Density of air	kg/m^3	Standard value
a^i	Floor area of zone i	m^2	Planning data
h	Room height (same for all rooms)	m	Planning data
γ_{infilt}	Natural air change rate (room volumes per second)	$1/s$	Assumption
Q_{RadMax}	Maximum heating power of a radiator	W	Planning data

Continued on next page

Table 6.7 – continued from previous page

$a_{\text{TABS,tot}}$	Area of all building elements with TABS piping	m^2	Planning data
P_{CTowMax}	Electrical power consumption of the cooling tower running at maximum capacity	W	Planning data
$Q_{\text{TABSHeatMax}}$	Maximum TABS heating power	W	Planning data
$a^i_{\text{win,tot}}$	Total window area in zone i	m^2	Planning data
$a^i_{\text{win,fac}}$	Total window area of the *fac* facade of zone i	m^2	Planning data
$a^i_{\text{BE,tot}}$	Total area of all building elements in zone i	m^2	Planning data
γ_{SecWinHG}	Secondary heat gains coefficient (due to solar radiation absorbed in the window)	-	EP simulations
U_{win}	U-Value of windows (area specific heat transfer coefficient)	W/(m^{2}K)	Planning data
f_{lumEffic}	Luminous efficacy of the lighting	lm/W	Planning data
f_{illum}	Conversion factor from transmitted solar radiation to illumination	lm/W	EP simulations
$\gamma^i_{\text{inflow,}j}$	Inflow from zone j to zone i as a fraction of total AHU mass flow rate	-	Planning data
γ^i_{AHU}	AHU inflow to zone i as a fraction of total AHU mass flow rate	-	Planning data
$P_{\text{AHU,Fan}}$	AHU fan electric power per air mass flow rate	W/(kg s)	Planning data
$P_{\text{AHU,Cool}}$	Electrical power consumption per mass flow rate of the evaporative cooler running at maximum capacity	W/(kg s)	Planning data
$\dot{m}_{\text{AHU,max}}$	Maximum achievable AHU mass flow rate	kg/s	Planning data
$Q_{\text{AHU,H,max}}$	Maximum heating power of the heating coil in the AHU	W	Planning data
η_{ERC}	Heat exchanger efficiency	-	Planning data
η_{Cool}	Fraction of the drybulb-wetbulb temperature difference by which the evaporative cooler can cool the return air	-	Planning data
a^i_{IM}	Surface area of the i-th zone's internal mass	m^2	Assumption

6.5.2.1 Opaque Building Hull

The heat flux to the opaque part of the building hull (i.e. without windows which are treated separately in Section 6.5.2.5) was modeled to have: i) a radiation component modeling the absorption of solar radiation and the thermal reradiation of the building hull; and ii) a convection component modeling the heat exchange between the hull and the ambient air.

We consider external wall j of room i. The absorbed radiation in component i) was modeled as the product of the solar radiation incident on the facade with orientation $fac(i, j)$, $v_{\text{Sol,}fac(i,j)}(t)$, and an absorption factor. The thermal (long wave) radiation exchange with the sky was simplified by using a combined heat transfer coefficient for convection and radiation, assuming the sky temperature[7] to coincide with the ambient air temperature.

---

[7]The equivalent temperature of all atmospheric elements making up the sky with which a surface (on the ground) is in thermal radiation exchange.

Table 6.8: Time-varying operating costs and constraints parameters of the EHF models. Computed prior to the optimization for the whole prediction horizon (see Section 6.6.2).

Parameter	Description	Unit
$f_{\text{gas}}^{(.)}$	Placeholder for the corresponding ("(.)" denotes money or NRPE) gas costs coefficients in Table 6.1 (converted to "per Joule")	J/J or CHF/J
$f_{\text{ele}}^{(.)}$	Placeholder for the corresponding ("(.)" denotes money or NRPE) electricity costs coefficients in Table 6.1 (converted to "per Joule")	J/J or CHF/J
$Q_{\text{TABSCoolMax}}$	Maximum TABS cooling power	W
$Q_{\text{TransmSolMin},fac}$	Transmitted solar radiation on facade fac corresponding to the maximum shading blinds setpoint allowed	W/m^2
$Q_{\text{TransmSolMax},fac}$	Transmitted solar radiation on facade fac corresponding to the minimum shading blinds setpoint allowed	W/m^2
I_{min}	Minimum illumination in office zones	lx
$\dot{m}_{\text{AHU,min}}$	Minimum AHU air mass flow rate	kg/s
$T_{\text{AHU,min}}$	Minimum AHU supply air temperature	°C
$T_{\text{AHU,max}}$	Maximum AHU supply air temperature	°C
$T_{\text{AHU,Ret}}$	AHU return air temperature	°C
T_{EN15251}	Maximum room temperature as a function of the running mean of the ambient temperature. Computed according to EN 15251 [39]	°C

Component ii) was modeled to be linearly proportional to the temperature difference between ambient air, $v_{\text{AmbT}}(t)$, and the external wall's outermost[8] layer's temperature, $x_{\text{EWo},j}^{i}(t)$. The corresponding thermal resistance considered the combined heat transfer coefficient and the conductive resistance.

Combining both, Equation (6.4) shows the EHF to the outermost layer of external wall j. This EHF applies to all facade zones.

$$
\begin{aligned}
\textbf{EHF} \quad q_{\text{EWo},j}^{i}(t) &= \gamma_{\text{absorp}} a_{\text{EW},j}^{i} v_{\text{Sol},fac(i,j)}(t) \\
&+ \frac{a_{\text{EW},j}^{i}}{1/\alpha_{\text{EW}} + r_{\text{EWo},j}^{i} d_{\text{EWo},j}^{i}/2}(v_{\text{AmbT}}(t) - x_{\text{EWo},j}^{i}(t))
\end{aligned}
\tag{6.4}
$$

Applicable Zones
$$
\mathcal{Z}^{\text{OpaqueBuildingHull}} = \{1\_\text{NW, 2a\_N, 2b\_N, 2c\_N, 2d\_N, 3\_NE, 4a\_E, 4b\_E,} \\
\text{5\_SE, 6\_S, 7\_SW, 8a\_W, 8b\_W, 9a\_L, 14}\}
$$

6.5.2.2 Infiltration

As commonly done, the heat flux due to infiltration (unintentional air exchange through cracks in the building hull) was modeled as an air exchange between the room and ambient air whose magnitude was proportional to the room's volume.

Equation (6.5) shows this EHF which applies to all facade zones.

---

[8]The layer in contact with the ambient air.

EHF	$q^i_{Z,\text{infilt}}(t) = c_{\text{air}} \rho_{\text{air}} a^i h \gamma_{\text{infilt}} (v_{\text{AmbT}}(t) - x^i_Z(t))$	(6.5)
Applicable Zones	$\mathcal{Z}^{\text{Infiltration}} = \{$1_NW, 2a_N, 2b_N, 2c_N, 2d_N, 3_NE, 4a_E, 4b_E, 5_SE, 6_S, 7_SW, 8a_W, 8b_W, 9a_L, 14$\}$	

6.5.2.3 Radiators

The radiators in the corner offices were locally controlled to ensure a minimum room air temperature. This local control could not be overwritten by the HL control. To consider their effects, the radiators were nevertheless modeled as controllable heat fluxes to the corner offices. The analysis of simulation data showed that almost all of the time this resulted in the same behavior as on the real building, i.e. MPC used the TABS and AHU to heat the non-corner zones to the lower temperature constraint and the radiators to provide the additional heat demand to achieve the same in the corner offices. In any case, the heat provided by the radiators was significantly smaller than of the TABS or AHU.

Equations (6.6)-(6.9) show this simple EHF for the NE, SE, SW, and NW cases. The operating costs (6.10) are proportional to the applied heating power.

The constraints (6.11) enforced the radiator heat fluxes to be non-negative and upper limited by a constant maximum heating power.

EHF	NE:	$q^i_{Z,\text{Rad}}(t) = u_{\text{Rad,NE}}(t)$	(6.6)
	SE:	$q^i_{Z,\text{Rad}}(t) = u_{\text{Rad,SE}}(t)$	(6.7)
	SW:	$q^i_{Z,\text{Rad}}(t) = u_{\text{Rad,SW}}(t)$	(6.8)
	NW:	$q^i_{Z,\text{Rad}}(t) = u_{\text{Rad,NW}}(t)$	(6.9)
Operating Costs		$J_{\text{Rad}}(t) = f^{(.)}_{\text{gas}}(t) \left(u_{\text{Rad,NE}}(t) + u_{\text{Rad,SE}}(t) + u_{\text{Rad,SW}}(t) + u_{\text{Rad,NW}}(t) \right)$	(6.10)
Constraints		$0 \le u_{\text{Rad},fac}(t) \le Q_{\text{RadMax}}$ $\forall fac \in \{\text{NE,SE,SW,NW}\}$	(6.11)
Applicable Zones	NE:	$\mathcal{Z}^{\text{Rad,NE}} = \{3_NE\}$	
	SE:	$\mathcal{Z}^{\text{Rad,SE}} = \{5_SE\}$	
	SW:	$\mathcal{Z}^{\text{Rad,SW}} = \{7_SW\}$	
	NW:	$\mathcal{Z}^{\text{Rad,NW}} = \{1_NW\}$	

6.5.2.4 Thermally Activated Building System

As shown in Equation (6.12), we modeled the heat flux to the TABS layer, $q^i_{\text{TABS}}(t)$, as a fraction of the total supplied TABS heating and cooling heat fluxes, $u_{\text{TABS,H}}(t)$ and $u_{\text{TABS,C}}(t)$,

respectively[9].

The operating costs (6.13) are the sum of the gas costs for heating and the electricity costs for operating the cooling tower fans. The latter are computed as a fraction, $\frac{u_{\text{TABS,C}}(t)}{Q_{\text{TABSCoolMax}}(t)}$, of the electrical power necessary for running the cooling tower at full capacity, P_{CTowMax}. The maximum cooling power, $Q_{\text{TABSCoolMax}}(t)$, is a function of the ambient and the average TABS core temperature (see Section 6.6.2). The pumping costs of the TABS could not be modeled accurately as a linear function of the control inputs due to the binary nature (fixed or no flow rate). However, they were an order of magnitude lower than the gas costs for heating or electricity costs for cooling (at full capacity). Hence, the resulting control actions were unlikely to be significantly influenced.

The total TABS heat fluxes were enforced by (6.14) and (6.15) to be non-negative and upper constrained by the maximum available heating power of the boiler, $Q_{\text{TABSHeatMax}}$, and $Q_{\text{TABSCoolMax}}(t)$, respectively.

EHF	$q_{\text{TABS}}^i(t) = \dfrac{a^i}{a_{\text{TABS,tot}}}(u_{\text{TABS,H}}(t) - u_{\text{TABS,C}}(t))$	(6.12)
Operating Costs	$J_{\text{TABS}}(t) = f_{\text{gas}}^{(\cdot)}(t)u_{\text{TABS,H}}(t) + f_{\text{ele}}^{(\cdot)}(t)P_{\text{CTowMax}}\dfrac{u_{\text{TABS,C}}(t)}{Q_{\text{TABSCoolMax}}(t)}$	(6.13)
Constraints	$0 \leq u_{\text{TABS,H}}(t) \leq Q_{\text{TABSHeatMax}}$	(6.14)
	$0 \leq u_{\text{TABS,C}}(t) \leq Q_{\text{TABSCoolMax}}(t)$	(6.15)
Applicable Zones	$\mathcal{Z}^{\text{TABS}} = \{$1_NW, 2a_N, 2b_N, 2c_N, 2d_N, 3_NE, 4a_E, 4b_E, 5_SE, 6_S, 7_SW, 8a_W, 8b_W, 9a_L, 9b_L$\}$	

6.5.2.5 Windows

We considered the heat flux through the windows in three parts: i) a transmitted solar radiation part absorbed by the innermost[10] layers of the zone's building elements; ii) a solar radiation part absorbed by the window and transmitted to the zone (also known as secondary heat gains); iii) a heat flux due to conduction through the window.

Part i) constitutes the heat fluxes $q_{\text{FLi}}^i(t)$, $q_{\text{CLi}}^i(t)$, $q_{\text{EWi},j}^i(t)$, $q_{\text{IWi},j}^i(t)$, and $q_{\text{IM}}^i(t)$. Since the transmitted solar heat flux is a function of the blinds position, we modeled it as a controllable heat flux, $u_{\text{TransmSol},\{\text{N,E,W,S}\}}(t)$. Recall that in the target building, the blinds can only be controlled facade-wise. We assumed that the solar radiation varied only insignificantly between

---

[9]An obvious alternative approach would have been to model the TABS heat flux proportional to the difference of a supply temperature setpoint and $x_{\text{TABS}}^i(t)$. However, in the target building the mass flows differed significantly between cooling and heating operation. This implied varying proportionality constants which could not have been considered and hence would have rendered this modeling approach less accurate than the one described.

[10]The layer in contact with the zone's air.

zones of the same facade and thus considered just one input per facade. The total transmitted solar heat flux, $\sum_{fac \in \{N,E,W,S\}} a^i_{\text{win},fac} u_{\text{TransmSolar},fac}(t)$, is then distributed area proportionally among all innermost building element layers of zone i. Equation (6.16) shows this EHF by example of interior wall j, $q^i_{\text{IWi},j}(t)$ (analogous for $q^i_{\text{FLi}}(t)$, $q^i_{\text{CLi}}(t)$, $q^i_{\text{EWi},j}(t)$, $q^i_{\text{IM}}(t)$).

Parts ii) and iii) are reflected in $q^i_{\text{Z},\text{win}}(t)$, see Equation (6.17). As commonly done, the conductive part was modeled with a *U-value* while the secondary heat gains were modeled to be proportional to the transmitted solar radiation.

Recall that only four blinds position setpoints could be set. Considering this exactly would obviously have resulted in integer constraints. To avoid that, we relaxed the integer constraints by assuming that the blinds could be set to any intermediate position between the maximum and the minimum shading blinds setpoint and computed corresponding lower and upper bounds on the transmitted solar heat fluxes $Q_{\text{TransmSolMin},fac}(t)$, $Q_{\text{TransmSolMax},fac}(t)$ as a function of the solar radiation and the blinds position (see Section 6.6.2). In the post-processing step (Section 6.6.4), those blinds positions were chosen whose heat flux best matched the $u_{\text{TransmSol},\{N,E,W,S\}}$ resulting from the solution of the MPC problem.

Throughout the study, it was assumed that the windows were closed and the blinds were at the position the MPC set them to (both could be changed by the occupants). Deviations from this assumption were only taken into account indirectly via the room temperature measurements. This was motivated by the expectation that any changes by the occupants were only made to improve comfort.

No operating costs were associated with $u_{\text{TransmSol},\{N,E,W,S\}}(t)$. This EHF applied to all facade zones.

EHF	$$q^i_{\text{IWi},j}(t) = \frac{a^i_{\text{IW},j}}{a^i_{\text{BE},\text{tot}}} \sum_{fac \in \{N,E,W,S\}} a^i_{\text{win},fac} u_{\text{TransmSolar},fac}(t)$$ $$\text{analogously to (6.16) for } q^i_{\text{FLi}}(t),\ q^i_{\text{CLi}}(t),\ q^i_{\text{EWi},j}(t),\ q^i_{\text{IM}}(t)$$ $$q^i_{\text{Z},\text{win}}(t) = U_{\text{win}} a^i_{\text{win},\text{tot}} (v_{\text{AmbT}}(t) - x^i_{\text{Z}}(t))$$ $$+ \gamma_{\text{SecWinHG}} \sum_{fac \in \{N,E,W,S\}} a^i_{\text{win},fac} u_{\text{TransmSolar},fac}(t)$$	(6.16) (6.17)
Constraints	$$Q_{\text{TransmSolMin},fac}(t) \le u_{\text{TransmSolar},fac}(t) \le Q_{\text{TransmSolMax},fac}(t)$$ $$\forall fac \in \{N, E, W, S\}$$	(6.18)
Applicable Zones	$$\mathcal{Z}^{\text{Windows}} = \{1\_\text{NW}, 2a\_\text{N}, 2b\_\text{N}, 2c\_\text{N}, 2d\_\text{N}, 3\_\text{NE}, 4a\_\text{E}, 4b\_\text{E},$$ $$5\_\text{SE}, 6\_\text{S}, 7\_\text{SW}, 8a\_\text{W}, 8b\_\text{W}, 9a\_\text{L}, 9b\_\text{L}, 14\}$$	

6.5.2.6 Internal Gains

Internal gains due to occupants, lighting, and appliances were considered as simple heat sources acting on the zone nodes. We distinguished between office and non-office zones. Recall that

the former have an illumination controlled lighting system (not controlled by MPC) while the lighting of the non-office zones was scheduled irrespective of the current illumination level. Even though the lighting in the office zones was not controlled by MPC, we modeled it as control inputs $u_{\text{Light},\{\text{N,E,W,S}\}}(t)$ to be able to take the lighting costs into account when determining the blinds positions.

The internal gains in the offices were modeled as the sum of $v_{\text{IG,Off}}(t)$ (not including lighting) and $u_{\text{Light},fac(i)}(t)$ (Equation (6.19)), where $fac(i)$ denotes the facade of zone i. For the non-offices (Equation (6.20)), it simply is $v_{\text{IG,NonOff}}(t)$ (including lighting).

The total lighting costs are given by expression (6.21). The total illumination level in the offices was modeled as the sum of the lighting illumination and the solar illumination. Constraint (6.22) enforced that the total illumination was not below $I_{\text{min}}(t)$. Again, we modeled only one lighting input per facade because we assumed the solar illumination only to vary little between zones of the same facade. The lighting inputs $u_{\text{Light},fac(i)}(t)$ were upper bounded by the power necessary to provide $I_{\text{min}}(t)$.

EHF	Offices:	$q^i_{\text{Z,IG}}(t) = a^i\left(v_{\text{IG,Off}}(t) + u_{\text{Light},fac(i)}(t)\right)$	(6.19)
	Non-Offices:	$q^i_{\text{Z,IG}}(t) = a^i v_{\text{IG,NonOff}}(t)$	(6.20)

$$J_{\text{Light}}(t) = f^{(.)}_{\text{ele}}(t) \sum_{i \in \mathcal{Z}^{\text{IG,Offices}}} a^i u_{\text{Light},fac(i)}(t) \qquad (6.21)$$

with the label **Operating Costs**.

Constraints

$$I_{\text{min}}(t) \le f_{\text{lumEffic}} u_{\text{Light},fac(i)}(t) + \frac{f_{\text{illum}}}{a^i} \sum_{fac \in \{\text{N,E,W,S}\}} a^i_{\text{win},fac} u_{\text{TransmSolar},fac}(t) \qquad (6.22)$$

$$0 \le u_{\text{Light},fac(i)}(t) \le I_{\text{min}}(t)/f_{\text{lumEffic}} \qquad (6.23)$$

$$\forall i \in \mathcal{Z}^{\text{IG,Offices}}$$

Applicable Zones

Offices:
$$\mathcal{Z}^{\text{IG,Offices}} = \{1\_\text{NW}, 2a\_\text{N}, 2b\_\text{N}, 2c\_\text{N}, 2d\_\text{N}, 3\_\text{NE}, 4a\_\text{E}, 4b\_\text{E}, 5\_\text{SE}, 6\_\text{S}, 7\_\text{SW}, 8a\_\text{W}, 8b\_\text{W}\}$$

Non Offices:
$$\mathcal{Z}^{\text{IG,NonOffices}} = \{9a\_\text{L}, 9b\_\text{L}, 10, 11, 12, 13, 14\}$$

6.5.2.7 Air Handling Unit

The derivation of a bilinear model of the AHU at hand was not trivial. For brevity, only a brief description is given here, for details see the technical report [42]. Since the supply ventilation ducts are located in the offices on the facades and the return ventilation are located in the core zones, two physical effects due to the AHU operation had to be modeled. First, Equation (6.24) describes the *direct heat flux* due to the air flow directly from the AHU to zone i, $q^i_{\text{Z,AHU,Dir}}(t)$. We denote by $\mathcal{Z}^{\text{All}}$ the set of all zones. Second, expression (6.25) models the *zone-to-zone* heat flux due to the air exchange from offices to the core zones.

The operating costs (6.26) consider the gas costs for the heating coil operation and the electricity costs for operating the supply and return air fans and the evaporative cooler.

The constraints (6.27)-(6.29) ensure non-negativity of the mass flows. Inequality (6.30) constrains the heater power to be non-negative and upper bounded by a constant maximum power. Inequality (6.31) enforces that the evaporative cooler is not used without using the energy recovery. Inequality (6.32) guarantees that the total mass flow rate is within the minimum required to ensure comfort, $\dot{m}_{\text{AHU,min}}(t)$, and the maximum possible, $\dot{m}_{\text{AHU,max}}$. Inequality (6.33) finally enforces the minimum and maximum supply air temperatures $T_{\text{AHU,min}}(t)$ and $T_{\text{AHU,max}}(t)$, respectively.

EHF

Direct:

$$
q^i_{\text{Z,AHU,Dir}}(t) = \gamma^i_{\text{AHU}} \Bigg[c_{\text{air}}(v_{\text{AmbT}}(t) - x^i_{\text{Z}}(t))(u_{\text{AHU},\dot{m},\text{ERC}}(t) + u_{\text{AHU},\dot{m},\text{NoERC}}(t))
$$

$$
+ u_{\text{AHU,H}}(t)
$$

$$
+ c_{\text{air}}\eta_{\text{ERC}} \Bigg(\Bigg(\sum_{l \in \mathcal{Z}^{\text{AHU,ZToZ}}} x^l_{\text{Z}}(t) \sum_{j \in \mathcal{Z}^{\text{All}}} \gamma^l_{\text{inflow},j} \Bigg) - v_{\text{AmbT}}(t) \Bigg) u_{\text{AHU},\dot{m},\text{ERC}}(t)
$$

$$
- c_{\text{air}}\eta_{\text{ERC}}\eta_{\text{Cool}}\delta_{\text{wb}} u_{\text{AHU},\dot{m},\text{EvapC}}(t) \Bigg] \tag{6.24}
$$

Zone-to-zone:

$$
q^i_{\text{Z,AHU,ZtoZ}}(t) = c_{\text{air}}(u_{\text{AHU},\dot{m},\text{ERC}}(t) + u_{\text{AHU},\dot{m},\text{NoERC}}(t)) \sum_{j \in \mathcal{Z}^{\text{All}}} \gamma^i_{\text{inflow},j}(x^j_{\text{Z}}(t) - x^i_{\text{Z}}(t)) \tag{6.25}
$$

Operating Costs

$$
J_{\text{AHU}}(t) = f^{(.)}_{\text{ele}}(t)P_{\text{AHU,Cool}}u_{\text{AHU},\dot{m},\text{EvapC}}(t)
$$

$$
+ f^{(.)}_{\text{ele}}(t)P_{\text{AHU,Fan}}(u_{\text{AHU},\dot{m},\text{ERC}}(t) + u_{\text{AHU},\dot{m},\text{NoERC}}(t))
$$

$$
+ f^{(.)}_{\text{gas}}(t)u_{\text{AHU,H}}(t) \tag{6.26}
$$

Constraints

$$
0 \le u_{\text{AHU},\dot{m},\text{ERC}}(t) \tag{6.27}
$$

$$
0 \le u_{\text{AHU},\dot{m},\text{NoERC}}(t) \tag{6.28}
$$

$$
0 \le u_{\text{AHU},\dot{m},\text{EvapC}}(t) \tag{6.29}
$$

$$
0 \le u_{\text{AHU,H}}(t) \le Q_{\text{AHU,H,max}} \tag{6.30}
$$

$$
u_{\text{AHU},\dot{m},\text{EvapC}}(t) \le u_{\text{AHU},\dot{m},\text{ERC}}(t) \tag{6.31}
$$

$$
\dot{m}_{\text{AHU,min}}(t) \le u_{\text{AHU},\dot{m},\text{ERC}}(t) + u_{\text{AHU},\dot{m},\text{NoERC}}(t) \le \dot{m}_{\text{AHU,max}} \tag{6.32}
$$

$$
(u_{\text{AHU},\dot{m},\text{ERC}}(t) + u_{\text{AHU},\dot{m},\text{NoERC}}(t))\, T_{\text{AHU,min}}(t) \le
$$

$$
v_{\text{AmbT}}(t)(u_{\text{AHU},\dot{m},\text{ERC}}(t) + u_{\text{AHU},\dot{m},\text{NoERC}}(t))
$$

$$
+ u_{\text{AHU,H}}(t)/c_{\text{air}}
$$

$$
+ \eta_{\text{ERC}}(T_{\text{AHU,Ret}}(t) - v_{\text{AmbT}}(t))u_{\text{AHU},\dot{m},\text{ERC}}(t) \tag{6.33}
$$

$$
- \eta_{\text{ERC}}\eta_{\text{Cool}}\delta_{\text{wb}} u_{\text{AHU},\dot{m},\text{EvapC}}(t)
$$

$$
\le (u_{\text{AHU},\dot{m},\text{ERC}}(t) + u_{\text{AHU},\dot{m},\text{NoERC}}(t))\, T_{\text{AHU,max}}(t)
$$

	Zone-to-zone:	$\mathcal{Z}^{\text{AHU,ZToZ}} = \{10, 11, 12, 13, 14\}$
Applicable Zones	Direct:	$\mathcal{Z}^{\text{AHU,Dir}} = \{1\_\text{NW}, 2a\_\text{N}, 2b\_\text{N}, 2c\_\text{N}, 2d\_\text{N},$ $3\_\text{NE}, 4a\_\text{E}, 4b\_\text{E}, 5\_\text{SE}, 6\_\text{S},7\_\text{SW},$ $8a\_\text{W}, 8b\_\text{W}, 9a\_\text{L}, 9b\_\text{L}\}$

6.5.2.8 Aggregation of EHF models

Constructing the aggregated EHF model (6.3) by parameterizing and aggregating for each zone in Figure 6.6 those EHFs[11] which are applicable is a cumbersome but straightforward task. The total operating costs $J_{\text{tot}}(t)$ are simply the sum of the radiators, TABS, AHU, and lighting costs and can be easily written as a linear function of $u(t)$

$$J_{\text{tot}}(t) = J_{\text{Rad}}(t) + J_{\text{TABS}}(t) + J_{\text{AHU}}(t) + J_{\text{Light}}(t) = c^T(t)u(t). \tag{6.34}$$

Similarly, constructing $F_x(t), F_u(t), F_v(t), f(t)$ such that the constraints[12] can be written as

$$F_x(t)x(t) + F_u(t)u(t) + F_v(t)v(t) \leq f(t) \tag{6.35}$$

is straightforward.

6.5.3 Outputs

Generally, the lower the number of outputs, the fewer states are necessary in the reduced order model to reproduce a similar input-output behavior (see Section 6.5.5). Hence, we chose the outputs describing the temperatures we wanted to constrain to be area-weighted temperature averages of zones that exhibit similar behavior (and not every individual zone). In particular, since the solar radiation is the most important cause of temperature differences among zones, we grouped them according to their facade orientation. Figure 6.6 indicates the zone groups for which the averaged operative temperature outputs were defined. Hence, using the zone group definitions in Table 6.9,

$$y_{\text{AvgOpRoomT},fac}(t) = \frac{\sum_{i \in \mathcal{Z}^{fac}} a^i T^i_{\text{Op}}(t)}{\sum_{i \in \mathcal{Z}^{fac}} a^i} \qquad \forall fac \in \{\text{N, E, W, S, C}\}, \tag{6.36}$$

where the operative temperature of room i, $T^i_{\text{Op}}(t)$, was as usual approximated as the average of the room air temperature and the *mean radiant temperature*, i.e. an area-weighted average of the room's building elements' surface temperatures,

$$
\begin{aligned}
T^i_{\text{Op}}(t) = {}& 0.5 \cdot x^i_{\text{Z}}(t) \\
& + 0.5 \cdot \frac{\sum_j a^i_{\text{EW},j} x^i_{\text{EWo},j}(t) + \sum_j a^i_{\text{IW},j} x^i_{\text{IWi},j}(t) + a^i x^i_{\text{FLi}}(t) + a^i x^i_{\text{CLi}}(t) + a^i_{\text{IM}} x^i_{\text{IM}}(t)}{a^i_{\text{BE,tot}}}.
\end{aligned}
\tag{6.37}
$$

---

[11]See Equations (6.6)-(6.9), (6.4), (6.5), (6.12), (6.16), (6.17), (6.19), (6.20), (6.24), (6.25).
[12]See Equations (6.11), (6.14), (6.15), (6.18) (6.22), (6.27)-(6.33).

Table 6.9: Definition of zone groups.

Set	Contained zones	Set	Contained zones
$\mathcal{Z}^{\mathsf{N}}$	2a_N, 2b_N, 2c_N, 2d_N	$\mathcal{Z}^{\mathsf{S}}$	6_S, 7_SW, 9a_L
$\mathcal{Z}^{\mathsf{E}}$	3_NE, 4a_E, 4b_E, 5_SE	$\mathcal{Z}^{\mathsf{C}}$	9b_L, 10, 11, 12, 13
$\mathcal{Z}^{\mathsf{W}}$	1_NW, 8a_W, 8b_W, 14		

The reason for constraining the operative room temperature instead of the room air temperature was that it better approximates the temperature felt by the occupants (which depends on convective *and* radiation heat transfer), see [43].

For the computation of the time-varying operating costs and constraints parameters (see Section 6.6.2), also predictions of the AHU return air temperatures and of the average TABS core temperature were required. They were modeled as follows

$$y_{\mathsf{AHU,ReturnT}}(t) = \sum_{l \in \mathcal{Z}^{\mathsf{AHU,ZToZ}}} x_{\mathsf{Z}}^{l}(t) \sum_{j \in \mathcal{Z}^{\mathsf{All}}} \gamma_{\mathsf{inflow},j}^{l} \tag{6.38}$$

$$y_{\mathsf{TABS,Core}}(t) = \frac{\sum_{j \in \mathsf{TABS\ zones}} a_{\mathsf{TABS}}^{j} x_{\mathsf{TABS}}^{j}(t)}{a_{\mathsf{TABS,tot}}}. \tag{6.39}$$

Note that $\sum_{j \in \mathcal{Z}^{\mathsf{All}}} \gamma_{\mathsf{inflow},j}^{l}$ is the sum of the fractions (of the total AHU air mass flow) that flow into zone *l*. Since zone *l* is an air returning zone, this also is the sum of the fractions which are returned from zone *l* to the AHU. Again, it is straightforward to construct *C* such that

$$y(t) = Cx(t). \tag{6.40}$$

The AHU return air temperature and the TABS core temperature were not constrained. The constraints on the average room temperatures were computed according to Section 6.3.1

Working hours: $\quad 22 \le y_{\mathsf{AvgOpRoomT},fac}(t) \le T_{\mathsf{EN15251}}(t), \quad \forall fac \in \{\mathsf{N,E,W,S}\}$
$\quad\quad\quad\quad\quad\quad\quad 20 \le y_{\mathsf{AvgOpRoomT,C}}(t) \quad \le 30$
Otherwise: $\quad\quad 20 \le y_{\mathsf{AvgOpRoomT},fac}(t) \le 30, \quad\quad\quad \forall fac \in \{\mathsf{N,E,W,S,C}\}$

from which, trivially, y_{min} and y_{max} can be derived such that

$$y_{\mathsf{min}}(t) \le y(t) \le y_{\mathsf{max}}(t). \tag{6.41}$$

6.5.4 Discretization

Combining (6.2) with (6.3) and discretizing at a sampling time of $T_s = 0.25\,\mathsf{h}$ as in Section 4.2

resulted in the full-order discrete-time model

$$x_{k+1} = Ax_k + B_u u_k + B_v v_k + \sum_{i=1}^{n_u}(B_{vu,i}v_k + B_{xu,i}x_k)u_{k,i} \tag{6.42a}$$

$$y_k = Cx_k. \tag{6.42b}$$

The continuous-time operating costs and constraints were assumed not to change within one sampling interval (i.e. the time-varying parameters were assumed to be constant within every sampling interval). Hence, for the operating costs to represent the actual monetary or energy costs of applying u_k for a period of T_s, J_k, the total continuous-time operating costs are multiplied by T_s (converted to seconds),

$$J_k = c_k^T u_k = (3600 \cdot T_s c(t))^T u_k. \tag{6.43}$$

The discrete-time constraints,

$$F_{x,k}x_k + F_{u,k}u_k + F_{v,k}v_k \leq f_k \tag{6.44}$$

$$y_{\min,k} \leq y_k \leq y_{\max,k}, \tag{6.45}$$

are identical to (6.35) and (6.41), i.e. $F_{x,k} = F_x(t)$, $F_{u,k} = F_u(t)$, $F_{v,k} = F_v(t)$, $f_k = f(t)$, $y_{\min,k} = y_{\min}(t)$ and $y_{\max,k} = y_{\max}(t)$.

6.5.5 Model Order Reduction

Partially, the time to solve the MPC optimization problem and in particular, the performance of the state estimation depend on the number of states in the model. Recall that system (6.42) contained $n_x = 390$ states. This large number made a model order reduction, which attempts to find a lower order representation approximating the original system's input-output behavior, attractive. One possible method is the balanced truncation model reduction described for instance in [44].

In this method, a linear (invertible) state transformation, $x = Tx'$, is applied to a stable, observable, and controllable linear system,

$$x_{k+1} = A_{\text{lin}}x_k + B_{\text{lin}}u_k \tag{6.46}$$

$$y_k = C_{\text{lin}}x_k . \tag{6.47}$$

The matrix T is computed such that the resulting system's states which are "easy to reach" are at the same time "easy to observe" (hence, "balanced"). Moreover, the states are ordered such that the higher a state's index the more "difficult to reach" and "difficult to observe" it is. *Truncating* (i.e. discarding) the higher index states results in a system with similar input-output behavior (bounds on the maximum model difference can be given). We refer to [44] for a mathematically precise description and the computation of T.

To apply this method to model (6.42), it had to be linearized. We considered typical operating conditions (time-averaged values from simulations), $\bar{x}$ and $\bar{v}$, as the linearization point.

The linearized system was stable, observable, and controllable. We computed the transformation matrix T using

$$A_{\mathrm{lin}} = A \tag{6.48}$$

$$B_{\mathrm{lin}} = (B_{\mathrm{u}} + (B_{\mathrm{xu},1}\bar{x}, B_{\mathrm{xu},2}\bar{x}, \cdots, B_{\mathrm{xu},n_{\mathrm{u}}}\bar{x}) + (B_{\mathrm{vu},1}\bar{v}, B_{\mathrm{vu},2}\bar{v}, \cdots, B_{\mathrm{vu},n_{\mathrm{u}}}\bar{v}), B_{\mathrm{v}}) \tag{6.49}$$

$$C_{\mathrm{lin}} = C \ . \tag{6.50}$$

Denote the number of states in the reduced model by $n_{\tilde{x}}$. Using

$$T = \left(T_1, T_2\right), \qquad T^{-1} = \left(\begin{array}{c} (T^{-1})_1 \\ (T^{-1})_2 \end{array} \right), \tag{6.51}$$

with $T_1 \in \mathbb{R}^{n_{\mathrm{x}} \times n_{\tilde{x}}}$ and $(T^{-1})_1 \in \mathbb{R}^{n_{\tilde{x}} \times n_{\mathrm{x}}}$, the transformation and truncation of the full-order model resulting in the matrices in (6.1) can also compactly be written as

Costs:	c_k as in (6.43)	(6.52a)
Model:	$\tilde{A} = \left(T^{-1}\right)_1 A T_1, \quad \tilde{B}_{\mathrm{u}} = \left(T^{-1}\right)_1 B_{\mathrm{u}}, \quad \tilde{B}_{\mathrm{v}} = \left(T^{-1}\right)_1 B_{\mathrm{v}}$	(6.52b)
	$\tilde{B}_{\mathrm{vu},i} = \left(T^{-1}\right)_1 B_{\mathrm{vu},i}, \quad \tilde{B}_{\mathrm{xu},i} = \left(T^{-1}\right)_1 B_{\mathrm{xu},i} T_1, \quad i \in \mathbb{N}_1^{n_{\mathrm{u}}}$	(6.52c)
	$C = C T_1$	(6.52d)
Constraints:	$y_{\mathrm{min},k}, y_{\mathrm{max},k}$ as in (6.45)	(6.52e)
	$\tilde{F}_{\mathrm{x}} = F_{\mathrm{x},k} T_1$	(6.52f)
	$F_{\mathrm{u},k}, F_{\mathrm{v},k}, f_k$ as in (6.44).	(6.52g)

The number of states in the reduced model, $n_{\tilde{x}}$, was chosen such that step responses of the full- and reduced-order model coincided within less than $0.1\,^{\circ}\mathrm{C}$, resulting in $n_{\tilde{x}} = 35$. Note that since we applied the balanced model order reduction method to the bilinear system (6.42), none of the approach's theoretical results for linear systems could be applied. Nevertheless, the results turned out to be very satisfying.

6.5.6 Model Validation

To assess the prediction quality of the model, a validation experiment was conducted around Christmas 2012 (December 21-27). During December 21-25, all blinds were closed and the AHU was turned off. During December 21-23, maximum TABS heating and during December 23-25 maximum TABS cooling was applied. For the rest of the experiment, MPC control was again activated. This set up was chosen such that until December 25, the building was subject to as few disturbances as possible while after December 25 the model's performance during regular operation could be analyzed. During the experiments, the control inputs and disturbances of Table 6.4 were measured. Model (6.1b)-(6.1c) was then simulated in open-loop using the measured control inputs and disturbances. The resulting averaged zone temperature outputs were compared with the corresponding measured values.

Figure 6.8 shows the simulated and measured temperatures for the north, east, west, and south facades. The results show a good correspondence during the TABS steps, except for

the zone group south where the simulated temperatures were too high, most likely due to underestimated solar gains. Further it can be seen that the response to the TABS actuation (December 21-25) was well simulated, but under regular operation the temperatures were less well reproduced. During regular operation, errors of about $0.5\,^{\circ}\text{C}$ with peaks of up to $1\,^{\circ}\text{C}$ have to be expected when making predictions over multiple days. This finding was underlined by further similar experiments conducted during regular operation.
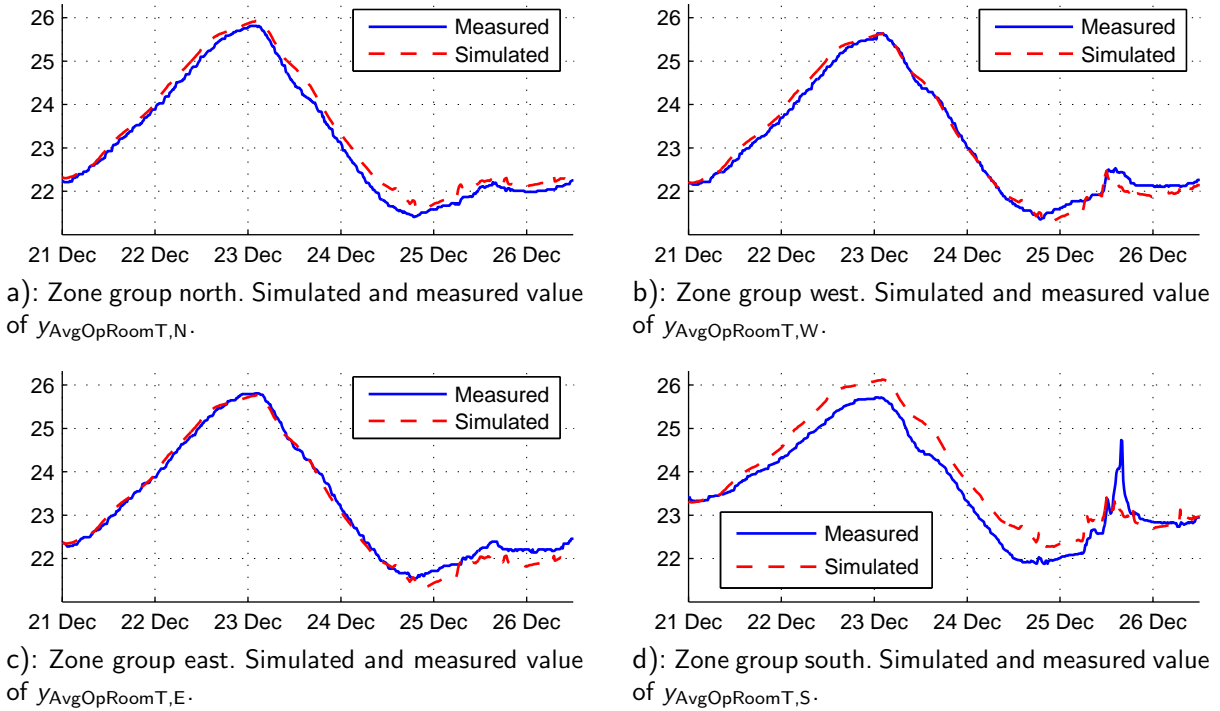

a): Zone group north. Simulated and measured value of $y_{\text{AvgOpRoomT,N}}$.

b): Zone group west. Simulated and measured value of $y_{\text{AvgOpRoomT,W}}$.

c): Zone group east. Simulated and measured value of $y_{\text{AvgOpRoomT,E}}$.

d): Zone group south. Simulated and measured value of $y_{\text{AvgOpRoomT,S}}$.

Figure 6.8: TABS experiment in December 2012.

6.5.7 Summary

In this section, we described how the model, the operating costs, and the constraints of the MPC optimization problem (6.1) were derived. We first extracted the thermal model data from an EnergyPlus model and generated the thermal model. The thermal model was then combined with the aggregated EHF model obtained by parameterizing and aggregating over all of the zones all the individual applicable EHFs. The resulting continuous-time full-order model and aggregated continuous-time operating costs and constraints were discretized with a sampling time of $T_s = 0.25\,\text{h}$ using the zero-order-hold assumption. We defined averaged operative room temperatures as model outputs and constrained them according to the temperature comfort requirements. Using the balanced truncation method, the order of the resulting discrete-time model was reduced and the MPC optimization problem (6.1) was obtained.

Note that in every iteration of the controller, the following components had to be available to completely specify (6.1). Their calculation is described in Section 6.6.2.

- The time-varying parameters in Table 6.8 for the whole prediction horizon to compute the operating costs and constraints;
- The state estimate $\hat{\tilde{x}}$;
- The disturbance predictions $V_{0 \to N}$.

Even though the BRCM toolbox was developed after the main OptiControl-2 experiments had been conducted, the modeling of the building used mostly the same algorithms as implemented in the toolbox. In fact, the identical thermal model and similar EHF models can be generated from the demonstration file made available in the BRCM toolbox installation.

6.6 Control Algorithm

In every iteration of the control, the algorithm outlined in Figure 6.9 was executed. The figure also serves as this section's outline. The steps of the control algorithm are described in the following.

6.6.1 Data Acquisition

As a first step, the current measurements listed in Table 6.2 were gathered via the OPC server. The latest (3 updates per day) available 72 h COSMO-7 forecast from MeteoSwiss of the ambient air temperature and global horizontal solar radiation (i.e. direct plus diffuse radiation on a horizontal surface) was downloaded, if not already locally available. Note that the COSMO-7 forecast did not correspond to the building's exact location, but represented an average of the closest 7 km $\times$ 7 km (hence the name) grid element of the meteorological model. If the download failed (very rarely), a persistence forecast was calculated assuming the weather of the next three days to be the same as that during the previous day.
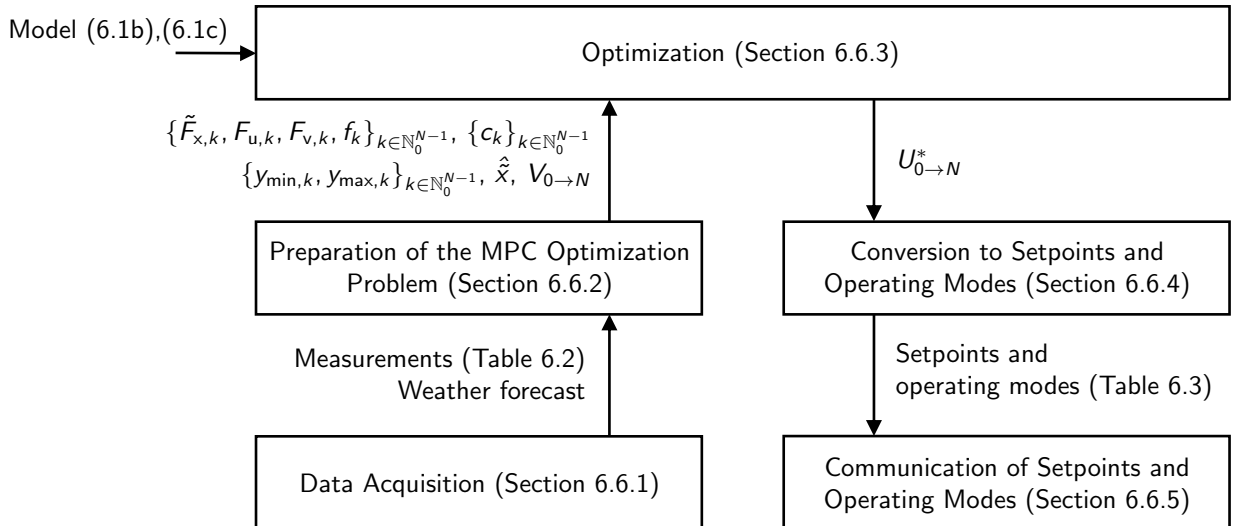

Figure 6.9: Control Algorithm.

6.6.2 Preparation of the MPC Optimization Problem

As mentioned in Section 6.5.7, the state estimate, the disturbance predictions, and the time-varying operating costs and constraints parameters must be provided to set up the MPC optimization problem (6.1). This is described in the following.

6.6.2.1 State Estimate

A standard extended Kalman filter (e.g. see [45]) was used to update the current state estimate $\hat{x}$. Its process and measurement noise covariance matrices as well as the initial estimation error covariance matrix were chosen based on physically motivated initial values and turned out to perform well for a large range of values.

6.6.2.2 Disturbance Predictions

The predictions of the disturbances in Table 6.4, $V_{0 \to N}$, were computed as follows.

The internal gains from people and equipment, $v_{IG,Off,k}$, $v_{IG,NonOff,k}$, were at first predicted based on standard schedules for office buildings and had subsequently been adjusted to measurements.

The predictions for $v_{AmbT,k}$ and $v_{Sol,\{N,E,W,S\},k}$ were based on the weather forecast. However, the COSMO-7 weather forecasts did not represent the predictions for the exact location of the controlled building. Hence, to account for local influences, we used another Kalman filter to combine the weather forecast with radiation and temperature measurements from the weather station on the building. This filter was based on an autoregressive model for the local correction coefficients. It is described in more detail in [46].

The predictions for $v_{AmbT,k}$ were directly obtained from the Kalman-filtered temperature forecast.

Computing the predictions of $v_{Sol,\{N,E,W,S\},k}$ consisted of two steps: i) the disaggregation of the Kalman-filtered global solar radiation on a horizontal surface forecast, $I_{Glob,Hor,k}$, into direct, $I_{Dir,Hor,k}$, and diffuse, $I_{Diff,Hor,k}$, components; and ii) the projection of the components onto the corresponding facades taking into account the shadowing of neighboring buildings. This is briefly outlined in the following, see [37] for a detailed description of the algorithms we employed.

The split of $I_{Glob,Hor,k}$ into $I_{Dir,Hor,k}$ and $I_{Diff,Hor,k}$ was achieved using the semi-empirical Maxwell Direct Insolation Simulation Code model [47]. To calculate the direct solar radiation on the inclined facade surfaces, $I_{Dir,\{N,E,W,S\},k}$, $I_{Dir,Hor,k}$ is projected taking into account the shadowing of neighboring buildings. For the calculation of the diffuse solar radiation on the inclined facade surfaces, $I_{Diff,\{N,E,W,S\},k}$, the simplified Perez Diffuse Irradiance model [48] was used. The global solar radiation on the facades was then simply calculated as the sum of the components

$$v_{Sol,fac,k} = I_{Dir,fac,k} + I_{Diff,fac,k} \qquad \forall fac \in \{N, E, W, S\}. \qquad (6.53)$$

This method was validated by applying it to the global horizontal solar radiation measured by the weather station and comparing its output to the corresponding north, east, west, south values also measured by the weather station. The very satisfying results are reported in Section 3.4.1 of [9].

6.6.2.3 Operating Costs and Constraints

The time-varying operating costs and constraints were constructed in every iteration of the control algorithm based on their formulation in Section 6.5. Their generation required values for the time-varying parameters in Table 6.8 over the whole prediction horizon. In this section, we describe the calculation of these parameters.

To this end, predictions of the return air temperature, $y_{\text{AHU,ReturnT}}$, and the TABS core temperature, $y_{\text{TABS,Core}}$, were required. They were obtained by shifting the optimal output trajectory calculated in the last control iteration. We denote them by $\{\bar{y}_{\text{AHU,ReturnT},k}\}_{k \in \mathbb{N}_0^{N-1}}$ and $\{\bar{y}_{\text{TABS,Core},k}\}_{k \in \mathbb{N}_0^{N-1}}$, respectively. The comfort constraints were only enforced while the building was occupied. Their description is facilitated by defining the occupancy prediction

$$\{o_k\}_{k \in \mathbb{N}_0^{N-1}}, \qquad o_k \in \{0, 1\}, \tag{6.54}$$

where $o_k = 1$ denotes occupancy and $o_k = 0$ denotes vacancy at time step k. We assumed as in Section 6.3.1 that the building was occupied during 08:00-19:00 on Mondays-Fridays (i.e. during weekends and nights it was assumed to be vacant).

Operating costs coefficients. The costs coefficients for gas and electricity, $f_{\text{gas},k}^{(.)}$, $f_{\text{ele},k}^{(.)}$, were calculated as in Table 6.1 according to the optimization objective (NRPE or monetary).

Comfort parameters. The minimum illumination, minimum AHU air mass flow, as well as the minimum and maximum supply air temperature parameters were calculated as

$$
\begin{aligned}
I_{\text{min},k} &= \begin{cases} 0 & \text{if } o_k = 0 \\ 500 & \text{otherwise} \end{cases} \\[6pt]
\dot{m}_{\text{AHU,min},k} &= \begin{cases} 0 & \text{if } o_k = 0 \\ 1.1 & \text{otherwise} \end{cases} \\[6pt]
T_{\text{AHU,min},k} &= \begin{cases} 10 & \text{if } o_k = 0 \\ 16 & \text{if } o_k = 1 \text{ and cooling season (May-August)} \\ 22 & \text{otherwise} \end{cases} \\[6pt]
T_{\text{AHU,max},k} &= \begin{cases} 35 & \text{if } o_k = 0 \\ 28 & \text{otherwise.} \end{cases}
\end{aligned}
\tag{6.55}
$$

The maximum room temperature constraint as a function of the recursively computed filtered ambient temperature, $T_{\text{Amb,Filtered},k}$, was calculated based on EN 15251 [39],

$$T_{\text{EN15251},k} = \max(25, \min(27, 21.3 + 0.33 \cdot T_{\text{Amb,Filtered},k})) \tag{6.56}$$

$$T_{\text{Amb,Filtered},k} = e^{-T_s/100} T_{\text{Amb,Filtered},k-1} + (1 - e^{-T_s/100}) v_{\text{AmbT},k}. \tag{6.57}$$

Return air temperature. The return air temperature was simply predicted by the corresponding output,

$$T_{\text{AHU,Ret},k} = \bar{y}_{\text{AHU,ReturnT},k}. \tag{6.58}$$

This notation was chosen to underline that the AHU supply air temperature constraint (6.33) in which $T_{\text{AHU,Ret},k}$ appears was linearized around $\bar{y}_{\text{AHU,ReturnT},k}$.

TABS cooling power. The maximum TABS cooling power was modeled as in [49] to be

$$Q_{\text{TABSCoolMax},k} = \frac{1}{R_{\text{TABS}}}\left(\bar{y}_{\text{TABS,Core},k} - v_{\text{AmbT},k}\right). \tag{6.59}$$

R_{TABS} was calculated based as a function of the TABS pipes' geometry and materials, see [49].

Transmitted solar radiation. The calculation of $Q_{\text{TransmSolMin},fac}$ and $Q_{\text{TransmSolMax},fac}$ required a function $f_{\text{InclToTransm}}(b_{fac,k}, I_{\text{Dir},fac,k}, I_{\text{Diff},fac,k}, P_{\text{sun},k})$ that maps the blinds position on facade fac at time k,

$$b_{fac,k} \in \{\text{Open, Shading Position 1, Shading Position 2, Closed}\}, \tag{6.60}$$

the solar irradiations on the inclined facade surface, $I_{\text{Dir},fac,k}$, $I_{\text{Diff},fac,k}$, and the sun position angles, $P_{\text{sun},k}$, to the solar heat flux transmitted through the blinds and windows. Evaluating it for every facade at the allowed maximum, $b_{\text{MaxShad},fac,k}$, and minimum, $b_{\text{MinShad},fac,k}$, shading blinds positions resulted in

$$Q_{\text{TransmSolMin},fac,k} = f_{\text{InclToTransm}}(b_{\text{MaxShad},fac,k}, I_{\text{Dir},fac,k}, I_{\text{Diff},fac,k}, P_{\text{sun},k}) \tag{6.61}$$

$$Q_{\text{TransmSolMax},fac,k} = f_{\text{InclToTransm}}(b_{\text{MinShad},fac,k}, I_{\text{Dir},fac,k}, I_{\text{Diff},fac,k}, P_{\text{sun},k}). \tag{6.62}$$

Having an EnergyPlus model at hand that performs detailed blinds and window physics simulations, such a function was found by a multivariate linear regression based on quarter hourly outputs from a year-long EnergyPlus simulation (see Section 4.3.3.4 of [9]). This dependence on EnergyPlus is discussed in Section 6.9. An alternative approach based on measuring temperature differences of rooms with and without solar irradiation is described in Section 3.4.1 of [9].

The allowed minimum and maximum shading blinds positions, $b_{\text{MinShad},fac,k}$ and $b_{\text{MaxShad},fac,k}$, were determined based on Section 6.3.1:

- The closed blinds position was only allowed if $o_k = 0$;
- Changes of blinds positions were only allowed if $o_k = 0$ or at 13:00;
- At 13:00, if measurements indicated more than 200 W/m^2 irradiation on a facade, only the high shading position Shading Position 2 was allowed for that particular facade.
- At night, blinds were opened during the cooling season (May-August) and closed otherwise[13].

---

[13]This was done to reduce / increase the insulation of the windows. This effect was not represented in the window EHF model (see Section 6.5.2.5), hence this heuristic had to be used.

6.6.3 Optimization

Given the bilinear model as well as the state estimate, the disturbance predictions, the operating costs, and the constraints prepared as in Section 6.6.2, the optimization problem (6.1) is completely specified. To avoid infeasibilities, we used soft constraints, i.e. we did not enforce the room temperature constraints strictly but heavily penalized their violation in the cost function (not shown in the MPC problem (6.1)). As described in Section 2.4, we solved the bilinear optimization problem with a sequential linear programming approach. Usually, less than five iterations were necessary. The linear programs were solved with CPLEX. The resulting optimal control input trajectory, $U^*_{0 \rightarrow N}$, was then converted to setpoints and operating modes as described in the next section.

6.6.4 Conversion to Setpoints and Operating Modes

As mentioned previously, the MPC problem (6.1) could not be formulated directly in terms of the setpoints and operating modes of Table 6.3. Hence, the first entry in $U^*_{0 \rightarrow N}$ had to be converted as follows.

Typically, all "Enable high-level control" signals except for the radiators (see below) were set to 1. The live check flag was set to 1. In the case that an operating mode of a subsystem (TABS, AHU, radiators, blinds) was set to "Off", default values for the remaining setpoints were sent (not listed below).

6.6.4.1 TABS heating

TABS heating was activated if $u^*_{\text{TABS,H},k} > 0$. The supply water temperature setpoint was computed analogously to (6.59). Note that the formulation of the TABS model in Section 6.5.2.4 ensured that $u^*_{\text{TABS,H},k} > 0$ and $u^*_{\text{TABS,C},k} > 0$ never occurred at the same time.

$$
\left.
\begin{aligned}
\text{Operating mode} &= \text{On} \\
\text{Flow temperature SP} &= y^*_{\text{TABS,Core},k} + R_{\text{TABS}}\, u^*_{\text{TABS,H},k}
\end{aligned}
\right\} \quad \text{if } u^*_{\text{TABS,H},k} > 0
$$

$$
\text{Operating mode} = \text{Off} \qquad\qquad\qquad\qquad \text{if } u^*_{\text{TABS,H},k} = 0
$$

6.6.4.2 TABS cooling

The TABS cooling settings were analogous to the heating case:

$$
\left.
\begin{aligned}
\text{Operating mode} &= \text{On} \\
\text{Flow temperature SP} &= y^*_{\text{TABS,Core},k} - R_{\text{TABS}}\, u^*_{\text{TABS,C},k}
\end{aligned}
\right\} \quad \text{if } u^*_{\text{TABS,C},k} > 0
$$

$$
\text{Operating mode} = \text{Off} \qquad\qquad\qquad\qquad \text{if } u^*_{\text{TABS,C},k} = 0
$$

6.6.4.3 AHU

In the case of a non-zero total mass flow rate $u^*_{\text{AHU,}\dot{m}\text{,ERC},k} + u^*_{\text{AHU,}\dot{m}\text{,NoERC},k}$, the desired supply

air temperature, T_{sup}^{*}, could be calculated as follows (see Section 6.5.2.7)

$$T_{\mathrm{sup}}^{*} = v_{\mathrm{AmbT},k}$$

$$+ \frac{u_{\mathrm{AHU,HCoil},k}^{*}/c_{\mathrm{air}} + \eta_{\mathrm{ERC}}(y_{\mathrm{AHU,Ret},k}^{*} - v_{\mathrm{AmbT},k})u_{\mathrm{AHU},\dot{m},\mathrm{ERC},k}^{*}}{u_{\mathrm{AHU},\dot{m},\mathrm{ERC},k}^{*} + u_{\mathrm{AHU},\dot{m},\mathrm{NoERC},k}^{*}}$$

$$- \frac{\eta_{\mathrm{ERC}}\eta_{\mathrm{Cool}}\delta_{\mathrm{wb}}u_{\mathrm{AHU},\dot{m},\mathrm{EvapC},k}^{*}}{u_{\mathrm{AHU},\dot{m},\mathrm{ERC},k}^{*} + u_{\mathrm{AHU},\dot{m},\mathrm{NoERC},k}^{*}}.$$

Using air flow measurements, we constructed look-up tables, $f_{\mathrm{P,Sup}}$ and $f_{\mathrm{P,Ret}}$ that converted the desired air mass flow rate to a differential pressure setpoint for the supply and exhaust fans,

$$\Delta P_{\mathrm{Sup}}^{*} = f_{\mathrm{P,Sup}}(u_{\mathrm{AHU},\dot{m},\mathrm{ERC},k}^{*} + u_{\mathrm{AHU},\dot{m},\mathrm{NoERC},k}^{*}) \tag{6.63}$$

$$\Delta P_{\mathrm{Ret}}^{*} = f_{\mathrm{P,Ret}}(u_{\mathrm{AHU},\dot{m},\mathrm{ERC},k}^{*} + u_{\mathrm{AHU},\dot{m},\mathrm{NoERC},k}^{*}). \tag{6.64}$$

Finally, the AHU settings were as follows

$$\left.\begin{array}{ll}
\text{Operating mode} & = \text{On} \\
\text{Supply air temperature SP heating} & = T_{\mathrm{sup}}^{*} \\
\text{Supply air temperature SP cooling} & = T_{\mathrm{sup}}^{*} \\
\text{Supply air temperature SP ERC} & = T_{\mathrm{sup}}^{*} \\
\text{Differential pressure SP supply} & = \Delta P_{\mathrm{Sup}}^{*} \\
\text{Differential pressure SP return} & = \Delta P_{\mathrm{Ret}}^{*}
\end{array}\right\} \text{ if } u_{\mathrm{AHU},\dot{m},\mathrm{ERC},k}^{*} + u_{\mathrm{AHU},\dot{m},\mathrm{NoERC},k}^{*} > 0$$

$$\text{Operating mode} \qquad\qquad = \text{Off} \qquad \text{ if } u_{\mathrm{AHU},\dot{m},\mathrm{ERC},k}^{*} + u_{\mathrm{AHU},\dot{m},\mathrm{NoERC},k}^{*} = 0.$$

6.6.4.4 Blinds

Blinds commands were only sent at the blinds command times 07:00, 13:00, or 20:00. In case an occupant locally set a different blinds position in his office, this ensured that it was not immediately overwritten again.

At the blinds command times 07:00 and 13:00, that blinds position was chosen from the allowed set, $\mathbb{B}_{fac}$, (defined by $b_{\mathrm{MinShad},fac,k}$, $b_{\mathrm{MaxShad},fac,k}$, and intermediate positions, see Section 6.6.2.3) that matched best the integrated heat flux over the next fixed period (i.e. 07:00-13:00 or 13:00-20:00), whose last step we denote by N_{s}, i.e.

$$b_{fac}^{*} = \arg\min_{b_{fac} \in \mathbb{B}_{fac}} \sum_{k=0}^{N_{\mathrm{s}}} u_{\mathrm{TransmSolar},fac,k}^{*} - f_{\mathrm{InclToTransm}}(b_{fac}, I_{\mathrm{Dir},fac,k}, I_{\mathrm{Diff},fac,k}, P_{\mathrm{sun},k}). \tag{6.65}$$

At 20:00, we set for all facades $b_{fac}^{*} = \text{Open}$ in cooling periods (May-August) while otherwise $b_{fac}^{*} = \text{Closed}$. Then, by example of the north facade, in the case of $b_{\mathrm{N}}^{*} = \text{Open}$, the command "Open North" was sent with value 1 while "Shading Position 1 North", "Shading Position 2 North", and "Close North" were sent with value 0.

6.6.4.5 Radiators

Since the radiators are locally controlled to a room air temperature setpoint which could not be influenced by the MPC[14], it was decided to simply keep the LL control in charge of the overall supply water temperature. Hence, "Enable high-level control" was set to 0 during all MPC experiments.

6.6.5 Communication of Setpoints and Operating Modes

Finally, the Matlab OPC toolbox was used to interface the OPC server on the (same) industry PC. The OPC server sent the setpoints and operating modes via the BACNet protocol to the LL control.

6.7 Experimental and Simulation Results

To assess the performance of the MPC strategy, two approaches were taken. Long-term experiments were used to demonstrate the feasibility, comfort satisfaction, and soundness of the control actions. This is described in Section 6.7.1. However, the sequential nature of on-site experiments and the varying operating conditions make the experimental comparison of controllers in terms of energy efficiency difficult. Therefore, for more rigorous comparative controller assessment, we also employed whole-year simulations based on an EnergyPlus model of the building's second floor. These results are reported in Section 6.7.2.

6.7.1 Experiments

The experimental setup was operational from October 7th, 2011 until April 2nd, 2013. Before and after, the pre-installed control strategy RBC-0 was active. During the experimental period, several controllers were tested. Here we report on the MPC experiments only.

The MPC controlled the building during three intervals: i) a 14-week cooling season period (CS) from May 1 to August 7, 2012; ii) a six-week heating season period (HS-1) from November 10 to December 22, 2012; iii) a nine-week heating season period (HS-2) from December 27, 2012 to March 1, 2013. During all of the experiments shown here, the MPC was optimizing NRPE usage except from February 05-14, 2013 during which a load shifting experiment with an artificial time-varying electricity price took place (see Section 6.7.1.1).

Figures 6.10a, 6.10b, 6.10c show for each of the periods: i) the ambient temperature; ii) the average and the individual room temperatures of the second floor (which was the most thoroughly equipped with sensors and meters) together with the room temperature comfort constraints; and iii) the cumulative comfort violations, respectively. Thermal comfort was assessed in terms of the time-integral of room temperature comfort range violations, measured in Kelvin-hours (Kh). Lower bound comfort violations in cold periods were only counted when the window contacts indicated closed windows. The measured AHU supply air temperature and mass flow rate (not shown) indicated that the respective constraints were satisfied. The blinds movement restrictions were satisfied by design. Visual comfort could not

---

[14]In other words, even with "Enable high-level control" set to 1 the LL radiator control was still actively controlling the room temperature to a setpoint.

be assessed via measurements, however the occupants were at all times able to set the blinds in their office to any desired position. For detailed energy consumption data during the MPC experiments we refer to Section 5.2.2 of [9].

In the CS period, the controller managed to keep the average room temperature within the prescribed comfort range except for one day around the end of June when temperatures were high enough to overwhelm the cooling capability of the system (MPC had operated the cooling for several days at maximum capacity up to this date). Several downward spikes due to the opening of windows can be observed. Maximum cumulative violations amounted to an acceptable[15] level of 10 Kh in 14 weeks or 37 Kh/a (Kelvin-hours per year).

In the HS-1 and HS-2 periods, the MPC controlled the building as expected at the lower constraint. The daily peaks above 22 °C were due to internal and solar gains. Maximum cumulative violations amounted to an again reasonable level of 10 Kh and 17 Kh or 86 Kh/a and 98 Kh/a, respectively.

A more qualitative assessment of thermal comfort was possible due to the feedback from the facility manager who was in direct contact with the occupants. Apart from the need for an adjustment of the minimum allowed supply air temperature, no issues were reported. Throughout all experiments, the controller was found to operate smoothly and the fallback strategy was never activated. The facility manager's response to a questionnaire showed that he was also very satisfied with the control system's overall performance.

6.7.1.1 Load Shifting

In this section, we evaluate in detail the experimental period February 05 - 14, 2013 in which we investigated the effect of time-varying electricity price signals. Simple time-varying electricity prices such as day / night tariffs have been used for a long time to incentivize the shift of electricity usage from high- to low-price periods. Recently, with the accelerating integration of renewable energy sources, the need for such *demand-side participation* is increasing. However, more complex price signals have basically not been introduced at the consumer level because of implementation difficulties. In particular in buildings, current RBC strategies have no means of systematically integrating a complex electricity price signal. MPC on the other hand is well suited for taking into account energy price predictions. This section is not intended to be a full analysis of this capability, but aims to illustrate it by means of an experimental study. All of the experimental data shown in this section are part of the heating season experiments shown in Figures 6.10b and 6.10c.

We compared the operation of the MPC during a period with an artificial time-varying electricity price (known to the MPC ahead of time) to its baseline operation with constant electricity costs[16]. In order for the electricity price signal to have a significant effect, we assumed during this period that the primary heat supply was a heat pump with a coefficient of performance of 4 instead of a gas boiler. Note that with this assumption all the contributions to the operating costs were electrical. To analyse the shifted load, we computed for each hour of the day the TABS and AHU heating power averaged over all days of a period. Two periods were considered:

---

[15]In [50] acceptable annual violations were defined to be around 70 Kh/a.
[16]Recall that baseline operation was to minimize NRPE with a constant electrical energy to NRPE conversion coefficient.
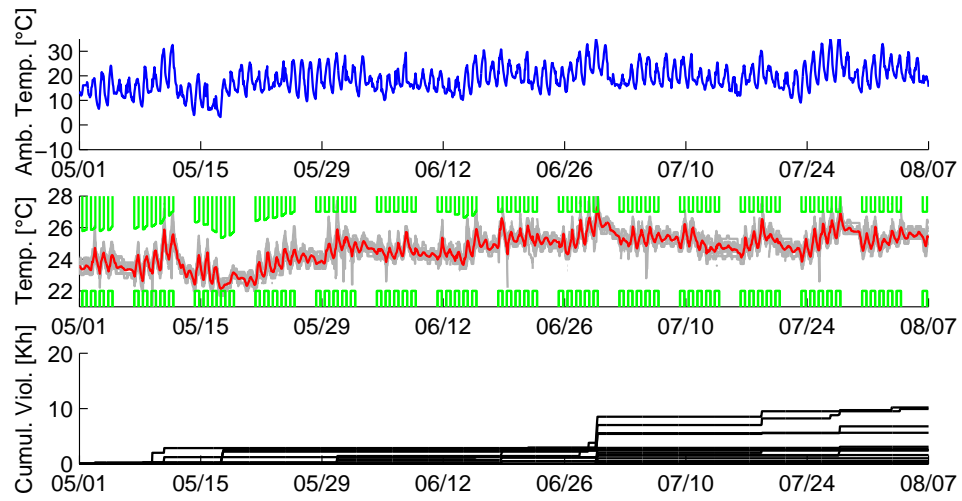
a): May 1 to August 7, 2012.
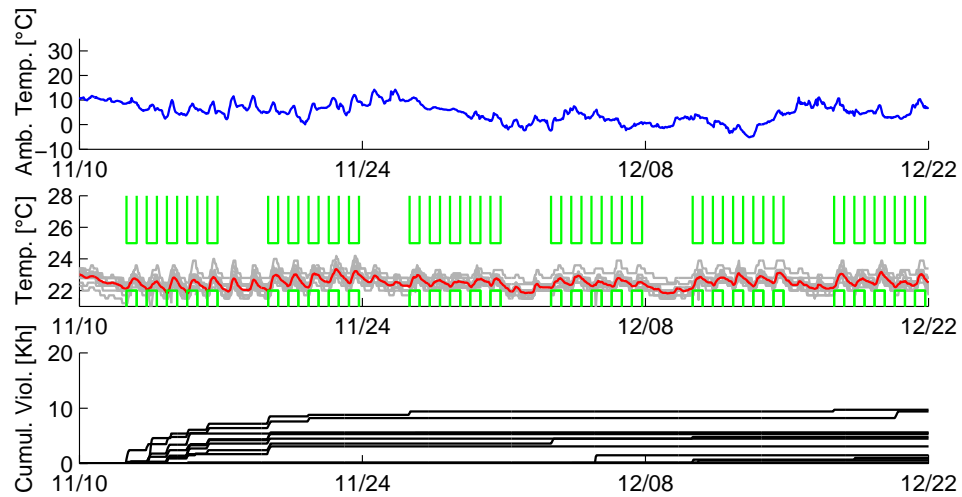
b): November 10 to December 22, 2012.
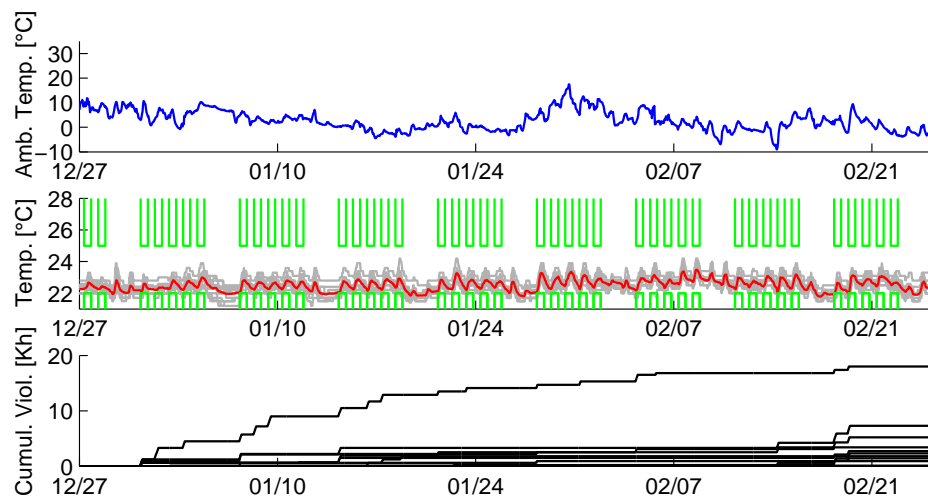
c): December 27, 2012 to March 1, 2013.

Figure 6.10: Experimental MPC results during three periods. Top plots: Ambient temperature. Middle plots: Average (red) and individual (grey) room temperatures and comfort bounds enforced from 08:00-19:00 during workdays (green). Bottom plots: Cumulative comfort violations for each room.

- **Period 1: Constant electricity price.** Since the MPC optimized NRPE, constant costs were associated with the consumption of electricity in the two heating season periods November 10 to December 12, 2012 and from December 27 to February 28, 2013 with the exception of Period 2 (see below). In Figure 6.11a, the hourly average heating power of the TABS and the AHU are depicted for this period.
- **Period 2: Time-varying electricity price.** A time-varying price signal (known to the MPC ahead of time) was applied from February 5 to February 14, 2013. The price pattern was repeated every day and consisted of two high-price times from 1:30 to 4:00 and from 6:30 to 21:00 and low-price times otherwise. The ratio of high- to low-price level was 3. The price pattern was chosen to achieve a large shifting of power consumption compared to the case of a constant price signal. In Figure 6.11b, the hourly average heating power of TABS and AHU are depicted for this period. Additionally, the time-varying price signal is indicated qualitatively.

Comparing Figures 6.11a and 6.11b, a clear shifting of most of the TABS heating power to low-price hours can be observed. The AHU heating power during high-price times could not be shifted, because otherwise the minimum supply air temperature constraint would have been violated. Note that the two experiments were carried out under different weather conditions and that the durations of the experiments were different. Since Period 1 and 2 were included in the data shown in Figures 6.10b and 6.10c, comfort satisfaction was similar and satisfying.

Figures 6.11a and 6.11b demonstrate that in similar office buildings controlled by MPC load shifting is feasible. This holds particularly if slow actuators such as TABS are available that allow a pre-heating of the building. Note that the price signal in Period 2 was constructed such that a maximum load shifting took place. Moreover, note that not all load at all times could be shifted and that a building can only have a significant electrical load shifting effect on the grid if most of its power consumption is electrical, i.e. the demonstrator building would only have a very small effect in reality.

6.7.2 Simulations

To assess the MPC's energy savings compared to the baseline control strategy RBC-0, we performed whole year simulations for both, RBC-0 and MPC, using a detailed and validated EnergyPlus model developed by the building simulation experts from Gruner-Roschi as the simulation model. Matlab (used for control calculations) and EnergyPlus (used for building simulation) were coupled with the aid of the Building Controls Virtual Test Bed (BCVTB) software. Details on the EnergyPlus model and the simulation environment are reported in [41] and Section 3.2 of [9]. In the simulations, MPC minimized NRPE. We used weather data recorded in Basel in 2010 and corresponding MeteoSwiss weather predictions.

Figures 6.12a and 6.12b show the simulation results in terms of energy and comfort. The left and right bars of the bar pairs correspond to the RBC-0 and the MPC strategy, respectively. Figure 6.12a shows in the left plot the annual and in the right plot the monthly NRPE energy consumption by load type for the simulated 2nd floor. Table 6.10 summarizes the operating costs for HVAC, lighting, and equipment, the latter two accounting for a significant part of the overall energy consumption. The MPC operation resulted in 16.6 % less NRPE energy compared to RBC-0, corresponding to annual absolute NRPE savings[17] for the 2nd floor

---

[17]The corresponding numbers for delivered energy usage, i.e. the energy amount unweighted by the NRPE factors, (not shown in the plots) were 25 %, 13.9 MWh/a, 26 kWh/(m^{2}a), respectively.
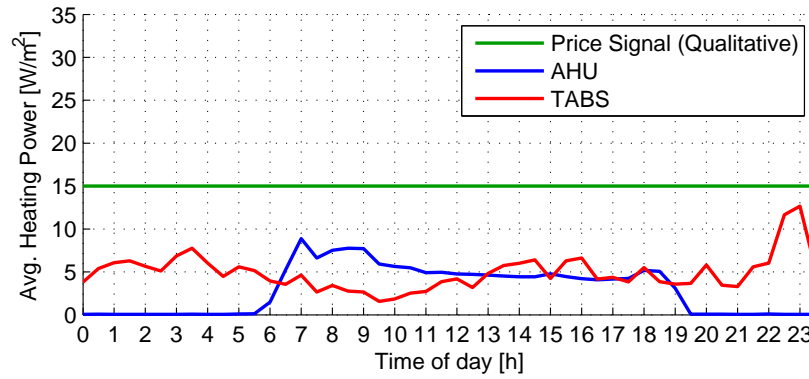
a): Period 1: Constant electricity price. Average heating power over 76 days.
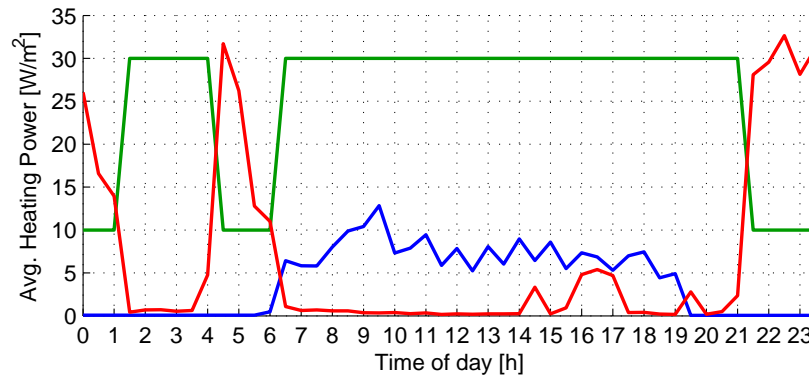
b): Period 2: Time-varying electricity price. Average heating power over 10 days.

Figure 6.11: Average heating power in [W/m²] of TABS (red) and AHU (blue) based on a time-varying price signal (shown qualitatively in green).

of 22 MWh/a or 40.4 kWh/(m²a). The corresponding numbers for monetary costs savings (not shown in the plots) were 16.9 %, 1'119 CHF/a and 2.1 CHF/(m²a), respectively. Most of the MPC's savings come from reduced lighting and substituting TABS with ventilation heating. The former is achieved when setting the blinds by considering the lighting costs that are necessary to satisfy the minimum illumination constraint. Using primarily the ventilation instead of the TABS heating allows a delayed start of the heating in the morning. Moreover, the MPC strategy allows an operation closer to the temperature constraints which is difficult in the case of the non-predictive RBC-0 strategy due to the slow building dynamics. MPC has somewhat higher cooling costs which are necessary to satisfy comfort in the cooling season. RBC-0 often fails to do so (see below) since it is not predictive but the main cooling has to take place during the night (cooling tower).

Table 6.10: Simulated annual total NRPE and monetary costs for RBC-0 and MPC. The costs include HVAC, lighting and equipment for the 2nd floor.

Controller	NRPE			Monetary		
	Relative [%]	Abs. (2nd floor) [MWh/a]	Specific [kWh/(m²a)]	Relative [%]	Abs. (2nd floor) [CHF/a]	Specific [CHF/(m²a)]
RBC-0	100	130	243	100	6'625	12.4
MPC	83.4	108	203	83.1	5'506	10.3
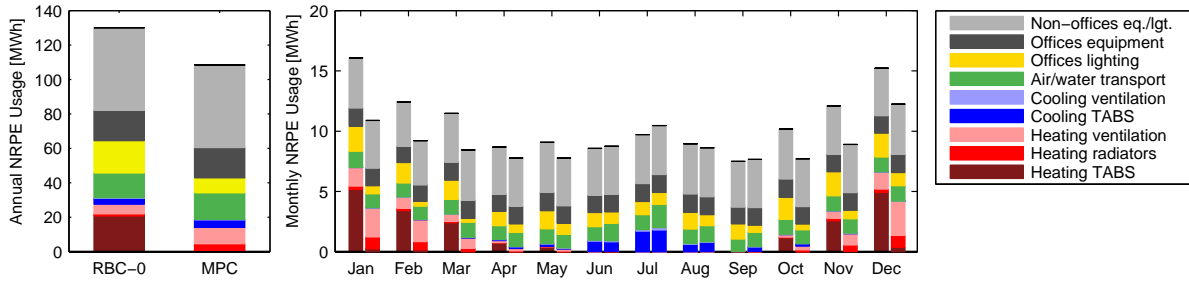
a): Simulation results: Energy. Left plot: annual. Right plot: monthly.
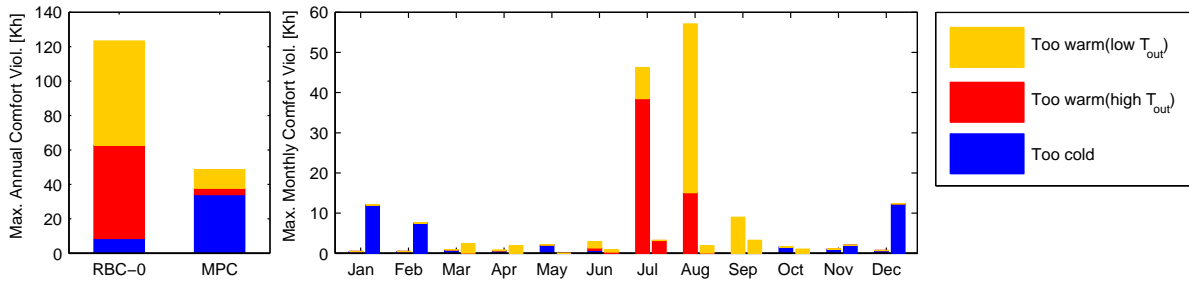
b): Simulation results: Comfort. Violations of the upper bound during warm ('Too warm (high out T)') and cold periods ('Too warm (low out T)') are distinguished to indicate when the violation could have been alleviated by opening the windows. Left plot: Maximum annual comfort violations (i.e. maximum over all zones of the annual sum of each of the three violation types). Right plot: Maximum monthly violations.

Figure 6.12: Simulation results for the second floor. Comparisons of RBC-0 (left bar of the bar pairs) and MPC (right bar).

Figure 6.12b shows the comfort violations in Kelvin-hours of the room with the most violations on an annual (left plot) and on a monthly (right plot) basis. We distinguish violations of the lower bound ('Too cold') and of the upper bound during warm ('Too warm (high T_{out})') and cold periods ('Too warm (low T_{out})') to indicate when the violation could have been alleviated by opening the windows.

Most of the savings were realized in the heating period. During the summer months, MPC used slightly more control energy but provided significantly improved thermal comfort. Even though the MPC control resulted in an increase in lower bound violations, overall comfort was improved.

6.7.2.1 Advanced RBC Results

In the context of the OptiControl-II project, the Siemens engineers developed and tested four advanced predictive RBC strategies. They all represented improved versions of the RBC-0 algorithm, ranging in complexity from simply an integrated and better tuned version of RBC-0 (called RBC-1) to an RBC / MPC hybrid strategy (called RBC-4). Since the development of the RBC strategies was not part of this thesis, we refer for a description of the algorithms as well as of their detailed simulation and experimental results to the project report [9]. Here, we simply present in Table 6.11 the results of the same simulation comparisons as were performed for MPC in order to show that there exist next to MPC also alternative improvements of the baseline building control strategy. Generally, the RBC algorithms are less complex than the MPC strategy but also result in somewhat lower energy savings. A detailed discussion of all strategies' benefits and costs is also provided in [9].

Table 6.11: Simulated annual total NRPE and monetary costs for RBC-0, RBC-1, RBC-2, RBC-3, and RBC-4. The costs include HVAC, lighting, and equipment for the 2nd floor.

Controller	NRPE			Monetary		
	Relative [%]	Abs. (2nd floor) [MWh/a]	Specific [kWh/(m²a)]	Relative [%]	Abs. (2nd floor) [CHF/a]	Specific [CHF/(m²a)]
RBC-0	100	130	243	100	6'625	12.4
RBC-1	88	114	214	87.6	5'804	10.86
RBC-2	86.7	113	211	85.8	5'686	10.64
RBC-3	88.5	115	215	88.6	5'873	10.99
RBC-4	85.9	112	209	85.6	5'674	10.62

6.8 Cost / Benefit Analysis

In mid-sized to large non-residential buildings, typically custom control systems are set up. Their application consists of several steps: the definition of the requirements, the choice and design of the control system, its implementation and commissioning (i.e. checking and testing), and its possible adaptation to changing requirements throughout the building's life cycle. From this, it is clear that although good control performance in terms of energy usage and occupant comfort is essential, the value of a control strategy also depends on the inherent effort of these steps. This is often neglected in the academic literature. This section gives a condensed version of the cost / benefit analysis reported in Section 7 of [9], which is backed by the practical experience of the Siemens team. Here we comment solely on cost / benefit *differences* of MPC when compared to an industry-standard control strategy such as RBC-0. The main goal is to point out which we, according to our experience, think are the current major obstacles for a wide-spread adoption of building MPC.

This section will show that MPC can be expected to have an improved performance (Section 6.8.1) at the expense of higher installation costs (Section 6.8.3). Since the technology still has to be developed to a product level, significant development costs also arise (Section 6.8.2). Maintenance and data costs are somewhat higher as well (Section 6.8.4).

6.8.1 Control Performance

The assessment of the achievable control performance in terms of energy and monetary costs is based on the simulation results of Section 6.7.2 while comfort-wise the assessment is also based on the experimental evidence.

The simulated savings reported in Section 6.7.2 for the second floor translate for all five upper (office) floors into 5'590 CHF/a. These values have been obtained using 2012 energy prices.

The MPC strategy achieved a good thermal comfort level in simulation and experiments. Air quality comfort was considered by enforcing a minimum supply air flow rate according to standards. Blinds movements were for both control strategies restricted by design to the desired behavior. A further analysis (not shown) of the simulations indicated comparable visual comfort levels of RBC-0 and MPC.

6.8.2 Development Costs

Here, we define the development costs for a new control strategy as the effort required by a building automation company to develop the control strategy to a product level and build the engineering expertise required to routinely apply it. To develop building MPC to this point, a significant effort is necessary that can mainly be attributed to the following points.

6.8.2.1 Control Framework

A product level MPC software framework needs to be developed from scratch, including a solver for the (moderately sized) linear programs. However, given a high-level / low-level control abstraction as used in the this study, the development of such a framework and its integration into existing building automation systems appears to be rather straightforward.

6.8.2.2 Model Generation Framework

The construction of the building model is central in the control design. Without appropriate tools, the necessary modeling effort most likely could not be justified by cost savings in the order of the ones reported in Section 6.8.1. Therefore, we believe that a framework allowing the fast generation of MPC suitable models is a key factor to the widespread adoption of MPC in building control.

6.8.2.3 Training

Since experience with MPC is currently very limited within the building industry, significant costs are related to the training of the engineering, commissioning and service personnel if it were to be included in the portfolio of an existing building automation company.

6.8.3 Installation Costs

Here, we consider the installation costs that would arise per building if a completely developed MPC framework as defined in Section 6.8.2 was available. Installation costs arise during the engineering (design of the control) and commissioning (tuning of the control) phases. Here, we consider the case of a typically (i.e. sparsely) instrumented building such as the OptiControl-II target building. In particular, we assume that: i) the control of the HVAC system is completely integrated, i.e. all HVAC actuators can be centrally accessed; ii) blinds control is *not* integrated; iii) ambient temperature but no solar radiation sensors are available. In the following, we distinguish costs for hardware installation and for software configuration.

6.8.3.1 Hardware Installation

The proposed setup with MPC as a high-level control requires at least the installation of: i) a dedicated high-level control device (e.g. industry PC[18]); ii) blinds control integration; iii) one room temperature sensor per facade and core facilities; iv) solar radiation sensors. Optional additional installations include presence detectors and electricity meters that can be used to

---

[18]Alternatively, the computation could also be performed in the "cloud", i.e. on a server hosted by a building automation company. Given a sufficient number of buildings having such a setup, this likely would lower the hardware costs compared to the here proposed local configuration. Other benefits include enabling the fast support by the company's experts and easy software updates.

Table 6.12: Additional hardware costs if instead of RBC the proposed MPC control was installed on a similar building.

Component	Costs
Industry PC	600-2'500 CHF
Blinds control integration	3'000 CHF
Room temperature sensors	1'200 CHF
Solar radiation sensors	400 CHF

improve internal gains predictions, TABS heat / cold meters to improve heat flux estimates, as well as further room temperature and window contact sensors.

For cases similar to the building studied here, the estimated additional hardware installation costs[19] are given in Table 6.12. The shown figures reflect the estimated lower limit of the investment costs required to implement MPC. In particular, the costs of optional measurements are not taken into account.

6.8.3.2 Software Configuration

When setting up a building MPC, the two main software related tasks are the modeling of the building and the setting up of the high-level control. Given the model and a control framework that only needs to be parameterized (model, interface, settings) to a certain building, the engineering and commissioning effort of the latter can be expected to be moderate and potentially even lower than for industry-standard control systems that may require difficult tuning.

Even given a modeling framework, the necessary engineering effort for constructing a model still remains the largest unknown factor on the cost side because it heavily depends on the realization of the framework and on the model accuracy required by the MPC. Without such control and modeling frameworks, the resulting per-case engineering effort will be prohibitive for a widespread commercial application.

6.8.4 Maintenance and Data Costs

Maintenance and data costs arise due to the need for equipment servicing, troubleshooting, and the procurement of weather forecast data from a meteorological service. According to our experience, servicing and troubleshooting costs for MPC should be comparable to the ones for industry-standard control systems. Our MPC controller requires two types of weather data: outside air temperature and global radiation on a horizontal surface. Today, typical fees for state-of-the-art weather forecasts by a meteorological service amount to 100-600 CHF per site, per year, and per meteorological variable. It can be expected that in future, fees will be lower.

---

[19]These include costs for sensors, wiring, and input / output modules as well as labor costs and depend to a large extent on the project size.

6.9 Discussion

In the following, we first discuss choices related to the setup of the MPC and second the economic aspects based on the cost / benefit analysis.

6.9.1 Technical Aspects

Two key design choices regarding the setup of the MPC have been made: i) implementing MPC as a high-level supervisory control; and ii) modeling the building using a physics-based approach.

An alternative to i) would be to implement MPC in the low-level control in order to save the expenses for a dedicated high-level control PC. However, this comes with several disadvantages such as individual programming, need for communication to achieve integrated control, a lack of computational power, and usually no access to weather forecasts. We believe that the additional expense for a dedicated high-level control device is greatly outweighed by its advantages.

The standard alternative to ii) is to model the building using identification methods. The most prominent downside of these approaches is the fact that due to time and building usage constraints, the effort of identifying detailed models may well be prohibitive or, due to limited excitation, even impossible in practice. In particular for the building studied here, identification experiments would have been only possible on weekends. Since the time-constant of the TABS is in the order of days, the identification of this aspect alone would have been difficult. The major downside with physics-based modeling is that geometry, construction, and building systems data are often not completely available and have to be estimated which requires expert know-how. Nevertheless, in particular for buildings exhibiting slow dynamics, we suggest the use of physics-based models, possibly together with an online adaptation of a few parameters related to the faster dynamics of the model.

In the development of the MPC model, we used the EnergyPlus model for a) parameter tuning (see parameters with source "EP simulations" in Table 6.6), and b) identifying a regression model for computing the transmitted solar radiation as a function of the incident solar radiation and the blinds position (see Section 6.6.2). If an EnergyPlus model of a given building is available, it certainly is useful to improve the MPC model as was done in this study. If however no detailed building simulation software model is at hand (which is likely), a) and b) need to be addressed. We believe that this dependence can be dropped with reasonable effort: Regarding a), the parameters identified from the EnergyPlus simulations have physical meanings such that reasonable values can be estimated and potentially be refined by measurements during online operation. As for b), the coefficients lie within 0 and 1 and can be approximated using standard window properties and estimates of the blinds' influence. Alternatively, they can be identified based on measuring temperature differences of rooms with and without solar irradiation as described in Section 3.4.1 of [9].

6.9.2 Economic Aspects

MPC is expected to have an improved performance (i.e. lower operating costs at a similar comfort level) but higher investment costs (i.e. engineering and commissioning of the software

and installation of additional hardware). Central to the success of MPC as a commercial product is the question whether customers are willing to pay for the higher investment costs of the control solution in return for lower operating costs. Unfortunately, investment and operating costs are usually paid by different entities, namely by the owner or the general contractor and the tenant, respectively. Other factors influencing the customer's decision are the user acceptance of MPC on the facility management side but also its innovativeness and "greenness" as a selling argument.

For cases similar to ours, net operating costs savings likely are in the order of 5'000 CHF/a. This figure was computed by subtracting the additional maintenance and data costs from the simulated energy savings for all floors. Under the assumption of a low-instrumented building, minimum additional installation costs are in the range of 3'000-6'000 CHF, the lower range corresponding to a case in which the blinds control is already integrated. The largest uncertainty on the cost side lies in the engineering effort. The availability of an efficient modeling framework may well become the decisive factor whether building MPC makes economic sense as a product. Note that even with a modeling framework, expert knowledge will still be required to handle issues such as missing construction data. Commissioning effort can be expected to be similar or lower than for industry-standard control strategies due to less parameter tuning.

The BRCM toolbox (see Chapter 4) was developed as a first step towards such a modeling framework. Given the experience from the OptiControl-II project, we believe that the toolbox is suitable for generating sufficiently accurate models for MPC controllers.

For several reasons, we expect the operating costs savings to increase with time. First, energy prices will likely increase in the future. Second, due the expected increase in the use of renewable energy sources, future energy prices are likely to show larger time-variations which can be exploited by MPC. Third, weather forecasts are expected to become cheaper and finally, advanced building climate control can improve the monitoring of the building system due to a usually increased number of sensors. This facilitates the detection of misconfigurations, which are commonly regarded as a reason for significant energy-efficiency reductions. Also, note that in the present study, the number of actuators was very small. The savings can be expected to be larger when room temperatures can be influenced on a more individual basis.

6.10 Conclusion

Our experiments have shown that an MPC strategy can successfully control the TABS, ventilation and blinds of a typical Swiss office building to the complete satisfaction of the building owner, the facility manager, and the occupants. The implementation of MPC as a high-level supervisory control was demonstrated to be a most promising approach for integrated HVAC control.

Simulations using the EnergyPlus software showed that the MPC's simulated energy savings for HVAC, lighting, and equipment were around 17 % of the simulated energy use under industry-standard rule-based control while providing an improved level of comfort. Subtracting annual costs for weather data, this corresponded to monetary savings of around 5'000 CHF per year for all floors.

Nevertheless, for similar buildings as ours, given present-day energy prices, and with the tools currently available, the required effort for model development and engineering appears

to be too high to justify the deployment of MPC in everyday building projects on the basis of operating costs savings alone. However, significant development investments in a model predictive building automation framework, a modeling tool, and the training of engineers together with the increasing importance of demand response and rising energy prices may push the technology into the net benefit range.

Part IV

Importance of Occupancy Information

Chapter 7

Importance of Occupancy Information for Building Climate Control

7.1 Introduction

One of the most important influences on the thermal behavior of buildings originates from its occupants, both in terms of the heat gains and of the constraints describing the occupants' comfort requirements. Today, occupancy information is used only in form of standard occupancy *schedules*[1] in building climate control, often in addition with instantaneous adjustments of lighting, sometimes in addition with instantaneous adjustment of both lighting and ventilation based on occupancy sensor measurements. The question arises whether the use of occupancy *predictions* has a significant energy savings potential.

In [51], the authors showed that significant energy savings can be achieved by employing a nighttime-setback strategy, i.e. the relaxation of comfort constraints during the night. This gives rise to the hypothesis that information about *long-term* vacancies in the range of days (business trips, holidays, illnesses) also provides an energy savings potential. This work aims at quantifying the savings potential of such long-term occupancy/vacancy information by means of closed-loop simulations with MPC. Such a setting allows the consistent incorporation of occupancy information in the control in form of comfort constraints and internal gains predictions. This facilitates the comparison of different types of occupancy information and results in a close-to-optimal control of the building for a given occupancy prediction assuming a perfect model and having a sufficiently long prediction horizon.

7.1.1 Use of Occupancy Information for Building Automation

As some of the first dealing with occupancy information for building automation, the authors in [52] tried to estimate the benefit of occupancy sensor based lighting control. The same question was addressed in [53] where a more detailed occupancy-based control coupled with an ESP-r simulation was considered. In [54] a learned pattern recognition algorithm was using multi-sensor data to identify how long occupants are typically staying in a room. If this expected period was long enough, the HVAC control would start to bring the room temperature to a certain comfort level while otherwise the room would stay at its setback temperature.

All these works focused on exploiting short-term (in the range of minutes) occupancy information for increasing energy efficiency in buildings. To the best of our knowledge, the influence of long-term (in the range of days) occupancy information on the building energy consumption has not yet been investigated systematically.

---

[1]Typically, occupancy is assumed during working hours on Mondays-Fridays and vacancy otherwise.

7.1.2 Occupancy Models in the Literature

Since occupancy is of stochastic nature, in this study the average energy use of a control taking into account occupancy information was evaluated by means of a Monte Carlo study. In order to generate random sequences of occupancy and vacancy days, a suitable model had to be found. There exist several works on modeling occupancy in the literature, some of which are summarized in the following.

The authors of [23] and [55] were interested in modeling occupancy to fuse sensor data with model predictions of a complex stochastic agent-based model for estimating the number of people present in an office. In [53] and [56] Markov models were used to model the occupant's behavior over a time period. In [57] a genetic programming algorithm was applied to learn the behavior of an occupant in a single-person office based on motion sensor data. In [58] it was hypothesized that the occupancy and vacancy intervals in a single person office are distributed exponentially. Using motion sensor data collected from 35 single room offices to verify the hypothesis, it was found to hold for the vacancy intervals but had to be rejected for the occupancy intervals.

All of the works on occupancy modeling found by the authors aim at modeling short-term occupancy. Hence, for the presented study a new model describing long-term occupancy had to be devised.

7.1.3 Main Idea and Outline

The aim of this work was to estimate the importance of occupancy information for energy-efficient building climate control by means of a simulation study.

First, current methods of taking into account occupancy information were compared, i.e. the use of standard occupancy schedules is compared with additionally adjusting the lighting according to instantaneous occupancy measurements and with additionally adjusting both lighting and ventilation according to instantaneous occupancy measurements. This quantified the importance of taking into account instantaneous measurements. Second, the question of how much an occupancy prediction could improve the energy use at best was addressed by comparing a controller using standard occupancy schedules with another having a perfect prediction of the upcoming occupancy (deviating from the occupancy schedule) available.

The focus of the investigation was to determine the energy savings potential in case of long-term vacancies which are not considered in the schedule. A randomized study was carried out with different, random realizations of occupancy. These random realizations were created by sampling from an occupancy model designed for this study.

To ensure the comparability of control approaches and to avoid dependency of the results on the numerous tuning parameters of RBC controllers, MPC controllers were used for all simulations.

The simulation study was carried out for different buildings and HVAC systems, summer and winter weather, high and low internal gains levels, and different occupancy parameters.

Section 7.2 introduces the building simulation framework including the formulation of the MPC problem and its components and also includes a description of the occupancy model used for creating the occupancy time series. A detailed description of the investigations performed using this simulation framework is given in Section 7.3. The results are presented in Section 7.4

and discussed in Section 7.5. Conclusions are drawn in Section 7.6.

7.2 Building Simulation Framework

This section provides an overview of the simulation setup used in this study. Its scheme is given in Figure 7.1. Double-lined boxes are parts that were varied in the investigations (see Section 7.3). In the following, all components in Figure 7.1 are described. All settings and parameters that were used throughout this study were based on [50].

7.2.1 MPC

Several model predictive controllers were considered in the investigations. They were all based on the MPC problem (2.16) but included explicitly formulated model outputs (7.1c) and output constraints (7.1d). Note that this formulation including outputs and output constraints is just a notational convenience and is completely equivalent to the MPC problem (2.16). The model predictive controllers only differed in terms of available occupancy information (see Section 7.3.1). The MPC problem is repeated here for convenience

$$\underset{U_{0 \to N}}{\text{minimize}} \quad \sum_{k=0}^{N-1} c_k^T u_k \tag{7.1a}$$

$$\text{subject to} \quad x_{k+1} = Ax_k + B_\mathrm{u} u_k + B_\mathrm{v} v_k + \sum_{i=1}^{n_\mathrm{u}} (B_{\mathrm{vu},i} v_k + B_{\mathrm{xu},i} x_k) u_{k,i} \quad \forall k \in \mathbb{N}_0^{N-1} \tag{7.1b}$$

$$y_k = Cx_k + Du_k \qquad\qquad\qquad\qquad\qquad\qquad \forall k \in \mathbb{N}_0^{N-1} \tag{7.1c}$$

$$y_{\mathrm{min},k} \leq y_k \leq y_{\mathrm{max},k} \qquad\qquad\qquad\qquad\qquad \forall k \in \mathbb{N}_0^{N-1} \tag{7.1d}$$

$$F_{\mathrm{x},k} x_k + F_{\mathrm{u},k} u_k + F_{\mathrm{v},k} v_k \leq f_k \qquad\qquad\qquad \forall k \in \mathbb{N}_0^{N-1} \tag{7.1e}$$

$$x_0 = \hat{x}. \tag{7.1f}$$

The costs (7.1a) are described in Section 7.2.5. The building model, (7.1b) and (7.1c), is outlined in Section 7.2.3. It was assumed that the model for simulation and the model used in the controller were identical. The comfort constraints, (7.1d), and the actuator constraints, (7.1e), are described in Section 7.2.4. The comfort constraints depended on the occupancy prediction, i.e. the occupancy information available to the controller. The generation of the occupancy realizations and predictions is described in Section 7.2.7. The MPC received measurements from the simulated building as described in Section 7.2.2. It was assumed that full state information was available, i.e. $\hat{x}$ in (7.1f) corresponded to the actual current state of the simulated building. Moreover, the MPC received information about the *current* occupancy realization which some of the controllers made use of to instantaneously adjust lighting and potentially ventilation (see Section 7.3.1). The predictions of the weather and internal gains disturbances, $V_{0 \to N}$, are described in Section 7.2.6. The weather disturbances were assumed to be perfectly predicted, while the internal gains predictions also depended on the occupancy
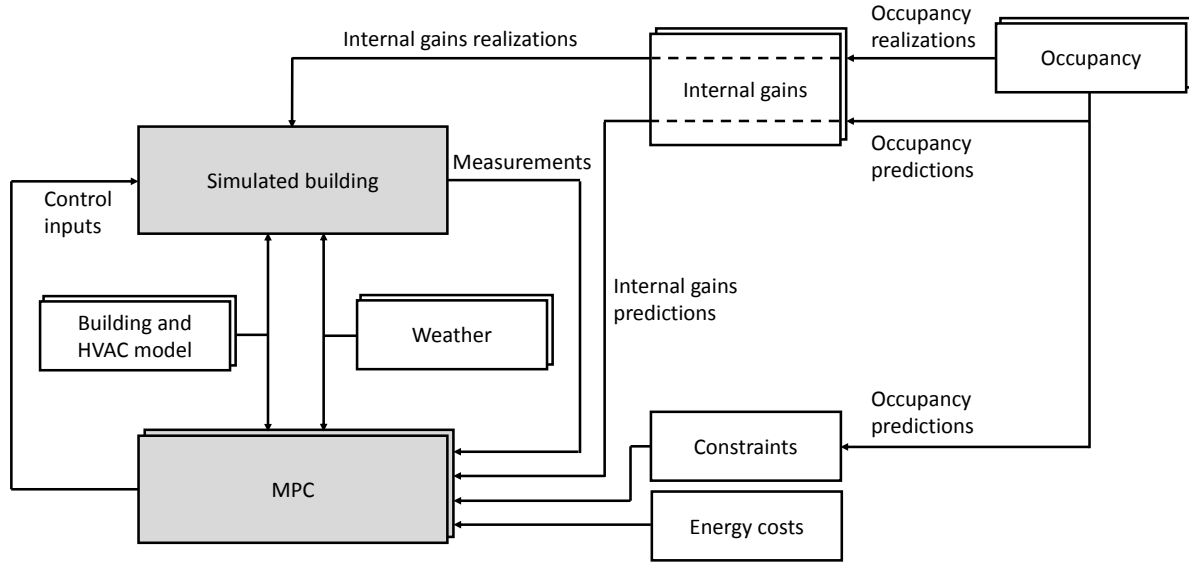
Figure 7.1: Scheme of the simulation setup. Boxes with double line indicate that different variants of this part were used in the investigation.

information available to the controller. The prediction horizon, N, was chosen to be 72 which corresponds to 3 days with a sampling time of 1 h. Choosing a longer prediction horizon was shown not to improve the energy use (below 1 % compared to a prediction horizon of one week).

7.2.2 Simulated Building

The model in the simulated building was identical to the control model in the MPC. One step in the simulation required the current control input from the MPC as well as the current weather and internal gains realization. The measurements obtained by the MPC include the current state of the system and the current occupancy realization.

7.2.3 Building Model

For this study we adapted the one-zone model of [34] which has been constructed and validated by building experts using the TRNSYS simulation software. The sampling time was 1 h.

The original one-zone model assumed that neighboring zones are identical to the modeled zone in terms of geometry, occupancy, and actuation and hence there is no heat transfer between the zones. Buildings with *inhomogeneous* occupancy usually have a heat transfer between zones which are occupied and zones which are vacant. In order to account for these effects, a two-zone model was constructed for this study. The two-zone model was obtained by connecting two one-zone models such that a chessboard-like structure as shown in Figure 7.2 was obtained. This two-zone model enables the description of two extreme occupancy layouts in the buildings: a *homogeneous* occupancy, where the occupancy in all zones is identical and an *alternating* occupancy, where the occupancy in the zones is different, i.e. while one zone is always occupied during working hours the other has random vacancies (see Section 7.2.7). Due to the chessboard-like structure of the model, these two layouts represent the extremes in terms of influence of different occupancy in neighboring rooms (no influence in the homogeneous
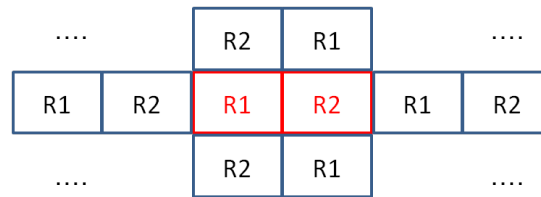
Figure 7.2: two-zone model. The building is composed of two types of rooms (R1 and R2) which are alternating horizontally and vertically resulting in a chessboard-like structure.

case and maximum influence in the alternating case). For simplicity, doors between offices are assumed to be closed. This is a reasonable assumption when offices are vacant. When offices are occupied, there is little heat transfer between offices due to regulated room temperatures, and hence, the position of doors is neglected and doors are assumed to be closed.

Throughout this investigation, it was assumed that the model for simulation and the model used in the controller are identical, i.e. there is no model-plant parameter mismatch.

In this study, two different building cases and two different HVAC systems were considered. The building cases were chosen such as to represent common building cases in Switzerland [50] as well as to have different thermal characteristics. The cases can be considered to be extreme cases in the sense that Building Case 1 has a normal insulation (swiss average) and little influence of solar gains due to small window area fraction, whereas Building Case 2 is very well insulated (passive house) and has high solar gains due to a large window area fraction. A description of the two building cases and their parameters is given in Table 7.1. The numerical values of the system matrices in (7.1b) and (7.1c), that reflect these two building cases can be found in [59].

Table 7.1: Building case definitions. The building cases represent common cases in Switzerland and are extreme cases in the sense that Building Case 1 has a normal insulation (swiss average) and little influence of solar gains due to a small window area fraction, whereas Building Case 2 is very well insulated (passive house) and has high solar gains due to a large window area fraction.

	Building Case 1	**Building Case 2**
Building standard	swiss average	passive house
Construction type	heavy	heavy
Window area fraction	low	high

An overview of the two HVAC systems considered in this study is given in Table 7.2. Both, HVAC system I and II, included blinds positioning and electric lighting, but differed in terms of availability of ventilation as well as means for heating and cooling. HVAC system I was chosen because it represents a simple HVAC system (e.g. no ventilation), which facilitates the analysis and is a common setup. HVAC system II includes TABS and an air handling unit. Tables 7.3 and 7.4 detail the actuators of HVAC systems I and II, respectively.

Table 7.2: Overview of the two HVAC systems and their automated subsystems. Both HVAC systems have blinds positioning and electric lighting, but differ in terms of availability of ventilation as well as means for heating and cooling.

Actuator	Description	Unit	Sys. I	Sys. II
Blinds positioning	Gain scaling maximal solar heatflux through windows	-	✓	✓
Electric lighting	Lighting power	W/m²	✓	✓
Mechanical ventilation ERC	Air change rate of forced ventilation preconditioned by energy recovery heat exchanger (ERC)	1/h	–	✓
Mechanical ventilation no ERC	Air change of unpreconditioned forced ventilation	1/h	–	✓
Heating mechanical ventilation	Heatflux due to heating coil in ventilation supply duct	W/m²	–	✓
Cooling mechanical ventilation	Heatflux due to cooling coil in ventilation supply duct (positive when cooling active)	W/m²	–	✓
Cooling tower	Gain scaling the maximum wet cooling tower power derived using outside wetbulb temperature. Power is delivered to cooled ceiling (see chiller)	-	✓	✓
Chiller	Cooling power from cooled ceiling (capillary tube system) using a chiller (positive when cooling active)	W/m²	✓	–
Radiator	Radiator heating power	W/m²	✓	–
Heating TABS	Heating power TABS	W/m²	–	✓
Cooling TABS	Cooling power TABS (positive when cooling active)	W/m²	–	✓

Table 7.3: Actuators of HVAC System I. $u_k := \left[u_{k,1}^I, u_{k,2}^I, u_{k,3}^I, u_{k,4}^I, u_{k,5}^I \right]^T$.

Input	Actuator	Unit	Constraints	Costs
$u_{k,1}^I$	Blinds positioning	-	$0 \leq u_{k,1}^I \leq 1$	$c_{k,1}^I = 0$
$u_{k,2}^I$	Electrical lighting	W/m²	$0 \leq u_{k,2}^I \leq 7.2$	$c_{k,2}^I = 3.32$
$u_{k,3}^I$	Chiller	W/m²	$0 \leq u_{k,3}^I \leq 80$	$c_{k,3}^I = 0.976$
$u_{k,4}^I$	Cooling tower	-	$0 \leq u_{k,4}^I \leq 1$	$c_{k,4}^I = 7.47$
$u_{k,5}^I$	Radiators	W/m²	$0 \leq u_{k,5}^I \leq 74$	$c_{k,5}^I = 1.107$

7.2.4 Constraints

Two types of constraints were considered: i) input constraints for formulating limitations on the actuator power; and ii) output constraints. The actuator constraints can be written in the form of (7.1e) with $F_{x,k} = 0$, $F_{v,k} = 0$ and constant $F_{u,k} = F_u$ and $f_k = f$ as in Tables 7.3 and 7.4.

The output constraints were time-varying and depended on the *occupancy prediction* available to the controller (including setbacks during nights and weekends). They are shown in Table 7.5. The output constraints can more compactly be written in the form

$$y_{\min,k} \leq y_k \leq y_{\max,k}, \tag{7.2}$$

Table 7.4: Actuators of HVAC System II. $u_k := \left[u_{k,1}^{II}, u_{k,2}^{II}, u_{k,3}^{II}, u_{k,4}^{II}, u_{k,5}^{II}, u_{k,6}^{II}, u_{k,7}^{II}, u_{k,8}^{II} \right]^T$.

Input	Actuator	Unit	Constraints	Costs
$u_{k,1}^{II}$	Blinds positioning	-	$0 \leq u_{k,1}^{II} \leq 1$	$c_{k,1}^{II} = 0$
$u_{k,2}^{II}$	Electrical lighting	W/m^2	$0 \leq u_{k,2}^{II} \leq 7.2$	$c_{k,2}^{II} = 3.32$
$u_{k,3}^{II}$	Mechanical ventilation ERC	1/h	$0 \leq u_{k,3}^{II} \leq 10^6$	$c_{k,3}^{II} = 0.396$
$u_{k,4}^{II}$	Mechanical ventilation no ERC	1/h	$0 \leq u_{k,4}^{II} \leq 10^6$	$c_{k,4}^{II} = 0.396$
$u_{k,5}^{II}$	Heating mechanical ventilation	W/m^2	$0 \leq u_{k,5}^{II} \leq 11$	$c_{k,5}^{II} = 1.071$
$u_{k,6}^{II}$	Cooling mechanical ventilation	W/m^2	$0 \leq u_{k,6}^{II} \leq 1.9$	$c_{k,6}^{II} = 0.949$
$u_{k,7}^{II}$	Cooling tower	-	$0 \leq u_{k,7}^{II} \leq 1$	$c_{k,7}^{II} = 7.47$
$u_{k,8}^{II}$	Heating TABS	W/m^2	$0 \leq u_{k,8}^{II} \leq 74$	$c_{k,8}^{II} = 0.949$
$u_{k,9}^{II}$	Cooling TABS	W/m^2	$0 \leq u_{k,9}^{II} \leq 80$	$c_{k,9}^{II} = 0.962$

Table 7.5: Occupancy prediction dependent output constraints.

Output	Description	Unit	Constraints if occupied	Constraints if not occupied
$y_{k,1}$	Room temperature	°C	$21 \leq y_{k,1} \leq 26$	$5 \leq y_{k,1} \leq 40$
$y_{k,2}$	Room illuminance	lux	$500 \leq y_{k,2}$	$0 \leq y_{k,2}$
$y_{k,3}$	Ceiling surface temp.	°C	$18 \leq y_{k,3}$	$18 \leq y_{k,3}$
$y_{k,4}$	Total air change rate	1/h	$1.54 \leq y_{k,4} \leq 4$	$0 \leq y_{k,4} \leq 4$

where the upper and lower bounds $y_{\min,k}$ and $y_{\max,k}$ are time-varying depending on the occupancy prediction as described above.

7.2.5 Energy Costs

The MPC controller was designed to minimize non-renewable primary energy consumption while satisfying the constraints. The cost function representing the sum of energy used by all actuators over a prediction horizon of N steps was given by

$$\sum_{k=0}^{N-1} c_k^T u_k, \tag{7.3}$$

where $c_k = c$ is constant and contains the costs of the different actuators as in the Tables 7.3 and 7.4.

7.2.6 Disturbances

The building was assumed to be subject to two kinds of disturbances, originating from weather and from internal gains (occupants, equipment). The disturbances v_k at time step k are given in Table 7.6. In the simulation, the disturbances were considered in two ways: a *prediction* of the disturbances N time steps into the future was taken into account in the controller in

Table 7.6: Disturbances.

Disturbance	Description	Unit
$v_{k,1}$	Solar radiation	W/m^2
$v_{k,2}$	Outside air temperature	°C
$v_{k,3}$	Outside air wetbulb temperature	°C
$v_{k,4}$	Internal gains occupancy	W/m^2
$v_{k,5}$	Internal gains equipment	W/m^2

order to make a good decision about the control input, and the *realization* (at the current time step) of the disturbances was considered for simulating the effect of the disturbances on the building, see Figure 7.1. The handling of predictions differed for the weather and internal gains variables. This is detailed in the following.

7.2.6.1 Weather

For the weather variables, it was assumed that all *predictions* are perfect, i.e. the weather *prediction* is equal to the (future) weather *realization*. The reason for the weather variables being assumed in this idealized fashion was the focus of this investigation on occupancy information and the aim to be able to isolate its effect on energy savings. All other parameter settings were therefore assumed ideal (i.e. perfect weather prediction, no model-plant parameter mismatch, idealized daily weather cycle, etc.).

For the *realization* of weather variables, only two seasons were considered, summer and winter, again to simplify the analysis of occupancy information. For creating weather data of the corresponding season, the average hourly values of the corresponding season from a design reference year (i.e. a representative annual data set, which follows the compilation of the standards of the SIA Merkblatt 2028 [60]) were taken and a daily cycle of the considered variables was created. The so created average daily cycle of the corresponding season was repeated in the simulation to create several days, such that it resulted in a periodic signal. This signal was used for two reasons: first, it had a realistic diurnal profile and second, it facilitated the analysis of the occupancy influence due to its simplicity.

7.2.6.2 Internal gains

Internal gains *realizations* used in the simulated building depended on occupancy *realizations* described in Section 7.2.7.1. Internal gains *predictions* used in the MPC depended on the occupancy *predictions* described in Section 7.2.7.2.

Internal gains due to *people*, $v_{k,4}$, and internal gains due to *equipment*, $v_{k,5}$, were assumed to be perfectly correlated, i.e. while people were present, the equipment was used, during vacancy times the equipment was not used. Only some base load from the equipment was assumed to be constant throughout the simulation. In the following, if referred to occupancy or vacancy, it is assumed that the equipment is varying accordingly.

In both, the internal gains realizations and predictions, the internal gains due to people were assumed to be constant during occupancy and zero otherwise while the internal gains

due to equipment were assumed to be constant high level during occupancy and constant low level otherwise. The value of the levels depended also on the simulated case: We distinguished an "internal gains high" (ih) and an "internal gains low" (il) scenario. This is summarized in Table 7.7.

Table 7.7: Internal gains.

Disturbance	Description	Unit	Occupied		Not Occupied	
			ih	il	ih	il
$v_{k,4}$	Internal gains people	W/m^2	6.3	3.5	0	0
$v_{k,5}$	Internal gains equipment	W/m^2	12	5.6	1.5	0.7

7.2.7 Occupancy

In this section, the occupancy realizations (used to generate internal gains realizations) and the occupancy predictions (used to generate the internal gains predictions and the comfort constraints) are described.

First, we define the *standard weekly occupancy profile*. It represents the baseline occupancy profile during a week. It was constructed based on the definitions in the building standards [61], with the exception that the occupancy level was held constant during the day. It is shown in Figure 7.3. Its definition is summarized as follows.

- A building zone is either occupied or vacant (no intermediate status reflecting partial occupancy was considered).
- A zone was considered to be occupied Monday to Friday between 7:00 and 18:00.
- During nights and weekends the zone is always vacant.
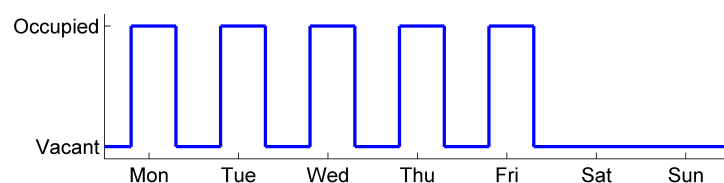
Figure 7.3: A standard weekly occupancy profile is constructed based on the standards [61] with the exception that the occupancy level is held constant during the day.

The actual occupancy *realizations* were assumed to differ from the standard weekly occupancy profile in terms of additional vacancies, i.e. vacancies occurring during whole working days due to illness, holiday, business trips, etc. This time series with additional vacancy days was randomly created and termed *stochastic varying occupancy profile* throughout this work. It is presented in the following Section 7.2.7.1.

7.2.7.1 Occupancy Realizations

This section describes the construction of occupancy *realizations* and the modeling of occupancy necessary for their generation.

The energy savings which may result from taking into account occupancy information compared to using only the standard weekly occupancy schedules can be expected to significantly depend on the occupancy realization. For instance, if the occupancy realization does not deviate much from the standard weekly profile, more sophisticated occupancy predictions are not important, whereas their importance likely grows with more deviating occupancy realizations. It was therefore decided to carry out a simulation study with different occupancy patterns. Hence, a model of occupancy was needed for generating random occupancy time series for a Monte Carlo study in which the relative energy savings were estimated.

In order to determine how to model occupancy, as a first step, occupancy data from an office building in Zurich were analyzed. These data comprised occupancy and vacancy days of 50 different persons throughout five years (not everyone was present throughout all years). Denote by $o_p(k) \in \{0, 1\}$ the occupancy data for person p on day k where $o_p(k) = 0$ denotes vacancy and $o_p(k) = 1$ denotes occupancy. Suppose $k = 1$ is a Monday (if it is not, shift the indices of the removed elements accordingly), then removing elements $6, 7, 13, 14, 20, 21, \ldots$ yields the occupancy data without weekends $o'_p(k)$. In this data, an *occupancy interval* is defined as a series of consecutive "1s" and a *vacancy interval* as a series of consecutive "0s" and their lengths are given by the number of consecutive "1s" and "0s", respectively. The histograms for the occupancy and vacancy interval lengths of all people throughout the five years are given in Figure 7.4. Both histograms resemble geometric distributions. Hence,

a)   b)
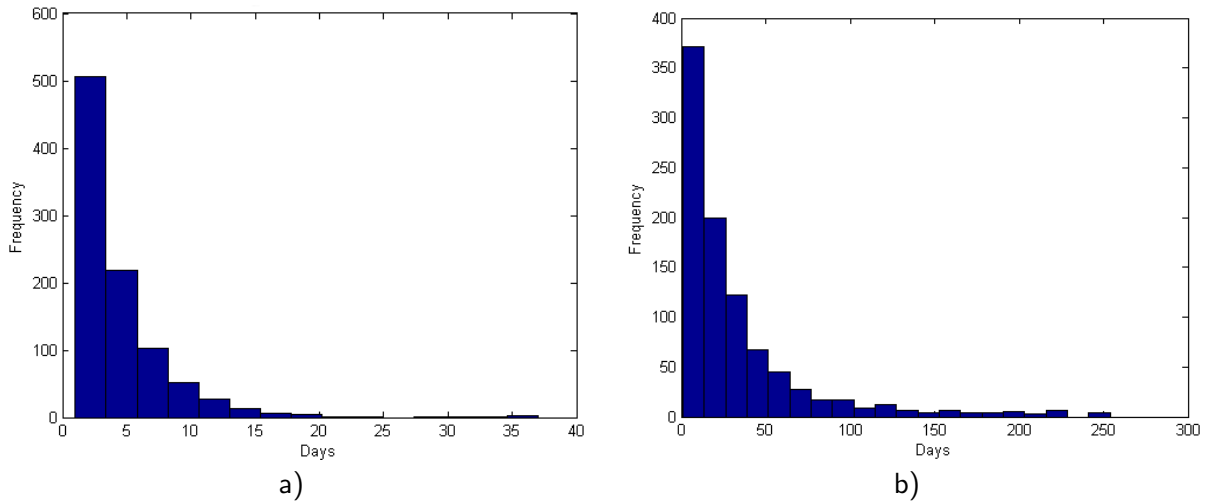
Figure 7.4: Vacancy (7.4a) and occupancy (7.4b) interval length histograms of 50 persons throughout five years. The lengths of the vacancy/occupancy intervals is plotted on the x-axis in days whereas on the y-axis the frequency of occurrence of the corresponding interval is shown.

motivated by the work in [58], where exponential distributions for vacancy and occupancy in the range of minutes are assumed, and the desire to use a simple model for occupancy in order to easily analyze effects of occupancy patterns, geometric distributions (i.e. the discrete analogy of the exponential distribution) for vacancy and occupancy intervals were assumed.

The geometric distribution's probability function is

$$\mathbf{P}(X = n) = \left(1 - \frac{1}{\beta}\right)^{n-1} \frac{1}{\beta} \tag{7.4}$$

with a support of $n = \{1, 2, 3, ...\}$. Its expected value is $\mathbf{E}(X) = \beta$.

With this assumption, occupancy time series were created with the procedure given in Algorithm 7.1. The time series of occupancy are created for a particular pair of (β_1, β_2)

Algorithm 7.1: Occupancy time series generation.

1) Choose expected number of consecutive vacancy days β_1 and expected number of occupancy days β_2.

2) Assume a geometric distribution f_1 for X_1, where $X_1 =$ number of consecutive vacancy days and $\mathbf{E}(X_1) = \beta_1$.

3) Assume a geometric distribution f_2 for X_2, where $X_2 =$ number of consecutive occupancy days and $\mathbf{E}(X_2) = \beta_2$.

4) Sample alternately from distributions f_1 and f_2 to create an occupancy status time series.

5) Insert a weekend (two vacant days) every five days.

---

and are representing the *stochastic varying occupancy profile*, which is used as *realization* of occupancy. For the Monte Carlo study, a large number of these time series were created. Many simulations with these realizations were performed and the average and standard deviation of the resulting energy use were computed assuming different levels of occupancy information (see Section 7.3). An example of the stochastic varying occupancy profile is shown in Figure 7.5.

Since a separate investigation (see Section 9.2 in the Appendix) showed the average energy savings to be a monotonously increasing function of β_1/β_2, the investigation was limited to the following set $(\beta_1, \beta_2) \in \{(1, 10), (1, 5), (5, 10)\}$. The assumption of geometrically distributed occupancy and vacancy intervals was investigated and supported in a second study presented in Chapter 8.
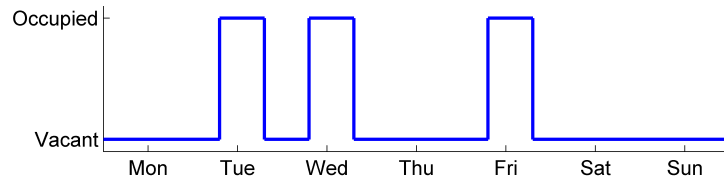

Figure 7.5: An example of an occupancy realization generated according to Algorithm 7.1.

7.2.7.2 Occupancy Predictions

The choice of the occupancy *prediction* was central to this study. In current practice, the standard weekly occupancy profile is assumed as a fixed schedule for occupancy prediction. This

is sometimes improved by additionally including an instantaneous *measurement* of occupancy, i.e. information about the *realization* at the current time step, and adjusting lighting and/or ventilation accordingly. To estimate the potential benefit of more sophisticated occupancy predictions, these methods were compared with a controller that had perfect information about the occupancy realization, i.e. the prediction was equal to the future realization (see also the definition of controllers in Section 7.3).

7.3 Investigations

First in this section, the set of performed simulations is described. In each, 90 days were simulated. In the set of simulations, we varied three components: the controller (chosen from some set $\mathbb{C}$), the occupancy pattern (chosen from some set $\mathbb{O}$) and the (remaining) simulation parameters (chosen from some set $\mathbb{P}$). The options among the three components are detailed in the following Sections 7.3.1, 7.3.2, and 7.3.3, respectively. In Section 7.3.4 the performance measures we defined to quantify the value of occupancy information are introduced.

7.3.1 Controllers

All controllers considered in this investigation were based on the MPC algorithm described in Section 7.2, although the current practice in building automation is to use RBC. The reason was the direct comparability and focus on the effect of occupancy prediction, which is easily achievable when using MPC. If one wanted to compare the value of different occupancy predictions with an RBC controller, the performance would highly depend on the rules applied and it would be very hard to isolate the effect of the occupancy prediction. In contrast, with MPC, the occupancy prediction directly enters in the optimization problem and, therefore, one can easily compare the same MPC controller with different predictions. The performance of an MPC controller with a particular occupancy information can be thought of as a bound on the performance of an RBC controller with the identical available occupancy information.

Four different levels of occupancy information were considered in this investigation, an overview can be found in Table 7.8.

$C_{-,-}^{\mathrm{std}}$ reflects the standard controller as currently implemented, where the superscript denotes the prediction and the subscript the adaptation to measurements. This controller assumes as occupancy prediction the standard weekly profile (std) and makes no further adjustments based on measurements (-,-).

$C_{\mathrm{li},-}^{\mathrm{std}}$ is identical to the first controller, with the exception that it adjusts lighting according to instantaneous measurements (li,-), i.e. if the occupancy sensor detects vacancy, the lighting is turned off, meaning that for the rest of the corresponding day the constraints on illuminance are set to their vacancy value in the MPC problem. The remaining constraints and predicted occupancy values are kept as in the first controller to ensure that the comfort requirements could be met again quickly in case the occupants returned.

$C_{\mathrm{li,ve}}^{\mathrm{std}}$ is identical to the first controller, but adjusts lighting and ventilation (li,ve) according to instantaneous measurements, i.e. if the occupancy sensor detects vacancy, lighting and ventilation are turned off, meaning that for the rest of the corresponding day the constraints on illuminance and air change rate are set to their vacancy value in the MPC problem. Again,

the remaining constraints and predicted occupancy values are kept.

Finally, $C^{\mathrm{perf}}_{-,-}$ reflects a controller which is possible at best, since it has a perfect prediction (perf) of the occupancy realization available, i.e. it knows a priori the occupancy that is realized in the future.

The key question of this paper is how big the energy savings potential of taking into account occupancy predictions is compared to using occupancy schedules. This savings potential is directly obtained by the comparison of $C^{\mathrm{perf}}_{-,-}$ and $C^{\mathrm{std}}_{-,-}$ since they only differ in terms of the considered occupancy prediction. One should note that both of these controllers, $C^{\mathrm{perf}}_{-,-}$ and $C^{\mathrm{std}}_{-,-}$, are idealized versions of building controllers (e.g. also RBC controllers) in the sense that they provide a bound on the performance given the model of the building is correct. However, in current building setups, if measurements of the occupancy are available, one can adjust lighting and ventilation based on instantaneous occupancy measurements. So, another equally important question is, whether occupancy *predictions* are necessary to realize significant energy savings or if already adjustments according to occupancy *measurements* provide a significant energy savings potential.

Note that it only makes sense to adjust lighting and ventilation to instantaneous occupancy measurements, but not heating and cooling, since the former two are very fast reacting systems, such that the comfort constraints can be guaranteed again after a short time when occupants have returned unexpectedly, whereas for heating and cooling there is no quick return to the comfort range once the room is at its setback temperature.

Also note that since in reality no perfect occupancy prediction is available, the energy savings potential of $C^{\mathrm{perf}}_{-,-}$ will be an upper bound on the energy savings which are possible to achieve in reality.

Controller	Description
$C^{\mathrm{std}}_{-,-}$	Baseline MPC controller, assumes standard weekly profile as prediction.
$C^{\mathrm{std}}_{\mathrm{li},-}$	Same as $C^{\mathrm{std}}_{-,-}$, but adjustment of lighting to instantaneous measurements.
$C^{\mathrm{std}}_{\mathrm{li,ve}}$	Same as $C^{\mathrm{std}}_{-,-}$, but adjustment of lighting and ventilation to instantaneous measurements.
$C^{\mathrm{perf}}_{-,-}$	MPC controller having a perfect prediction of occupancy.

Table 7.8: Overview of controllers.

7.3.2 Occupancy Patterns

The occupancy pattern is defined by its layout (homogeneous or alternating) denoted with a superscript and by the choice of combination of average vacancy days and average occupancy days (β_1, β_2) denoted with a subscript.

As already introduced in Section 7.2.3, two occupancy layouts were considered, an overview can be found in Table 7.9. $O^{\mathrm{hom}}_{(\beta_1,\beta_2)}$ denotes homogeneous occupancy in the building, which means that the stochastic varying occupancy profile is applied in both simulated zones. $O^{\mathrm{alt}}_{(\beta_1,\beta_2)}$ denotes alternating occupancy, which means that in one of the zones the stochastic varying occupancy profile and in the other the standard occupancy profile is applied. The two different

zones are arranged in a chessboard-like structure, see Figure 7.2.

For the average vacancy days and average occupancy days (β_1, β_2), it is sufficient to investigate only a subset of possible combinations $\{(1,10),(1,5),(5,10)\}$ due to the monotonicity of the resulting energy savings (see Section 9.2 in the Appendix). These choices reflect that (excluding weekends) one out of eleven days is vacant, one out of six days is vacant, and five out of 15 days are vacant on the average, respectively. Let $\mathbb{O}$ denote the set of considered occupancy layouts, with $\mathbb{O} := \{ O^{hom}_{(1,10)}, O^{hom}_{(1,5)}, O^{hom}_{(5,10)}, O^{alt}_{(1,10)}, O^{alt}_{(1,5)}, O^{alt}_{(5,10)} \}$.

Table 7.9: Overview of occupancy patterns.

Occupancy pattern	Description
$O^{hom}_{(\beta_1,\beta_2)}$	Occupancy is identical in all zones
$O^{alt}_{(\beta_1,\beta_2)}$ $\qquad (\beta_1, \beta_2) \in \{(1,10),(1,5),(5,10)\}$	Chessboard-like structure of two different zones, one zone is always occupied, the other has random vacancies

7.3.3 Parameters

In order to determine the influence of the building and HVAC system, the season, and the internal gains level on the energy savings potential of occupancy information, the parameters listed in Table 7.10 were varied in this study. Two different building cases $\{1,2\}$, two different HVAC systems $\{I,II\}$, summer and winter season $\{sum,win\}$, as well as two different levels for the internal gains $\{ih,il\}$ were simulated. Let

$$P := (\text{building case}, \text{HVAC system}, \text{season}, \text{internal gains level}) \qquad (7.5)$$

denote a particular combination of parameters, and let $\mathbb{P}$ denote the set of possible parameter combinations, with

$$\mathbb{P} := \{ (1, I, sum, ih), (1, I, sum, il), (1, I, win, ih), (1, I, win, il), (1, II, sum, ih), (1, II, sum, il),$$
$$(1, II, win, ih), (1, II, win, il), (2, I, sum, ih), (2, I, sum, il), (2, I, win, ih), (2, I, win, il),$$
$$(2, II, sum, ih), (2, II, sum, il), (2, II, win, ih), (2, II, win, il) \}.$$

Table 7.10: Table of simulation parameters.

Parameter	Value
Building Case	1, 2; see Table 7.1
HVAC system	I, II; see Table 7.2
Season	summer(sum), winter(win); see Section 7.2.6.1
Internal gains level	high(ih), low(il); see Section 7.2.6.2

7.3.4 Performance Measures

As a first step, the simulations for homogeneous occupancy were carried out and in a second step the simulations for alternating occupancy. Denote by $E(C, O, P)$ the average energy use for a particular choice of a controller C, an occupancy layout O, and a combination of parameters P.

The energy use when applying the standard controller assuming a standard weekly profile $C_{-,-}^{std}$ was used as a benchmark. The aim was to identify the savings potential relative to this benchmark when applying the other three controller options: $C_{li,-}^{std}$, $C_{li,ve}^{std}$, and $C_{-,-}^{perf}$. These performance measures were computed as

$$\Delta E_{li,-}^{std}(O, P) := \frac{E(C_{-,-}^{std}, O, P) - E(C_{li,-}^{std}, O, P)}{E(C_{-,-}^{std}, O, P)} \tag{7.6}$$

$$\Delta E_{li,ve}^{std}(O, P) := \frac{E(C_{-,-}^{std}, O, P) - E(C_{li,ve}^{std}, O, P)}{E(C_{-,-}^{std}, O, P)} \tag{7.7}$$

$$\Delta E_{-,-}^{perf}(O, P) := \frac{E(C_{-,-}^{std}, O, P) - E(C_{-,-}^{perf}, O, P)}{E(C_{-,-}^{std}, O, P).} \tag{7.8}$$

It can clearly be expected that $0 \leq \Delta E_{li,-}^{std}(O, P) \leq \Delta E_{li,ve}^{std}(O, P) \leq \Delta E_{-,-}^{perf}(O, P)$. Whereas the controllers deviated in the occupancy *prediction* and instantaneous adjustment of lighting and ventilation, they all encountered the same occupancy *realization* in the simulations, which was obtained from creating occupancy time series according to Algorithm 7.1. The number of simulated realization scenarios per (O, P) combination was determined such that the estimator of the relative energy savings potential had a standard deviation of less than 1.5% with a confidence interval of 90%.

7.4 Results

7.4.1 Homogeneous occupancy

Figure 7.6 depicts the simulation results for the case of homogeneous occupancy. It shows the relative energy savings $\Delta E_{li,-}^{std}$, $\Delta E_{li,ve}^{std}$, and $\Delta E_{-,-}^{perf}$ as defined in (7.6), (7.7), and (7.8) for all $P \in \mathbb{P}$ and all $O_{(\beta_1,\beta_2)}^{hom} \in \mathbb{O}$, i.e. for all building cases and HVAC systems, both seasons {sum,win}, both internal gains levels {il,ih}, and the three combinations of (β_1, β_2). Note that HVAC system I does not have ventilation, therefore, only two bars are shown.

It can clearly be seen that for all cases the energy savings potential is increasing for an increasing vacancy to occupancy ratio β_1/β_2. The savings potential is significant, ranging up to 34%. However, for almost all cases, a large fraction of this potential can already be captured by adjusting lighting and ventilation to instantaneous measurements. This can be seen from the fact that $\Delta E_{-,-}^{perf}$ is not significantly higher than $\Delta E_{li,ve}^{std}$. Only for very high vacancy to occupancy ratios as $(\beta_1, \beta_2) = (5, 10)$ there is still a significant savings potential of $C_{-,-}^{perf}$ compared to $C_{li,ve}^{std}$ (for Building Case 1 mainly in winter, for Building Case 2 mainly in summer).
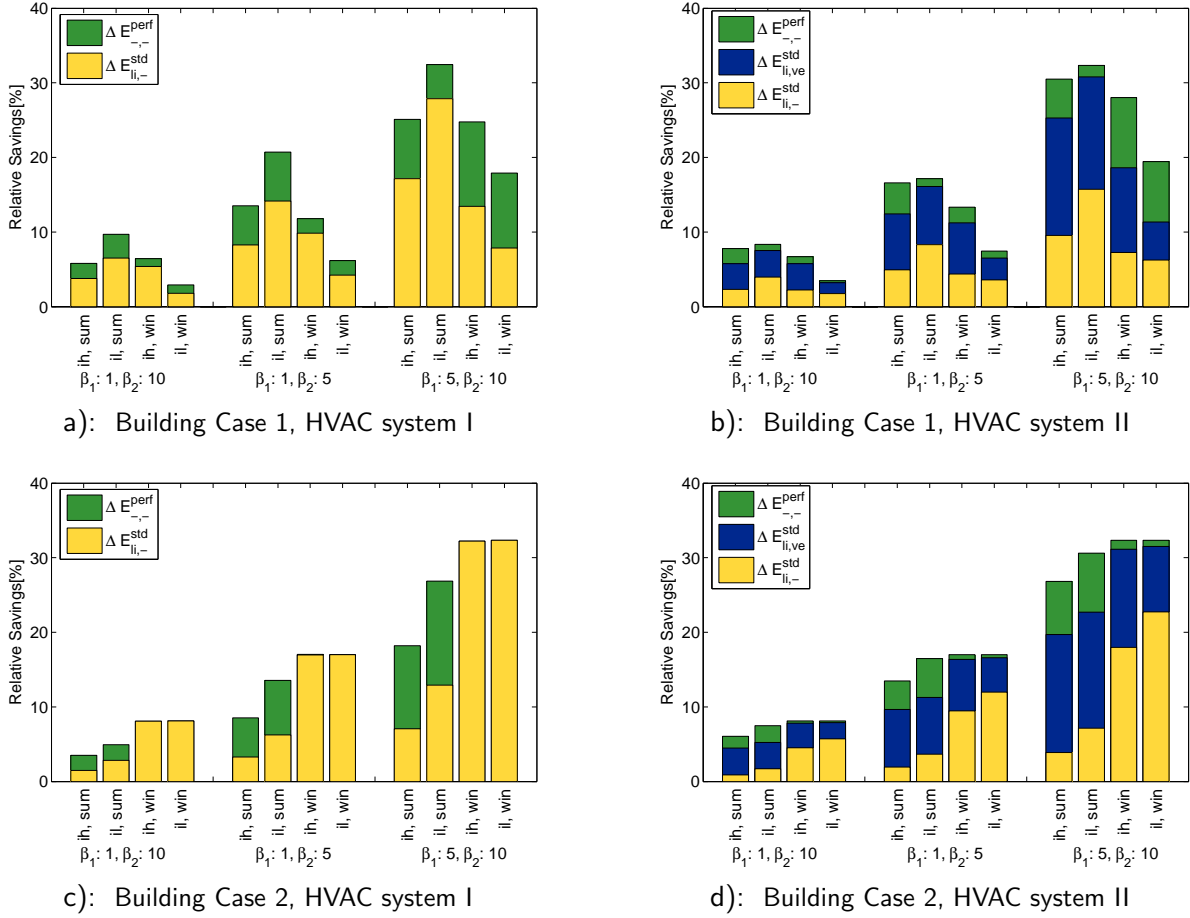
Figure 7.6: Homogeneous occupancy. The relative energy savings $\Delta E_{li,-}^{std}$, $\Delta E_{li,ve}^{std}$, and $\Delta E_{-,-}^{perf}$ as defined in (7.6), (7.7), and (7.8) are plotted for all $P \in \mathbb{P}$ and all $O_{(\beta_1,\beta_2)}^{hom} \in \mathbb{O}$, i.e. for all building cases and HVAC systems, both seasons {sum,win}, both internal gains levels {il,ih}, and the three combinations of (β_1, β_2).

Furthermore, for Building Case 2 in winter there is almost no energy savings potential with $C_{-,-}^{perf}$ compared to $C_{li,ve}^{std}$. A closer analysis revealed that due to the good insulation and large window area of this building, the controller is able to meet the comfort constraints almost only by changing the blinds position, which does not contribute to the energy use.

7.4.2 Alternating occupancy

This investigation was carried out to analyze the sensitivity of the savings potential if vacancies only appear in every second room of the building. Figure 7.7 depicts the simulation results for alternating occupancy. It shows the relative energy savings $\Delta E_{li,-}^{std}$, $\Delta E_{li,ve}^{std}$, and $\Delta E_{-,-}^{perf}$ as defined in (7.6), (7.7), and (7.8) for all $P \in \mathbb{P}$ and all $O_{(\beta_1,\beta_2)}^{alt} \in \mathbb{O}$, i.e. for all building cases and HVAC systems, both seasons {sum,win}, both internal gains levels {il,ih}, and the three combinations of (β_1, β_2).

Similarly to the case of homogeneous occupancy, the energy savings are increasing with an increasing vacancy to occupancy ratio β_1/β_2. Furthermore, for the investigated cases, the energy savings are about 50 % of the corresponding cases with homogeneous occupancy. This is similar to what can be expected if one neglects the heat transfer between zones, since the
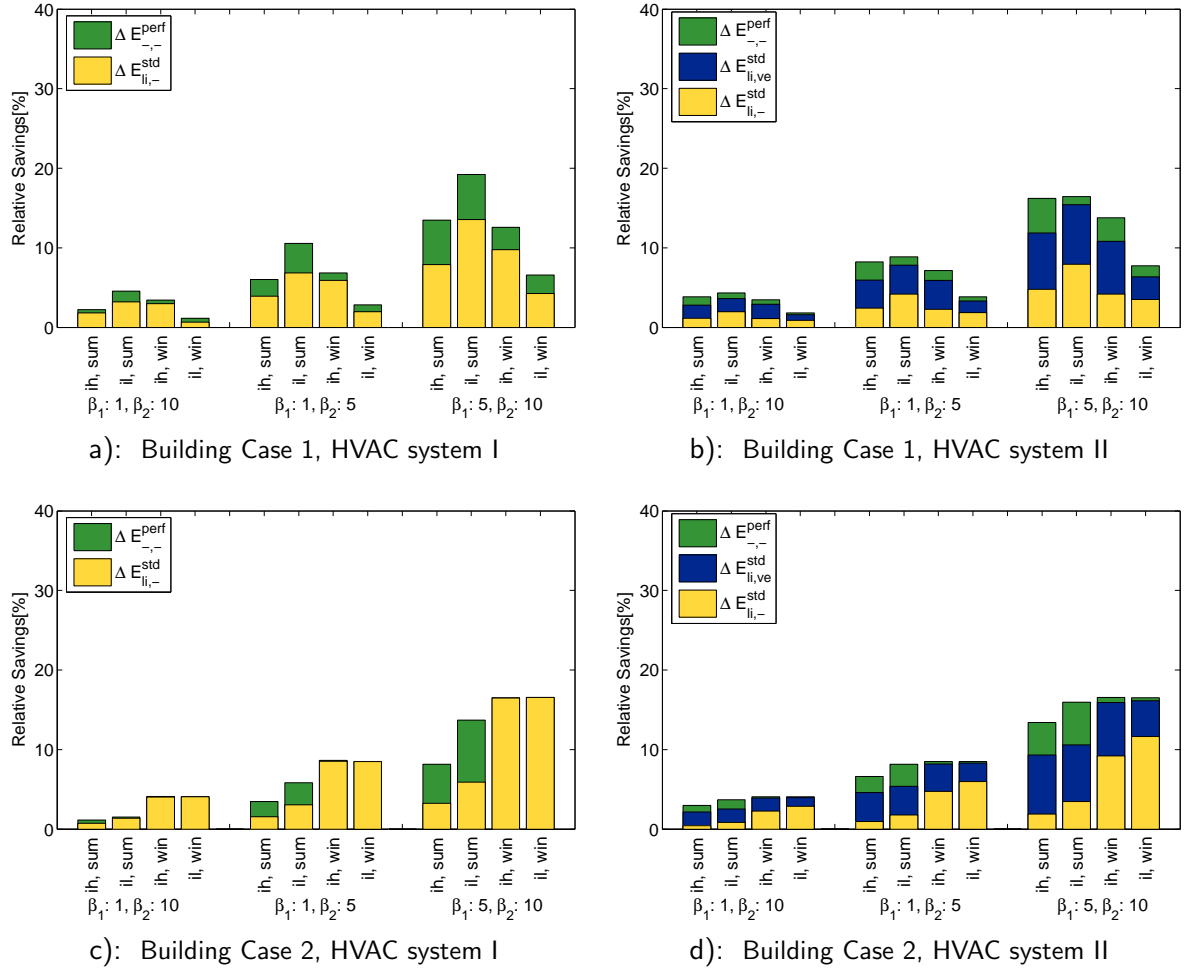
Figure 7.7: Alternating occupancy. The relative energy savings $\Delta E_{li,-}^{std}$, $\Delta E_{li,ve}^{std}$, and $\Delta E_{-,-}^{perf}$ as defined in (7.6), (7.7), and (7.8) are plotted for all $P \in \mathbb{P}$ and all $O_{(\beta_1,\beta_2)}^{alt} \in \mathbb{O}$, i.e. for all building cases and HVAC systems, both seasons {sum,win}, both internal gains levels {il,ih}, and the three combinations of (β_1, β_2).

savings are only realized in every second building zone. Therefore it can be concluded, that the influence of heat transfer between different zones had no significant effect on the energy savings potential in the current setup.

7.5 Discussion

In this section, first the investigation setup and then the obtained results are discussed.

7.5.1 Investigation Setup

All controllers considered in this investigation are based on MPC since this enables a direct comparability and focus on the effect of different occupancy information. If one wanted to compare the value of different occupancy predictions with RBC, which is current practice in building control, the performance would highly depend on the rules applied and it would be very hard to isolate the effect of the occupancy prediction. In contrast, with MPC, the

occupancy prediction directly enters in the optimization problem and therefore one can easily compare the same MPC controller with different predictions. The performance of an MPC controller with a particular occupancy information can be thought of as an upper bound on the performance of a RBC controller with the identical available occupancy information. Hence, the use of MPC provides a unifying and coherent framework for this investigation.

When investigating the energy savings potential of occupancy predictions, a perfect prediction of the occupancy realization was considered. In reality, one could think of using for instance corporate calendars in order to be aware of business trips, holidays, etc. in advance. However, illnesses can appear suddenly or people can also make mistakes when scheduling business trips. Therefore, in reality a perfect prediction of the realization will never be achieved and it should be pointed out that the computed energy savings potential reflects an upper bound on the realizable potential.

For generating stochastically varying occupancy profiles, we assumed a geometric distribution of the vacancy and occupancy profile. This choice was motivated by analysing real occupancy data. In an additional study described in Chapter 8, this assumption is further supported by comparing energy savings in simulations with a different set of measured occupancy data to simulations with occupancy profiles generated according to Algorithm 7.1 using appropriately chosen parameters β_1 and β_2.

In all simulations, it was assumed that the model of the building and HVAC system is perfectly known and that the weather is perfectly predicted. This is clearly not the case in reality. However, since this assumption was made for all investigations, the effect on the relative savings can be expected to be small (i.e. in reality both controllers will perform worse, but the difference should not be much affected).

The choice of buildings and HVAC systems was driven by two factors: first, the choices represent common setups in Switzerland and second, they were chosen to represent rather extreme outcomes of energy savings potentials, e.g. HVAC system II has TABS and is a slow reacting system, whereas HVAC system I is faster and has no ventilation. Also the buildings represent extreme scenarios, since Building Case I has an average insulation with small windows, whereas Building Case II is a passive house which is well insulated and has large windows. The choice was made such that is can be expected that the resulting energy saving potentials of most other relevant building cases lie in the spanned range of these cases.

Summarizing, the described investigation setup provides a general methodology for investigating questions related to energy savings potentials of occupancy information in building control.

7.5.2 Simulation Results

The most relevant case of average vacancy and average occupancy interval lengths arguably is $(\beta_1, \beta_2) = (1, 5)$ since it represents a case which is still reasonable for many offices, but has quite a large energy savings potential of taking into account occupancy information. However, for this case, the relative energy savings of $C_{-,-}^{\text{perf}}$ compared to $C_{\text{li},-}^{\text{std}}$ and $C_{\text{li,ve}}^{\text{std}}$ are only significant in summer and even for these cases, the absolute energy savings are only about $1\,\text{kWh/m}^2\text{a}$ (see Section 9.3 in the Appendix).

One can clearly see that even though there is a significant energy savings potential, a large part of it can already be obtained by taking into account instantaneous occupancy

measurements, i.e. using $C_{li,-}^{std}$ and $C_{li,ve}^{std}$. Hence, there is strong indication that adjustments based on instantaneous measurements have a significant energy savings potential, in particular the adjustment of ventilation (see Section 9.3 in the Appendix). Using on top of that more sophisticated occupancy prediction is questionable in terms of energy savings potential since the estimated savings potential is already very small and represents an upper bound on the energy savings which can be achieved in reality with occupancy predictions that are not perfect.

The comparison of homogeneous and alternating occupancy revealed that the influence of heat transfer between different zones had no significant effect on the energy savings potential in the current simulation setup, where doors between offices are assumed to be closed (see Section 7.2.3). In case of open doors, the heat transfer between offices can be expected to be more important. The effect of this depends on the season; in winter, heat transfer to vacant rooms is expected to increase energy use, whereas in summer the effect of heat transfer on the energy use is unclear since there can be a heat transfer to the cooled room, which would increase energy use or a heat transfer to the vacant room because this is colder due to missing internal gains. This effect could be investigated with a more detailed model. However, there is no significant change in the relative energy savings potential expected.

7.6 Conclusion

This investigation estimated the energy savings potential of using occupancy information for common office buildings in Switzerland depending on the occupancy pattern (i.e. frequency of vacancy days) as well as on the building case, HVAC system, season and internal gains level. It was found that energy savings are increasing with respect to increasing vacancy and decreasing occupancy days.

The simulations with homogeneous occupancy showed a savings potential of up to 34 % for the case of average vacancy and occupancy intervals of 5 and 10 days, respectively. This savings potential can to a large part be captured by using a schedule as prediction and adjusting lighting and ventilation to instantaneous measurement of the occupancy status.

In the simulations with alternating occupancy, the savings are in the range of 50 % of the savings with homogeneous occupancy. It apprears that the influence of heat transfer between different zones had no significant effect on the energy savings potential in the current simulation setup.

Taking into account occupancy information in building control has a significant energy savings potential. However, a large part of this potential can already be captured by taking into account instantaneous occupancy information.

To summarize, adjusting lighting and especially ventilation to instantaneous measurement can clearly be recommended for saving energy in building climate control. Using on top of that more sophisticated occupancy predictions does not provide a significant energy savings potential, considering that the estimated potential in this study is an upper bound, but only quite small.

Chapter 8

Investigating the Occupancy Interval Distribution Assumption Using Measured Data

8.1 Introduction

This chapter describes a follow up study to Chapter 7 aiming at validating the assumptions on the occupancy patterns. The main idea is as follows. Using the same simulation framework as described in Section 7.2, we calculated the energy savings of occupancy information from simulations using as occupancy realizations occupancy data measured on the OptiControl-II demonstrator building (see Section 6.2). We calculated from these measured data empirical occupancy distribution parameters $(\hat{\beta}_1, \hat{\beta}_2)$. We then calculated the energy savings of occupancy information from simulations using as occupancy realizations randomly generated occupancy patterns with $(\hat{\beta}_1, \hat{\beta}_2)$. If both energy savings coincided, the assumption of geometrically distributed occupancy intervals for the purpose of estimating the energy savings potential of occupancy information would be supported.

8.1.1 Measured Occupancy Data

The daily occupancy data were obtained as follows. In eight single person offices, occupancy measurements on a sub-hourly timescale were acquired by motion detection sensors. The reasons for focusing on the single person offices were: i) the initial assumption of geometrically distributed vacancy/occupancy intervals was based on an analysis of single person data; and ii) internal gains associated with occupancy are proportional to the number of persons in an office and the installed sensors were not capable of distinguishing whether one or more persons were in the office. The available data ranged from October 2011 to October 2012. For this investigation, we were interested in daily occupancy. However, simply requiring that the sub-hourly occupancy measurements indicated vacancy throughout a whole day was not accurate, since it was possible that other persons briefly entered the office in question. Hence the office was defined to be vacant (in daily terms) if the sub-hourly measurements indicated less than 30 minutes of occupancy during one particular day. Data for the summer and winter simulation period were taken from 90 days starting in May and December, respectively.

8.2 Investigations

We performed simulations varying

$$C \in \mathbb{C} = \{C_{-,-}^{\text{std}}, C_{\text{li,ve}}^{\text{std}}, C_{-,-}^{\text{perf}}\}$$
$$P \in \mathbb{P} = \{(1,\text{II,sum,ih}), (1,\text{II,win,ih})\}$$
$$O \in \mathbb{O}$$

For simplicity, the parameter set, $\mathbb{P}$, was limited to the cases that closely matched the building from which the measured occupancy data originated. The set of occupancy patterns $\mathbb{O}$ containing the random and measured occupancy patterns is described in the following Section 8.2.1.

8.2.1 Occupancy Patterns

To compare for each room i from which we obtained measured data and for every season, *seas*, the simulations with measured occupancy data, $O_{\text{meas},seas,i}^{\text{alt}}$, to a set of Monte-Carlo simulations with random occupancy patterns, $O_{\text{rand},seas,i}^{\text{alt}}$, generated as in Section 7.2.7, we needed to compute from the measured data the respective empirical values of (β_1, β_2). This is outlined in this section. A straightforward choice of calculating estimates of (β_1, β_2) from the measured data would have been to identify all n_{vac} vacancy interval lengths Δv_i, all n_{occ} occupancy interval lengths Δo_i (both calculated after excluding weekends) and to compute

$$\hat{\beta}_1 = \frac{1}{n_{\text{vac}}} \sum_{j=1}^{n_{\text{vac}}} \Delta v_i \tag{8.1a}$$

$$\hat{\beta}_2 = \frac{1}{n_{\text{occ}}} \sum_{j=1}^{n_{\text{occ}}} \Delta o_i. \tag{8.1b}$$

However, since we simulated a fixed period of 90 days, it was not guaranteed that $n_{\text{occ}} = n_{\text{vac}}$ although, by definition, $|n_{\text{vac}} - n_{\text{occ}}| \leq 1$. Denote by

$$A_{\text{meas}} = \frac{\sum_{j=1}^{n_{\text{occ}}} \Delta o_i}{\sum_{j=1}^{n_{\text{occ}}} \Delta o_i + \sum_{j=1}^{n_{\text{vac}}} \Delta v_i} \tag{8.2}$$

the average presence during working days as calculated from the measured data. The expected value of the corresponding quantity of the random data was approximated[1] by

$$\mathbf{E}(A_{\text{rand}}) \approx \hat{A}_{\text{rand}} = \frac{\beta_2}{\beta_1 + \beta_2}. \tag{8.3}$$

It turned out that $\hat{A}_{\text{rand}} = A_{\text{meas}}$ was a critical condition for a proper comparison. This was not satisfied in the case of $n_{\text{vac}} \neq n_{\text{occ}}$ (check by replacing (8.1) in (8.3) and comparing with

---

[1]Simulations showed that this approximation holds well.

(8.2)). Thus we calculated $\hat{\beta}_2$ according to (8.1) and $\hat{\beta}_1$ as

$$\hat{\beta}_1 = \hat{\beta}_2 \left(\frac{1 - A_{\text{meas}}}{A_{\text{meas}}} \right) \tag{8.4}$$

which trivially yielded $\hat{A}_{\text{rand}} = A_{\text{meas}}$. Note that both ways of calculating empirical values for (β_1, β_2) yield the same result if either $n_{\text{vac}} = n_{\text{occ}}$ or in the case of long time intervals (i.e. $n_{\text{vac}}, n_{\text{occ}} \to \infty$). Table 8.1 shows $\hat{\beta}_1$, $\hat{\beta}_2$, and A_{meas} as calculated from the measurement data of all eight rooms for winter and summer periods. The weather used in the simulations corresponded to these periods.

The set of occupancy patterns was

$$\mathbb{O} = \{ O^{\text{alt}}_{\text{meas},seas,i}, O^{\text{alt}}_{\text{rand},seas,i} \} \qquad i \in \{1, 2, \ldots, 8\}, \quad seas \in \{summer, winter\}. \tag{8.5}$$

Table 8.1: Empirically estimated values of (β_1, β_2) and corresponding A_{meas} as calculated from the measurement data of all eight rooms for winter and summer periods.

Room	Season	$\hat{\beta}_1$	$\hat{\beta}_2$	A_{meas}	Room	Season	$\hat{\beta}_1$	$\hat{\beta}_2$	A_{meas}
1	Summer	2.33	18	0.89	5	Summer	9	1.67	0.16
	Winter	3	12.5	0.81		Winter	1.5	3.58	0.70
2	Summer	1.88	3.25	0.63	6	Summer	2.4	9.8	0.80
	Winter	2.8	9.4	0.77		Winter	1.6	10.6	0.87
3	Summer	4	2.78	0.41	7	Summer	3.25	12	0.79
	Winter	4.67	15.67	0.77		Winter	3.83	6.33	0.62
4	Summer	2.33	18	0.89	8	Summer	1.33	5.44	0.80
	Winter	2.67	17.67	0.87		Winter	3	12.25	0.80

8.2.2 Simulations

We focused on the relative energy savings if lighting and ventilation are instantaneously adjusted and on the relative energy savings of an MPC with perfect occupancy information, i.e.

$$\Delta E^{std}_{li,ve}(O, P) := \frac{E(C^{\text{std}}_{-,-}, O, P) - E(C^{\text{std}}_{li,ve}, O, P)}{E(C^{\text{std}}_{-,-}, O, P)} \tag{8.6a}$$

$$\Delta E^{perf}_{-,-}(O, P) := \frac{E(C^{\text{std}}_{-,-}, O, P) - E(C^{\text{perf}}_{-,-}, O, P)}{E(C^{\text{std}}_{-,-}, O, P)}. \tag{8.6b}$$

In every simulation, a period of 90 days was simulated. Note that we only computed (8.6a) and (8.6b) for those O and P combinations with corresponding seasons, i.e. the simulation

set was given by

$$\left\{ (O, P) \,\middle|\, \begin{array}{l} P = (1, \mathrm{II}, seas, \mathrm{ih}),\, O \in \{O^{\mathrm{alt}}_{\mathrm{meas}, seas, i},\, O^{\mathrm{alt}}_{\mathrm{rand}, seas, i}\} \\ i \in \{1, 2, \ldots, 8\},\, seas \in \{sum, win\} \end{array} \right\}. \qquad (8.7)$$

8.3 Results

In every bar of Figure 8.1, the relative savings $\Delta E^{\mathrm{std}}_{\mathrm{li,ve}}(O, P)$ and $\Delta E^{\mathrm{perf}}_{-,-}(O, P)$ are shown in green and blue, respectively. We compared the influence of the occupancy pattern by plotting for every room i and both seasons, $seas$, next to each other the values using $O^{\mathrm{alt}}_{\mathrm{meas}, seas, i}$ and $O^{\mathrm{alt}}_{\mathrm{rand}, seas, i}$. The relative savings with $O^{\mathrm{alt}}_{\mathrm{rand}, seas, i}$ corresponded to average values over a set of Monte-Carlo simulations. The number of simulations was chosen such that the estimator for a particular comparison of two controllers with different occupancy information had a standard deviation of less than $1.5\,\%$ with a confidence interval of $90\,\%$.

Clearly, as expected, $\Delta E^{\mathrm{std}}_{\mathrm{li,ve}}(O, P) \leq \Delta E^{\mathrm{perf}}_{-,-}(O, P)$. The savings ranged from $5\,\%$-$45\,\%$ and depended mainly on the average presence time during weekdays A_{meas}. When comparing $\Delta E^{\mathrm{std}}_{\mathrm{li,ve}}(O, P)$ and $\Delta E^{\mathrm{perf}}_{-,-}(O, P)$, it can be seen in accordance to the previous results that a major part of the savings with perfect occupancy information could be captured by instantaneously adjusting lighting and ventilation. Crucially for answering the question posed at the beginning of this study, the energy savings of the simulations with measured and randomly generated data for a particular room and season corresponded very closely.
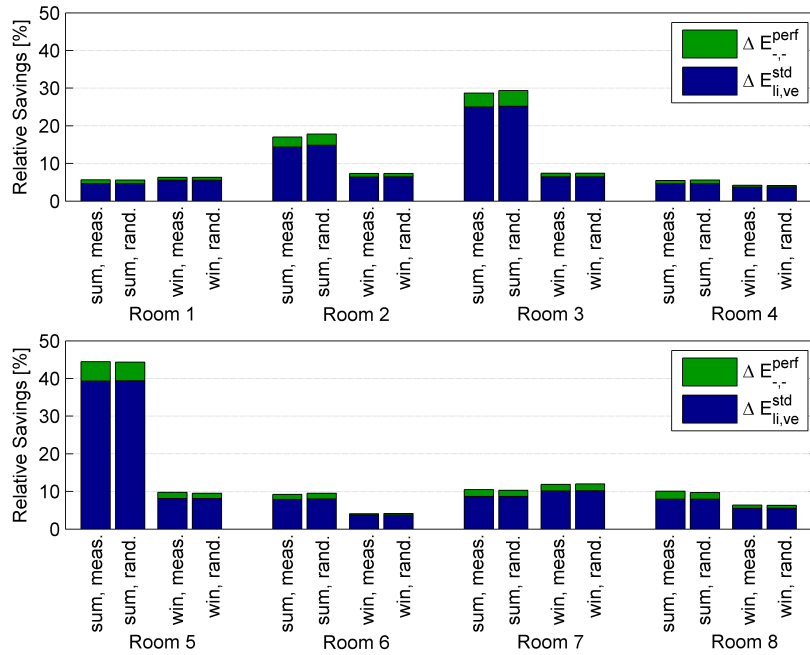
Figure 8.1: Relative savings $\Delta E^{\mathrm{std}}_{\mathrm{li,ve}}(O, P)$ and $\Delta E^{\mathrm{perf}}_{-,-}(O, P)$ for the measured and the randomly generated data of all eight rooms for winter and summer seasons.

8.4 Conclusion

In this study, the value of occupancy information was assessed by comparing the energy consumption of three MPC controllers that varied only in the available occupancy information. The same simulation framework as in Chapter 7 was used which is based on the assumption that occupancy and vacancy intervals are geometrically distributed. This study aimed at validating the geometric distribution assumption by comparing simulations using measured occupancy data to such using randomly generated occupancy data with empirically estimated parameters.

The energy savings potential was in many cases significant, however, in all cases the largest part of it could already be captured by using instantaneous occupancy measurements. This is in line with the findings of the previous study.

For all investigated cases the estimated savings potential with randomly created data was very close to the savings potential obtained with measured data. The close correspondence gives strong support for the occupancy model proposed in Chapter 7 to be a valid choice for the purpose of estimating the savings potential of occupancy information.

Chapter 9

Appendices

9.1 External Heat Flux Models

In this section, we describe how – based on the EHF model input data files (described below for every EHF model) and the thermal model data (see Section 4.3.1) – the aggregated EHF model,

$$q(x(t), u(t), v(t)) = A_{\mathsf{q}}x(t) + B_{\mathsf{q,u}}u(t) + B_{\mathsf{q,v}}v(t) + \sum_{i=1}^{n_u}(B_{\mathsf{q,vu},i}v(t) + B_{\mathsf{q,xu},i}x(t))u_i(t)], \quad (9.1)$$

is constructed. Moreover, we show how the costs and constraints matrices returned by the Matlab commands (see Section 4.5)

```
[Fx_k,Fu_k,Fv_k,f_k] = B.building_model.getConstraintsMatrices(constrParam);
c_k = B.building_model.getCostVector(costsParam);
```

are formulated. For every EHF model that is included, one input data file (again, Excel or CSV) with a well defined structure must be provided. To generate the costs and constraints, parameter values must be provided in the structures `constrParam` and `costsParam`. Which parameters have to be provided depends on the included EHF models. In the following, we describe for every EHF model first the required input data file as well as the required costs and constraints parameters. Then, we introduce the notation and describe the modeling of the EHF. Finally, we describe the formulation of the costs and constraints. Note that the EHF are modeled in continuous-time, while the costs and constraints are formulated in discrete-time assuming that the parameters provided in `constrParam` and `costsParam` are constant during the sampling interval. For brevity, we omit the time indication in the rest of this section.

Since the number of modeled control inputs and disturbances resulting from a particular EHF model depends on its input data, we use the following notation. By example of the internal gains EHF model (see Section 9.1.1), the number of distinct "*<disturbance_identifier>*" specified in the input data determines how many separate disturbances, $v_{\mathsf{IG},<disturbance\_identifier>}$, are modeled. Analogously, for example in the case of radiators, a control input $u_{\mathsf{Rad},<control\_identifier>}$ is modeled for every "*<control_identifier>*" specified in the radiators input data (see Section 9.1.2). In Table 9.1, we define the symbols we use to denote a particular heat flux and the state it is influencing. Note that several of the EHF models may model heat fluxes to the same state. We use the notation "$+=$" to denote that the right-hand side is *added* to the heat flux on the left-hand side (and not set equal to). That is, if the heat fluxes to zone i are

written as

$$q_Z^i \mathrel{+}= a^i v_{\mathrm{IG},<\mathit{disturbance\_identifier}>} \tag{9.2}$$

$$q_Z^i \mathrel{+}= a^i u_{\mathrm{Rad},<\mathit{control\_identifier}>} \ , \tag{9.3}$$

this is equivalent to writing

$$q_Z^i = a^i v_{\mathrm{IG},<\mathit{disturbance\_identifier}>} + a^i u_{\mathrm{Rad},<\mathit{control\_identifier}>} \ . \tag{9.4}$$

Table 9.1: This table lists the EHFs, the state they apply to, and the state's location.

EHF	State	Location
q_Z^i	x_Z^i	Zone i
$q_{\mathrm{BE},j,L,l}$	$x_{\mathrm{BE},j,L,l}$	Layer l of building element j.
$q_{\mathrm{BEo},j}$	$x_{\mathrm{BEo},j}$	j-th building element's outermost layer.
$q_{\mathrm{BEi},j}$	$x_{\mathrm{BEi},j}$	j-th building element's innermost layer.

9.1.1 Internal Gains

This EHF model considers internal gains due to occupants, lighting, and appliances. The heat gains are modeled to be purely convective (i.e. their influence is directly added to the zone states). The internal gains are considered as disturbances in $[\mathrm{W/m^2}]$.

9.1.1.1 Input Data

Table 9.2 shows the structure of the file specifying the internal gains EHF model. Its fields are described in Table 9.3. This EHF model models no costs or constraints, hence no costs and constraints parameters are shown.

Table 9.2: File structure of the internal gains EHF model.

zone_identifier	disturbance_identifier
. . .	. . .
. . .	. . .

Table 9.3: Fields of the internal gains EHF model input data file.

Field	Description
zone_identifier	Must be an existing zone identifier. Not all zones need to be specified. The same zone can be influenced by multiple distinct <*disturbance_identifier*>.
disturbance_identifier	An identifier string starting with a letter and only containing alphanumeric characters and "_". For every distinct identifier a corresponding disturbance is created.

9.1.1.2 Heat Flux Model

Table 9.4 shows the nomenclature used in this section.

Table 9.4: Nomenclature.

Symbol	Description
Disturbances	
$v_{\text{IG},<disturbance\_identifier>}$	Internal gains due to equipment and occupants for every distinct $<disturbance\_identifier>$ specified in the input data file (Table 9.3). In $[\text{W/m}^2]$.
Model parameters	
a^i	Area of zone i. From thermal model data. In $[\text{m}^2]$.
Other nomenclature	
$\mathcal{Z}^{\text{IG}}$	Set of all zones for which internal gains have been specified in the input data file (Table 9.3).

Internal gains heat flux

for $i \in \mathcal{Z}^{\text{IG}}$
    for all $<disturbance\_identifier>$ corresponding to zone i
        $q_{\text{Z}}^i \; += a^i v_{\text{IG},<disturbance\_identifier>}$
    end
end

9.1.2 Radiators

This EHF model considers heat gains from radiators. The heat gains are modeled to be purely convective (i.e. their influence is directly added to the zone states). The radiator heat gains are considered as control inputs in $[\text{W/m}^2]$.

9.1.2.1 Input Data

Table 9.5 shows the structure of the file specifying the radiators EHF model. Its fields are described in Table 9.6. Finally, Table 9.7 shows the costs and constraints parameters that must be part of `constrParam` and `costsParam`, respectively, when generating the costs and constraints.

Table 9.5: File structure of the radiator EHF model.

zone_identifier	control_identifier
. . .	. . .
. . .	. . .

Table 9.6: Fields of the radiator EHF model input data file.

Field	Description
zone_identifier	Must be an existing zone identifier. Not all zones need to be specified.
control_identifier	An identifier string starting with a letter and only containing alphanumeric characters and "_". For every identifier a corresponding control input is created.

Table 9.7: Parameters that must be part of `constrParam` and `costsParam`, respectively, when generating the costs and constraints.

Parameter Name	Description
Constraints	
Q_Rad_<*control_identifier*>_max	Maximum heating power. Must be specified for every distinct <*control_identifier*> specified in the input data file (Table 9.5). In [W/m^2].
Costs	
Ts	Sampling time. In [h].
costPerJouleHeated	Costs per Joule heating power [1/J].

9.1.2.2 Heat Flux Model

Table 9.8 shows the nomenclature used in this section.

Table 9.8: Nomenclature.

Symbol	Description
Control inputs	
$u_{\mathrm{Rad},<control\_identifier>}$	Radiator heating power for every <*control_identifier*> specified in the input data file (Table 9.6). In [W/m^2].
Parameters	
a^i	Area of zone i. From thermal model data. In [m^2].
T_s	Value of Ts (see Table 9.7).
$Q_{\mathrm{Rad},<control\_identifier>,\max}$	Value of Q_Rad_<*control_identifier*>_max (see Table 9.7).
c_{Rad}	Value of costPerJouleHeated (see Table 9.7).
Other nomenclature	
$\mathcal{Z}^{\mathrm{Rad}}$	Set of all zones for which radiators have been specified in the input data file (Table 9.6).
J_{Rad}	Total costs related to the use of radiators.

Radiator heat flux

Conductive heat transfer from ground.
for $i \in \mathcal{Z}^{\mathrm{Rad}}$
    for all <*control_identifier*> corresponding to zone i
        $q^i_{\mathrm{Z}} \mathrel{+}= a^i u_{\mathrm{Rad},<control\_identifier>}$
    end
end

9.1.2.3 Costs and Constraints

Costs

for $i \in \mathcal{Z}^{\text{Rad}}$
    for all $<control\_identifier>$ corresponding to zone i
        $J_{\text{Rad}} \mathrel{+}= c_{\text{Rad}} a^i u_{\text{Rad},<control\_identifier>}(3600 \cdot T_s)$
    end
end

Constraints

for all $<control\_identifier>$
    $0 \le u_{\text{Rad},<control\_identifier>} \le Q_{\text{Rad},<control\_identifier>,\text{max}}$
end

9.1.3 Building Hull

This EHF model considers convective and radiation heat transfer to all opaque facade parts as well as convective and radiation heat transfer through windows to the zones. Additionally, this EHF model models air infiltration through the building hull and the conductive heat exchange of building elements with a *ground* boundary condition (see Section 4.3).

Global solar radiation onto the facades is modeled as disturbance inputs in $[\text{W/m}^2]$. Solar heat gains to the opaque facade parts are modeled by an absorption coefficient scaling the global solar radiation. Thermal radiation exchange of the opaque facade parts is considered in the convective coefficients. Solar heat gains through windows are considered by scaling the incident solar radiation with a constant Solar Heat Gain Coefficient (SHGC) and the current blinds position (if present, modeled as a controllable gain between 0 and 1). The primary solar heat gains (the transmitted radiation) are distributed among the innermost building element layers proportionally to their surface area while the secondary heat gains (due to radiation absorbed by the windows and frames) are added to the zone air. Infiltration is modeled as a fixed air change rate to the zones.

9.1.3.1 Input Data

Table 9.9 shows the file structure of the building hull model input data. It contains three parts identified by facade_solar_group, window_solar_group, and infiltration_specification, respectively. Their fields are described separately in the Tables 9.10, 9.11, and 9.12, respectively. Finally, Table 9.13 shows the costs and constraints parameters that must be part of constrParam and costsParam, respectively, when generating the costs and constraints.

Table 9.9: File structure of the building hull EHF model. ***: secondary_gains_fraction**

facade_solar_group	buildingelement_identifier	disturbance_identifier	absorptance	
	. . .	. . .	. . .	
	. . .	. . .	. . .	
window_solar_group	**buildingelement_identifier**	**disturbance_identifier**	**control_identifier**	*****
	. . .	. . .	. . .	. . .
	. . .	. . .	. . .	. . .
infiltration_specification	**zone_identifier**	**airchangerate**		
	. . .	. . .		
	. . .	. . .		

Table 9.10: Fields of the window_solar_group part of the building hull EHF model input data file.

Field	Description
buildingelement_identifier	An identifier of an existing building element that has an *ambient* boundary condition (see Section 4.3). All building elements that have an *ambient* boundary condition must appear exactly once in this list.
disturbance_identifier	An identifier string starting with a letter and only containing alphanumeric characters and "_". For every identifier a corresponding solar radiation disturbance is created.
absorptance	Numerical value in [0,1]. Models the fraction of the solar radiation absorbed by the outermost layer of the corresponding building element.

Table 9.11: Fields of the facade_solar_group part of the building hull EHF model input data file.

Field	Description
buildingelement_identifier	Must be an identifier of an existing building element that has a window. All building elements that have a window must appear exactly once in this list.
disturbance_identifier	An identifier string starting with a letter and only containing alphanumeric characters and "_". For every identifier a corresponding solar radiation disturbance is created.
control_identifier	An identifier string starting with a letter and only containing alphanumeric characters and "_". For every identifier a corresponding blinds control input is created.
secondary_gains_fraction	Numerical value in $[0, 1]$. Specifying the fraction of the total solar heat gains which is added to the zone node (i.e. secondary heat gains).

Table 9.12: Fields of the infiltration_specification part of the building hull EHF model input data file.

Field	Description
zone_identifier	Must be an identifier of an existing zone. Every identifier most appear at most once.
airchangerate	Air change rate per hour. The volumetric infiltration flow in $[m^3/s]$ is calculated as the product of the air change rate and the zone's volume divided by 3600.

Table 9.13: Parameters that must be part of `constrParam` and `costsParam`, respectively, when generating the costs and constraints.

Parameter Name	Description
Constraints	
BPos_<*control_identifier*>_max	Maximum blind position. Must be specified for every distinct <*control_identifier*> in the input data file (Table 9.9). Must lie in [0,1].
BPos_<*control_identifier*>_min	Minimum blind position. Must be specified for every distinct <*control_identifier*> in the input data file (Table 9.9). Must lie in [0,1].

9.1.3.2 Heat Flux Model

Table 9.14 shows the nomenclature used in this section.

Table 9.14: Parameter table of the air handling unit EHF model.

Symbol	Description
Control inputs	
$u_{\text{blinds},<control\_identifier>}$	Blinds position control input corresponding to <*control_identifier*>. [-].
Disturbances	
v_{AmbT}	Ambient temperature. [°C].
v_{GndT}	Ground temperature. [°C].
$v_{\text{Sol},<disturbance\_identifier>}$	Global solar radiation on the facade disturbance corresponding to <*disturbance_identifier*>. [W/m²].
Model parameters	
$\rho_{\text{BEo},j}$	Specific thermal resistance of the j-th building element's outermost layer. [mK/W]. From thermal model data.
$d_{\text{BEo},j}$	Thickness of the j-th building element's outermost layer. [m]. From thermal model data.
$f_{\text{secHG},j}$	Secondary heat gain fraction of the j-th building element's window. [-]. From EHF model input data (Table 9.11).
$f_{\text{SHGC},j}$	Solar heat gain coefficient of the j-th building element's window. [-]. From thermal model data.
$a_{\text{BE},j}$	Net area of the j-th building element (i.e. discounting window and frame area). In [m²]. From thermal model data.
$\alpha_{\text{BEo},j}$	Convective coefficient between the j-th building element's outermost layer and ambient air. In [W/m²K]. From thermal model data.
$a_{\text{win},j}$	(Glass) area of the j-th building element's window. In [m²]. From thermal model data.
$a_{\text{frame},j}$	Area of the j-th building element's window frame. In [m²]. From thermal model data.
$\gamma_{\text{BEo},j}$	Solar absorptance of the j-th building element's outermost layer. [-]. From EHF model input data (Table 9.10).
$a^{i}_{\text{BE,tot}}$	Total area of all building elements of zone i (not including no-mass constructions). In [m²]. From thermal model data.

Continued on next page

Table 9.14 – continued from previous page

γ_{infilt}^i	Air change rate (zone volumes per hour) of zone i. In [1/h]. From EHF model input data (Table 9.12).
$U_{\text{win},j}$	Combined frame and window heat transfer coefficient of the j-th building element. In [W/m^{2}K]. From thermal model data.
V_{Z}^i	Volume of zone i. [m^3]. From thermal model data.
c_{air}	Heat capacity of air (assumed independent of the temperature). In [J/kgK]. From standard gas properties.
ρ_{air}	Heat capacity of air (assumed independent of the temperature). In [kg/m^3]. From standard gas properties.
$b_{\text{Pos},<control\_identifier>,\text{max}}$	Value of BPos_<*control_identifier*>_max (see Table 9.13).
$b_{\text{Pos},<control\_identifier>,\text{min}}$	Value of BPos_<*control_identifier*>_min (see Table 9.13).
Other nomenclature	
$\mathcal{B}_{\text{amb}}$	Set of all building elements which have an *ambient* boundary condition. From thermal model data.
$\mathcal{B}_{\text{win}}$	Set of all building elements which have an *ambient* boundary condition and contain a window. From thermal model data.
$\mathcal{B}_{\text{gnd}}$	Set of all building elements which have an *ground* boundary condition. From thermal model data.
$\mathcal{B}_{\text{Z},i}$	Set of all building elements adjacent to zone i. From thermal model data.
$\mathcal{Z}_{\text{inf}}$	Set of all zones for which infiltration has been specified in the input data file (Table 9.12).

Convective/conductive heat flux

Conductive heat transfer from ground.

for $j \in \mathcal{B}_{\text{gnd}}$

    compute thermal resistance $R = \rho_{\text{BEo},j} \dfrac{d_{\text{BEo},j}}{2}$

    $q_{\text{BEo},j} \mathrel{+}= \dfrac{a_{\text{BE},j}}{R}(v_{\text{GndT}} - x_{\text{BEo},j})$

end

Convective/conductive heat transfer to opaque facade parts

for $j \in \mathcal{B}_{\text{amb}}$

    compute total thermal resistance $R = \dfrac{1}{\alpha_{\text{BEo},j}} + \rho_{\text{BEo},j} \dfrac{d_{\text{BEo},j}}{2}$

    $q_{\text{BEo},j} \mathrel{+}= \dfrac{a_{\text{BE},j}}{R}(v_{\text{AmbT}} - x_{\text{BEo},j})$

end

Convective/conductive heat transfer through windows to the zones

for $j \in \mathcal{B}_{\text{win}}$

    determine zone i to which building element j is adjacent

    $q_{\text{Z}}^i \mathrel{+}= U_{\text{win},j}(a_{\text{win},j} + a_{\text{frame},j})(v_{\text{AmbT}} - x_{\text{Z}}^i)$

end

Heat flux due to solar radiation

for $j \in \mathcal{B}_{\mathrm{amb}}$

    Determine $<$*disturbance_identifier*$>$ corresponding to building element j

    $q_{\mathrm{BEo},j} \;\;+= a_{\mathrm{BE},j}\gamma_{\mathrm{BEo},j}v_{\mathrm{Sol},<disturbance\_identifier>}$

end

for $j \in \mathcal{B}_{\mathrm{win}}$

    determine zone i to which building element j is adjacent

    determine $<$*disturbance_identifier*$>$ corresponding to building element j

    if building element j has a $<$*control_identifier*$>$

        determine $<$*control_identifier*$>$ corresponding to building element j

        $q_{\mathrm{Z}}^{i} += f_{\mathrm{secHG},j}a_{\mathrm{win},j}f_{\mathrm{SHGC},j}v_{\mathrm{Sol},<disturbance\_identifier>}\,u_{\mathrm{blinds},<control\_identifier>}$

        for $k \in \mathcal{B}_{\mathrm{Z},i}$

$$q_{\mathrm{BEi},k} += \frac{a_{\mathrm{BE},k}}{a_{\mathrm{BE,tot}}^{i}}\left(1 - f_{\mathrm{secHG},j}\right)a_{\mathrm{win},j}f_{\mathrm{SHGC},j}v_{\mathrm{Sol},<disturbance\_identifier>}\,u_{\mathrm{blinds},<control\_identifier>}$$

        end

    else

        $q_{\mathrm{Z}}^{i} \;\;+= f_{\mathrm{secHG},j}a_{\mathrm{win},j}f_{\mathrm{SHGC},j}v_{\mathrm{Sol},<disturbance\_identifier>}$

        for $k \in \mathcal{B}_{\mathrm{Z},i}$

$$q_{\mathrm{BEi},k} += \frac{a_{\mathrm{BE},k}}{a_{\mathrm{BE,tot}}^{i}}\left(1 - f_{\mathrm{secHG},j}\right)a_{\mathrm{win},j}f_{\mathrm{SHGC},j}v_{\mathrm{Sol},<disturbance\_identifier>}$$

        end

    end

end

Infiltration

for $i \in \mathcal{Z}_{\mathrm{inf}}$

    $q_{\mathrm{Z}}^{i} += \frac{1}{3600}\rho_{\mathrm{air}}c_{\mathrm{air}}\gamma_{\mathrm{infilt}}^{i}V_{\mathrm{Z}}^{i}\left(v_{\mathrm{AmbT}} - x_{\mathrm{Z}}^{i}\right)$

end

9.1.3.3 Costs and Constraints

Constraints

for every $<$*control_identifier*$>$

    $b_{\mathrm{min},<control\_identifier>} \leq u_{\mathrm{blinds},<control\_identifier>} \leq b_{\mathrm{max},<control\_identifier>}$

end

9.1.4 Building Element Heat Fluxes

This EHF model considers heating and cooling from building systems located within layers of building elements, e.g. TABS, floor heating, etc.. The heating/cooling systems are modeled as control inputs in $[W/m^2]$ and act directly on the states of the corresponding layers.

9.1.4.1 Input data

Table 9.15 shows the file structure of the building element heat flux model input data. Its fields are described in Table 9.16. Finally, Table 9.17 shows the costs and constraints parameters that must be part of `constrParam` and `costsParam`, respectively, when generating the costs and constraints.

Table 9.15: File structure of the building element heat flux model.

buildingelement_identifier	layer_number	control_identifier	heating_cooling_selection
...	...	...	...
...	...	...	...

Table 9.16: Fields of the building element heat flux EHF model input data file.

Field	Description
buildingelement_identifier	An identifier of an existing building element.
layer_number	Positive integer. Number of the building element's layer to which the heating/cooling is applied.
control_identifier	An identifier string starting with a letter and only containing alphanumeric characters and "_". For every identifier a corresponding heating/cooling control input is created.
heating_cooling_selection	Either 'h' or 'c'. Determines whether the input is cooling or heating. Must be the same for a particular *<control_identifier>*.

Table 9.17: Parameters that must be part of `constrParam` and `costsParam`, respectively, when generating the costs and constraints.

Parameter Name	Description
Constraints	
Q_BEH_*<control_identifier>*_max	Maximum heating power for every distinct *<control_identifier>* specified in the input data file (Table 9.15). $[W/m^2]$.
Costs	
Ts	Sampling time. In [h].
costPerJouleHeated	Costs per Joule heating power [1/J].
costPerJouleCooled	Costs per Joule cooling power [1/J].

9.1.4.2 Heat Flux Model

Table 9.18 shows the nomenclature used in this section.

Table 9.18: Nomenclature.

Symbol	Description
Control inputs	
$u_{\mathrm{BEH},<control\_identifier>}$	Heating/cooling power corresponding to $<control\_identifier>$. In [W/m²].
Model parameters	
$a_{\mathrm{BE},j}$	Area of building element j. In [m^2]. From thermal model data.
T_s	Value of Ts (see Table 9.17).
c_{heat}	Value of costPerJouleHeated (see Table 9.17).
c_{cool}	Value of costPerJouleCooled (see Table 9.17).
$Q_{<control\_identifier>,\mathrm{Max}}$	Value of Q_BEH_$<control\_identifier>$_max (see Table 9.17).
Other nomenclature	
$\mathcal{B}_{\mathrm{BEH},<control\_identifier>}$	Set of all building elements that are influenced by $<control\_identifier>$. From EHF model input data (Table 9.16)
J_{BEH}	Total costs related to the use of heating/cooling systems located within building elements.

Heat flux to building elements

for all $<control\_identifier>$
    for $j \in \mathcal{B}_{\mathrm{BEH},<control\_identifier>}$
        determine layer l of building element j on which the heat flux is acting
        if $<control\_identifier>$ is a heating input
            $q_{\mathrm{BE},j,L,l} \mathrel{+}= a_{\mathrm{BE},j} u_{\mathrm{BEH},<control\_identifier>}$
        else
            $q_{\mathrm{BE},j,L,l} \mathrel{-}= a_{\mathrm{BE},j} u_{\mathrm{BEH},<control\_identifier>}$
        end
    end
end

9.1.4.3 Costs and Constraints

Costs

for every $<control\_identifier>$
    if $<control\_identifier>$ is a heating input
        $J_{\mathrm{BEH}} \mathrel{+}= c_{\mathrm{heat}} u_{\mathrm{BEH},<control\_identifier>}(3600 \cdot T_s)$
    else
        $J_{\mathrm{BEH}} \mathrel{+}= c_{\mathrm{cool}} u_{\mathrm{BEH},<control\_identifier>}(3600 \cdot T_s)$
    end
end

Constraints

for every $<control\_identifier>$
$\qquad 0 \leq u_{\mathrm{BEH},<control\_identifier>} \leq Q_{<control\_identifier>,\mathrm{Max}}$
end

9.1.5 Air Handling Unit

This EHF models an air handling unit. Since the supply ventilation ducts are often located in different zones than the return ventilation ducts, two physical effects due to the AHU operation are modeled: i) the direct heat flux due to the air flow directly from the AHU to the room; ii) the zone-to-zone air exchange heat flux.

The individual components of the AHU are depicted in Figure 9.1. At a minimum, the model includes a controlled unconditioned air mass flow from the ambient air to the zones. Additionally, it is possible to include a combination of the following: A heater and/or cooler in the supply air (modeled as simple positive / negative heat fluxes), an energy recovery (ERC) system (i.e. a heat exchanger between return and supply air) and an evaporative cooler[1]. To any zone a flow fraction can be assigned defining how much of the total AHU air mass flow enters it. Moreover, it is possible to define air flows between zones by additionally specifying flow fractions originating from other zones. We present here simply the final model, its derivation is described in [42].
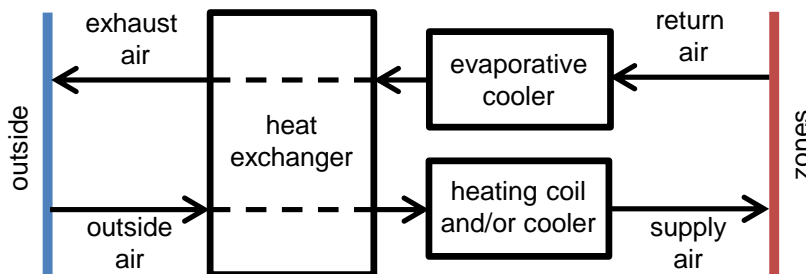

Figure 9.1: AHU schematic.

9.1.5.1 Input data

Table 9.19 shows the structure of the file specifying the AHU EHF model. It contains tow parts identified by AHU_specification and airflow_specification, respectively. Their fields are described separately in the Tables 9.20 and 9.21. Finally, Table 9.22 shows the costs and constraints parameters that must be part of `constrParam` and `costsParam`, respectively, when generating the costs and constraints.

---

[1]An evaporative cooler cools the return air by spraying water into it. The cold is then added to the supply air via the ERC (this implies that the evaporative cooler cannot be present without the ERC).

Table 9.19: File structure of the air handling unit EHF model.

AHU_specification	key	value	
	hasERC	...	
	ERCEfficiency	...	
	hasEvapCooler	...	
	evapCoolerEfficiency	...	
	hasHeater	...	
	hasCooler	...	
	has_AHU_Tin	...	
airflow_specification	**zone_identifier**	**from_identifier**	**flow_fraction**
	...	...	...
	...	...	...

Table 9.20: Fields of the AHU_specification part of the AHU EHF model input data file.

Field	Description
hasERC	Binary value (0/1). Specifies whether the AHU has an ERC.
ERCEfficiency	Numerical value in $[0, 1]$. Specifies the efficiency of the AHU's ERC.
hasEvapCooler	Binary value (0/1). Determines whether the AHU has an evaporative cooler in the return path.
evapCoolerEfficiency	Numerical value in $[0, 1]$. Specifies the efficiency of the evaporative cooler.
hasHeater	Binary value (0/1). Specifies whether a heater is installed in the supply path.
hasCooler	Binary value (0/1). Specifies whether a cooler is installed in the supply path.

Table 9.21: Fields of the airflow_specification part of the AHU EHF model input data file.

Field	Description
zone_identifier	Zone identifier. Zone into which the air flow of magnitude flow_fraction and from source from_identifer is considered.
from_identifier	Either a zone identifier or 'AHU'. Describes the air flow source into the specific zone.
flow_fraction	Numerical value in $[0, 1]$. Fraction of the the total AHU air mass flow coming from the corresponding from_identifier source. Sum of air flow fractions, where from_identifier is 'AHU' must be equal to 1 and for all zones $\Delta\gamma_{\text{inflow}} = $ "total inflow" $-$ "total outflow" ≥ 0. The remaining $\Delta\gamma_{\text{inflow}}$ is assumed to be air returned to the AHU.

Table 9.22: Parameters that must be part of `constrParam` and `costsParam`, respectively, when generating the costs and constraints.

Parameter Name	Description
Constraints	
T_supply_max	Maximum supply air temperature. In [°C].
T_supply_min	Minimum supply air temperature. In [°C].
Q_heater_max	Maximum supplied heating power by the heater. In [W].
Q_cooler_max	Maximum supplied cooling power by the cooler. In [W].
mdot_min	Minimum supplied air flow. In [kg/s].
mdot_max	Maximum supplied air flow. In [kg/s].
v	Current disturbance vector.
x	Current state of the system.
Costs	
Ts	Sampling time. In [h].
costPerJouleHeated	Costs per Joule heating power [1/J].
costPerJouleCooled	Costs per Joule cooling power of the cooling coil [1/J].
costPerKgAirTransported	Costs per kg air transported [1/kg].
costPerKgCooledByEvapCooler	Costs per kg air cooled by the evaporative cooler at maximum usage [1/kg].

9.1.5.2 Heat Flux Model

Table 9.23 contains the nomenclature used in this section. Additionally, we use the notation $\{0,1\}^{(.)}$ where "(.)" either is "H", "C", "EvapC", or "ERC". The expression should be read as "0" if according to the fields in Table 9.6. the corresponding component is unavailable and as "1" otherwise. For example, suppose the value entered for "hasERC" in the input data file is 0. Then the expression $\{0,1\}^{ERC} u_{AHU,\dot{m},ERC} + u_{AHU,\dot{m},NoERC}$ should be read as $u_{AHU,\dot{m},NoERC}$. If "hasERC" is 1, then the expression should be read as $u_{AHU,\dot{m},ERC} + u_{AHU,\dot{m},NoERC}$.

Table 9.23: Nomenclature.

Symbol	Description
Control inputs	
$u_{AHU,\dot{m},ERC}$	Air mass flow through fully active ERC. In [kg/s].
$u_{AHU,\dot{m},NoERC}$	Air mass flow bypassing ERC. In [kg/s].
$u_{AHU,\dot{m},EvapC}$	Air mass flow through fully active evaporative cooler. In [kg/s].
$u_{AHU,H}$	Heating power. In [W].
$u_{AHU,C}$	Cooling power. In [W].
Disturbances	
v_{AmbT}	Ambient temperature. In [°C].

Continued on next page

Table 9.23 – continued from previous page

$v_{\Delta wb}$	Drybulb / wetbulb temperature difference in the return air assumed independent of the actual return air temperature. In [°C].
Model parameters	
η_{ERC}	Efficiency of the heat exchanger, i.e. the fraction of the maximum possible heat exchange between supply and return air. [-]. See Table 9.20.
η_{Cool}	Efficiency of the evaporative cooler, i.e. the fraction of the maximum possibly achievable temperature difference $v_{\Delta wb}$. [-]. See Table 9.20.
$\gamma^i_{\mathrm{inflow},j}$	Inflow from zone j to zone i as a fraction of total AHU mass flow rate. Calculated from EHF model input data Table 9.21.
γ^i_{AHU}	AHU inflow to zone i as a fraction of total AHU mass flow rate. Calculated from EHF model input data Table 9.21.
γ^i_{Ret}	AHU inflow from zone i to the AHU as a fraction of total AHU mass flow rate. Calculated from EHF model input data Table 9.21.
c_{air}	Specific heat capacity of air. In [J/(kg K)]. From standard gas properties.
T_s	Value of Ts (see Table 9.22).
$T_{\mathrm{AHU,max}}$	Value of T_supply_max (see Table 9.22)
$T_{\mathrm{AHU,min}}$	Value of T_supply_min (see Table 9.22)
$Q_{\mathrm{AHU,H,max}}$	Value of Q_heater_max (see Table 9.22)
$Q_{\mathrm{AHU,C,max}}$	Value of Q_cooler_max (see Table 9.22)
$\dot{m}_{\mathrm{AHU,min}}$	Value of mdot_min (see Table 9.22)
$\dot{m}_{\mathrm{AHU,max}}$	Value of mdot_max (see Table 9.22)
$\bar{v}$	Value of v (see Table 9.22)
$\bar{x}$	Value of x (see Table 9.22)
$c_{\mathrm{AHU,H}}$	Value of costPerJouleHeated (see Table 9.22)
$c_{\mathrm{AHU,C}}$	Value of costPerJouleCooled (see Table 9.22)
$c_{\mathrm{AHU},\dot{m}}$	Value of costPerKgAirTransported (see Table 9.22)
$c_{\mathrm{AHU,evapC}}$	Value of costPerKgCooledByEvapCooler (see Table 9.22)
Other nomenclature	
$\mathcal{Z}^{\mathrm{all}}$	Set of all zones.
J_{AHU}	Total costs related to the operation of the AHU.

AHU influence on directly supplied zones

for $i \in \mathcal{Z}^{\mathsf{sup}}$

$$q_{\mathsf{Z}}^i \mathrel{+}= \gamma_{\mathsf{AHU}}^i \Bigg(c_{\mathsf{air}} \big(v_{\mathsf{AmbT}} - x_{\mathsf{Z}}^i \big) \big(\{0,1\}^{\mathsf{ERC}} u_{\mathsf{AHU},\dot{m},\mathsf{ERC}} + u_{\mathsf{AHU},\dot{m},\mathsf{NoERC}} \big) + \{0,1\}^{\mathsf{H}} u_{\mathsf{AHU},\mathsf{H}}$$

$$- \{0,1\}^{\mathsf{C}} u_{\mathsf{AHU},\mathsf{C}} + \{0,1\}^{\mathsf{ERC}} u_{\mathsf{AHU},\dot{m},\mathsf{ERC}} c_{\mathsf{air}} \eta_{\mathsf{ERC}} \Bigg(\sum_{j \in \mathcal{Z}^{\mathsf{All}}} \gamma_{\mathsf{Ret}}^j x_{\mathsf{Z}}^j - v_{\mathsf{AmbT}} \Bigg)$$

$$- \{0,1\}^{\mathsf{EvapC}} u_{\mathsf{AHU},\dot{m},\mathsf{EvapC}} c_{\mathsf{air}} \eta_{\mathsf{ERC}} \eta_{\mathsf{Cool}} v_{\Delta wb} \Bigg)$$

end

Air flow model between zones

for $i \in \mathcal{Z}_{\mathsf{all}}$

$$q_{\mathsf{Z}}^i \mathrel{+}= c_{\mathsf{air}} \big(\{0,1\}^{\mathsf{ERC}} u_{\mathsf{AHU},\dot{m},\mathsf{ERC}} + u_{\mathsf{AHU},\dot{m},\mathsf{NoERC}} \big) \sum_{j \in \mathcal{Z}^{\mathsf{All}}} \gamma_{\mathsf{inflow},j}^i \big(x_{\mathsf{Z}}^j - x_{\mathsf{Z}}^i \big)$$

end

9.1.5.3 Costs and Constraints

Costs

$$J_{\mathsf{AHU}} = \Big(c_{\mathsf{AHU},\dot{m}} \big(\{0,1\}^{\mathsf{ERC}} u_{\mathsf{AHU},\dot{m},\mathsf{ERC}} + u_{\mathsf{AHU},\dot{m},\mathsf{NoERC}} \big)$$

$$+ \{0,1\}^{\mathsf{H}} c_{\mathsf{AHU},\mathsf{H}} u_{\mathsf{AHU},\mathsf{H}}$$

$$+ \{0,1\}^{\mathsf{C}} c_{\mathsf{AHU},\mathsf{C}} u_{\mathsf{AHU},\mathsf{C}}$$

$$+ \{0,1\}^{\mathsf{EvapC}} c_{\mathsf{AHU},\mathsf{EvapC}} u_{\mathsf{AHU},\dot{m},\mathsf{EvapC}} \Big) \big(3600 \cdot T_s \big)$$

Constraints

if $\{0,1\}^{\text{ERC}}$

$\quad \dot{m}_{\text{AHU,min}} \leq u_{\text{AHU},\dot{m},\text{ERC}} + u_{\text{AHU},\dot{m},\text{NoERC}} \leq \dot{m}_{\text{AHU,max}}$

$\quad 0 \leq u_{\text{AHU},\dot{m},\text{ERC}}$

$\quad 0 \leq u_{\text{AHU},\dot{m},\text{NoERC}}$

else

$\quad \dot{m}_{\text{AHU,min}} \leq u_{\text{AHU},\dot{m},\text{ERC}} + u_{\text{AHU},\dot{m},\text{NoERC}} \leq \dot{m}_{\text{AHU,max}}$

$\quad 0 \leq u_{\text{AHU},\dot{m},\text{NoERC}}$

end

if $\{0,1\}^{\text{H}}$

$\quad 0 \leq u_{\text{AHU,H}} \leq Q_{\text{AHU,H,max}}$

end

if $\{0,1\}^{\text{C}}$

$\quad 0 \leq u_{\text{AHU,C}} \leq Q_{\text{AHU,C,max}}$

end

if $\{0,1\}^{\text{EvapC}}$

$\quad 0 \leq u_{\text{AHU},\dot{m},\text{EvapC}} \leq u_{\text{AHU},\dot{m},\text{ERC}}$

end

$$c_{\text{air}}\left(\{0,1\}^{\text{ERC}} u_{\text{AHU},\dot{m},\text{ERC}} + u_{\text{AHU},\dot{m},\text{NoERC}}\right) T_{\text{AHU,min}} \leq$$
$$c_{\text{air}} \bar{v}_{\text{AmbT}}\left(\{0,1\}^{\text{ERC}} u_{\text{AHU},\dot{m},\text{ERC}} + u_{\text{AHU},\dot{m},\text{NoERC}}\right)$$
$$+ \{0,1\}^{\text{H}} u_{\text{AHU,H}} - \{0,1\}^{\text{C}} u_{\text{AHU,C}}$$
$$+ \{0,1\}^{\text{ERC}} c_{\text{air}} \eta_{\text{ERC}} u_{\text{AHU},\dot{m},\text{ERC}}\left(\bar{T}_{\text{Return}} - \bar{v}_{\text{AmbT}}\right)$$
$$- \{0,1\}^{\text{EvapC}} c_{\text{air}} \eta_{\text{ERC}} \eta_{\text{Cool}} v_{\Delta wb} u_{\text{AHU},\dot{m},\text{EvapC}}$$
$$\leq c_{\text{air}}\left(\{0,1\}^{\text{ERC}} u_{\text{AHU},\dot{m},\text{ERC}} + u_{\text{AHU},\dot{m},\text{NoERC}}\right) T_{\text{AHU,max}} \,,$$

where $\bar{T}_{\text{Return}} = \sum\limits_{k \in \mathcal{Z}^{\text{All}}} f^k_{\text{ret,AHU}} \bar{x}^k_{\text{Z}}$ and $\bar{v}_{\text{AmbT}}$ have been calculated from $\bar{v}$ and $\bar{x}$.

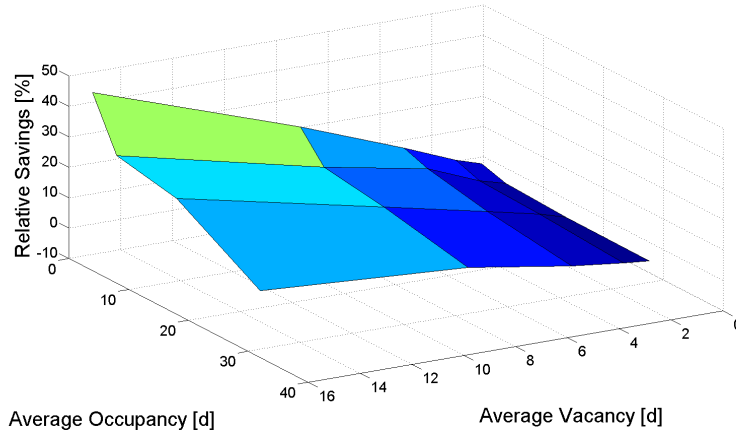## 9.2 Energy Savings as a Function of Occupancy and Vacancy Lengths

Figure 9.2: Homogeneous occupancy. The relative energy savings $\Delta E_{li,-}^{std}$ are plotted versus different values of (β_1, β_2) for the parameters $P = $ (Building Case 1, HVAC system I, il, win).

In order to analyze the behavior of energy use depending on the average occupancy β_1 and average vacancy β_2 the relative energy savings $\Delta E_{li,-}^{std}$ are plotted versus all combinations of $\beta_1 \in \{2, 4, 8, 16\}$ and $\beta_2 \in \{4, 8, 16, 32\}$ and the parameters $P = $ (Building Case 1, HVAC system I, il, win). The behavior of the savings with respect to changes in vacancy and occupancy appears to be monotonous. As can be expected, for increasing vacancy and decreasing occupancy values the relative energy consumption increases. For the investigated range of parameters and the investigated case the dependency appears to be approximately linear. This observation justifies the choice of only three different (β_1, β_2) combinations, i.e. (1,10), (1,5), (5,10), used in all investigations.

9.3 Absolute Energy Savings of Occupancy Information

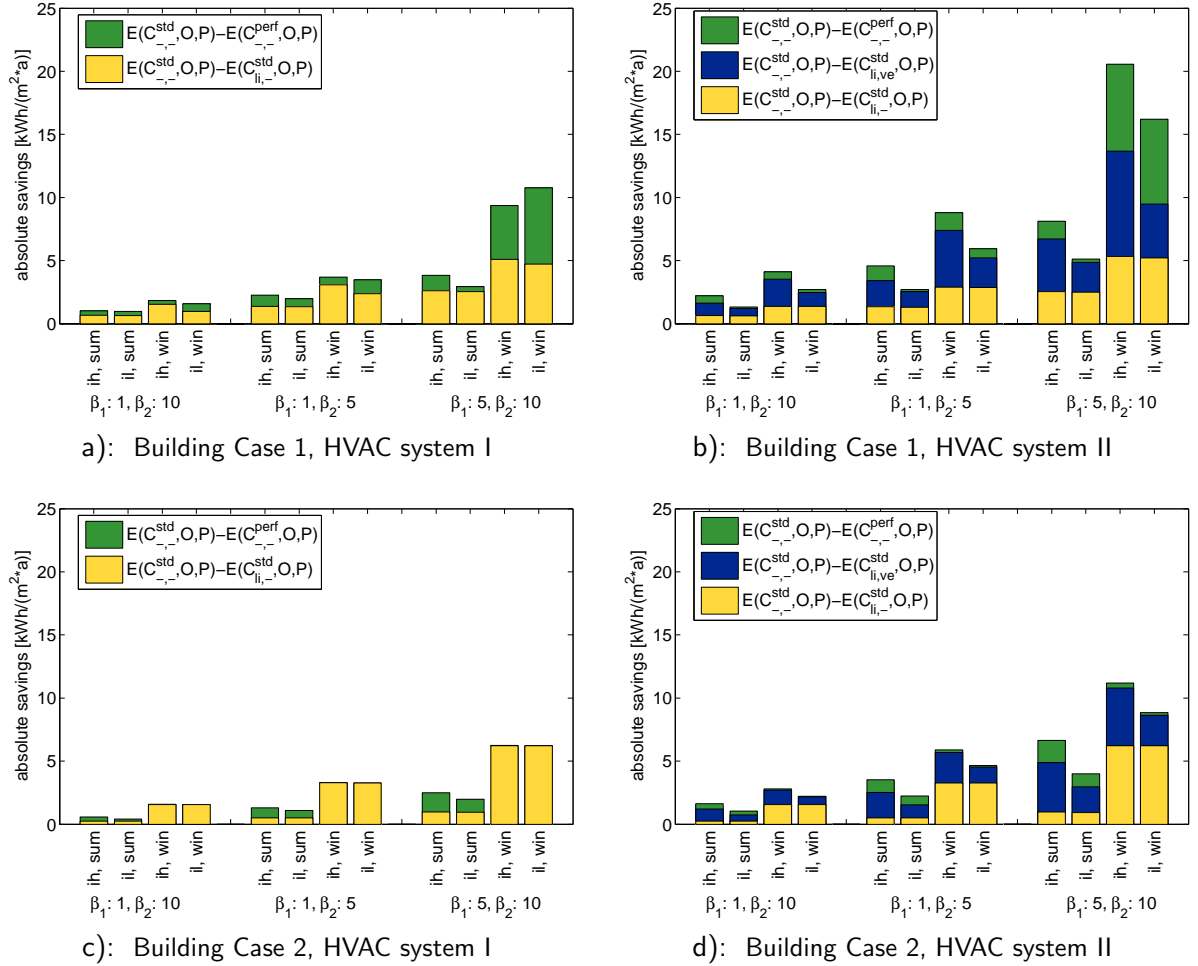Figure 9.3 shows absolute savings in the homogeneous occupancy case.

Figure 9.3: Homogeneous occupancy. The absolute energy savings $E(C_{-,-}^{\text{std}}, O, P) - E(C_{-,-}^{\text{perf}}, O, P)$, $E(C_{-,-}^{\text{std}}, O, P) - E(C_{\text{li,ve}}^{\text{std}}, O, P)$ and $E(C_{-,-}^{\text{std}}, O, P) - E(C_{\text{li,-}}^{\text{std}}, O, P)$ are plotted in [kWh/(m^2a)] for all $P \in \mathbb{P}$ and all $O_{(\beta_1, \beta_2)}^{\text{hom}} \in \mathbb{O}$, i.e. for all building cases and HVAC system, both seasons {sum,win}, both internal gains levels {il,ih}, and the three combinations of (β_1, β_2).

Bibliography

[1] Bert Metz, Ogunlade Davidson, Peter Bosch, Rutu Dave, and Leo Meyer (editors). In: Climate Change 2007: Mitigation. Contribution of Working Group III to the fourth assessment report of the Intergovernmental Panel on Climate Change. Technical report, `http://www.ipcc.ch/publications_and_data/publications_ipcc_fourth_assessment_report_wg3_report_mitigation_of_climate_change.htm`.

[2] Luis Pérez-Lombard, José Ortiz, and Christine Pout. A review on buildings energy consumption information. *Energy and buildings*, 40(3):394–398, 2008.

[3] Murthy Balijepalli, Vedanta Pradhan, SA Khaparde, and RM Shereef. Review of demand response under smart grid paradigm. In *Innovative Smart Grid Technologies-India (ISGT India), 2011 IEEE PES*, pages 236–243. IEEE, 2011.

[4] David Sturzenegger, Dimitrios Gyalistras, Manfred Morari, and Roy S. Smith. Semi-automated modular modeling of buildings for model predictive control. *BuildSys'12 Proc. of the Fourth ACM Workshop on Embedded Sensing Systems for Energy-Efficiency in Buildings*, pages 99–106, 2012.

[5] David Sturzenegger, Dimitrios Gyalistras, Vito Semeraro, Manfred Morari, and Roy S Smith. BRCM Matlab toolbox: Model generation for model predictive building control. In *American Control Conference*, pages 1063–1069, Portland, June 2014.

[6] David Sturzenegger, Dominik Keusch, Leonardo Muffato, Dominique Kunz, and R. Smith. Frequency-domain identification of a ventilated room for model-based control. In *IFAC World Congress on Automatic Control*, pages 593–598, Cape Town, South Africa, August 2014.

[7] David Sturzenegger, Dimitrios Gyalistras, Manfred Morari, and Roy S. Smith. Model predictive control of a Swiss office building: Implementation, results and cost-benefit analysis. *IEEE Transactions on Control Systems Technology (conditionally accepted)*.

[8] David Sturzenegger, Dimitrios Gyalistras, Markus Gwerder, Carina Sagerschnig, Manfred Morari, and Roy S. Smith. Model predictive control of a Swiss office building. In *11th REHVA World Congress Clima 2013*, 2013.

[9] Markus Gwerder, Dimitrios Gyalistras, Carina Sagerschnig, Roy S. Smith, and David Sturzenegger. Final report: Use of weather and occupancy forecasts for optimal building climate control Part II: Demonstration (OptiControl-II). Technical report, ETH Zurich, `http://www.opticontrol.ethz.ch/Lit/Gwer_13_Rep-OptiCtrl2FinalRep.pdf`, 2013.

[10] Frauke Oldewurtel, David Sturzenegger, and Manfred Morari. Importance of occupancy information for building climate control. *Applied Energy*, 101:521–532, 2013.

[11] David Sturzenegger, Frauke Oldewurtel, and Manfred Morari. Importance of long-term occupancy information - a validation with real occupancy data. In *11th REHVA World Congress Clima 2013*, 2013.

[12] Frauke Oldewurtel, David Sturzenegger, Göran Andersson, Manfred Morari, and Roy S. Smith. Towards a standardized building assessment for demand response. In *Conference on Decision and Control*, 2013.

[13] Xiaojing Zhang, Georg Schildbach, David Sturzenegger, and Manfred Morari. Scenario-based MPC for energy-efficient building climate control under weather and occupancy uncertainty. In *Control Conference (ECC), 2013 European*, pages 1029–1034. IEEE, 2013.

[14] Frauke Oldewurtel, David Sturzenegger, Peyman Mohajerin Esfahani, Göran Andersson, Manfred Morari, and J. Lygeros. Adaptively Constrained Stochastic Model Predictive Control for Closed-Loop Constraint Satisfaction. In *American Control Conference*, Washington, DC, USA, June 2013.

[15] Markus Gwerder, Stefan Boetschi, Dimitrios Gyalistras, Carina Sagerschnig, David Sturzenegger, Roy Smith, and Bruno Illi. Integrated predictive rule-based control of a Swiss office building. In *11th REHVA World Congress Clima*, 2013.

[16] James B. Rawlings and David Q. Mayne. *Model Predictive Control: Theory and Design*. Nob Hill Publishing, 2009.

[17] Stephen Boyd and Lieven Vandenberghe. *Convex Optimization*. Cambridge University Press, New York, NY, USA, 2004.

[18] Abdul Afram and Farrokh Janabi-Sharifi. Theory and applications of HVAC control systems - A review of model predictive control. *Building and Environment*, 72(0):343 – 355, 2014.

[19] JA Clarke, J Cockroft, S Conner, JW Hand, NJ Kelly, R Moore, T O'Brien, and P Strachan. Simulation-assisted control in building energy management systems. *Energy and buildings*, 34(9):933–940, 2002.

[20] Gregor P Henze, Doreen E Kalz, Simeng Liu, and Clemens Felsmann. Experimental analysis of model-based predictive optimal control for active and passive building thermal storage inventory. *HVAC&R Research*, 11(2):189–213, 2005.

[21] Matthias Schuss, Robert Zach, Kristina Orehounig, and Ardeshir Mahdavi. Empirical evaluation of a predictive simulation-based control method. In *Proceedings of the 12th International IBPSA Conference*, pages 14–16, 2011.

[22] P M Ferreira, A E Ruano, S Silva, and E Z E Conceição. Neural networks based predictive control for thermal comfort and energy savings in public buildings. *Energy and Buildings*, 55:238–251, 2012.

[23] Zaiyi Liao and Arthur L Dexter. An inferential model-based predictive control scheme for optimizing the operation of boilers in building space-heating systems. *Control Systems Technology, IEEE Transactions on*, 18(5):1092–1102, 2010.

[24] Jan Širokỳ, Frauke Oldewurtel, Jiří Cigler, and Samuel Prívara. Experimental analysis of model predictive control for an energy efficient building heating system. *Applied Energy*, 88(9):3079–3087, 2011.

[25] Anil Aswani, Neal Master, Jay Taneja, David Culler, and Claire Tomlin. Reducing transient and steady state electricity consumption in hvac using learning-based model-predictive control. *Proceedings of the IEEE*, 100(1):240–253, 2012.

[26] Yudong Ma, Francesco Borrelli, Brandon Hencey, Brian Coffey, Sorin Bengea, and Philip Haves. Model predictive control for the operation of building cooling systems. *Control Systems Technology, IEEE Transactions on*, 20(3):796–803, 2012.

[27] M Castilla, J D Álvarez, J E Normey-Rico, and F Rodríguez. Thermal comfort control using a non-linear MPC strategy: A real case of study in a bioclimatic building. *Journal of Process Control*, 2013.

[28] Sorin C. Bengea, Anthony D. Kelman, Francesco Borrelli, Russell Taylor, and Satish Narayanan. Implementation of model predictive control for an HVAC system in a mid-size commercial building. *HVAC&R Research*, 20(1):121–135, 2014.

[29] Poul O Fanger and et al. *Thermal comfort. Analysis and applications in environmental engineering.* Copenhagen: Danish Technical Press., 1970.

[30] Frauke Oldewurtel, Alessandra Parisio, Colin N Jones, Dimitrios Gyalistras, Markus Gwerder, Vanessa Stauch, Beat Lehmann, and Manfred Morari. Use of model predictive control and weather forecasts for energy efficient building climate control. *Energy and Buildings*, 45:15–27, 2012.

[31] MM Gouda, S Danaher, and CP Underwood. Building thermal model reduction using nonlinear constrained optimization. *Building and Environment*, 37(12):1255–1265, 2002.

[32] Gabrielle Masy. *Definition and validation of a simplified multizone dynamic building model connected to heating system and HVAC unit.* PhD thesis, Université de Liege, 2008.

[33] James E Braun and Nitin Chaturvedi. An inverse gray-box model for transient building load prediction. *HVAC&R Research*, 8(1):73–99, 2002.

[34] Beat Lehmann, Dimitrios Gyalistras, Markus Gwerder, Katharina Wirth, and Stephan Carl. Intermediate complexity model for model predictive control of integrated room automation. *Energy and Buildings*, 58:250–262, 2013.

[35] Jiří Cigler, Dimitrios Gyalistras, Jan Širokỳ, Vinh-Nghi Tiet, and Lukàš Ferkl. Beyond theory: the challenge of implementing model predictive control in buildings. In *Proceedings of 11th Rehva World Congress, Clima*, 2013.

[36] Gene F. Franklin, Michael L. Workman, and Dave Powell. *Digital Control of Dynamic Systems.* Addison-Wesley Longman Publishing Co., Inc., Boston, MA, USA, 3rd edition, 1997.

[37] Nino Hail. Extension of the BRCM toolbox to include solar calculations, Semester thesis, 2014.

[38] RS Smith and JC Doyle. Closed loop relay estimation of uncertainty bounds for robust control models. 9:57–60, 1993.

[39] EN 15251:2007. Indoor environmental input parameters for design and assessment of energy performance of buildings addressing indoor air quality, thermal environment, lighting and acoustics. European committee for standardization (2007).

[40] Desigo^{TM} system description (2010). Siemens Building Technologies. Document CM110660.

[41] Dimitrios Gyalistras, Carina Sagerschnig, and Markus Gwerder. A multi-stage approach for building and HVAC model validation and its application to a Swiss office building. In *13th International Conference of the International Building Performance Simulation Association*, 2013.

[42] David Sturzenegger. Bilinear modeling for model predictive control of an air handling unit. Technical report, ETH Zurich, 2012. `http://control.ee.ethz.ch/index.cgi?page=publications&action=details&id=4184`.

[43] *Thermal Environmental Conditions for Human Occupancy*. ANSI/ASHRAE Standard 55, 2010.

[44] Athanasios C Antoulas. *Approximation of large-scale dynamical systems*, volume 6. Siam, 2005.

[45] Greg Welch and Gary Bishop. An introduction to the kalman filter. Technical report, 1995. `http://clubs.ens-cachan.fr/krobot/old/data/positionnement/kalman.pdf`.

[46] Vanessa Stauch, Francis Schubiger, and Philippe Steiner. Local weather forecasts and observations. Technical report, 2009. in [50].

[47] Eugene L Maxwell. *A quasi-physical model for converting hourly global horizontal to direct normal insolation*. Solar Energy Research Institute, Golden, CO, 1987.

[48] Richard Perez, Robert Seals, Pierre Ineichen, Ronald Stewart, and David Menicucci. A new simplified version of the perez diffuse irradiance model for tilted surfaces. *Solar energy*, 39(3):221–231, 1987.

[49] Jürg Tödtli, Markus Gwerder, and Beat Lehmann. *TABS-control: Steuerung und Regelung von thermoaktiven Bauteilsystemen [in German]*. Faktor Verlag Zürich, Switzerland, ISBN: 978-3-905711-05-9, 2009.

[50] Dimitrios Gyalistras and Markus Gwerder (editors). Use of weather and occupancy forecasts for optimal building climate control (OptiControl): Two years progress report. Technical report, ETH Zurich and Siemens Building Technologies Division, Siemens Switzerland Ltd., 2009.

[51] DP Bloomfield and DJ Fisk. The optimisation of intermittent heating. *Building and Environment*, 12(1):43–55, 1977.

[52] GR Newsham, A Mahdavi, and I Beausoleil-Morrison. Lightswitch: A stochastic model for predicting office lighting energy consumption. In *Proceedings of Right Light Three, 3rd European Conference on Energy Efficient Lighting*, pages 59–66, 1995.

[53] Denis Bourgeois, Christoph Reinhart, and Iain Macdonald. Adding advanced behavioural models in whole building energy simulation: a study on the total energy impact of manual and automated lighting control. *Energy and Buildings*, 38(7):814–823, 2006.

[54] Bing Dong and Burton Andrews. Sensor-based occupancy behavioral pattern recognition for energy and comfort management in intelligent buildings. In *Proceedings of building simulation*, 2009.

[55] Chenda Liao, Yashen Lin, and Prabir Barooah. Agent-based and graphical modelling of building occupancy. *Journal of Building Performance Simulation*, 5(1):5–25, 2012.

[56] Jessen Page, Darren Robinson, Nicolas Morel, and J-L Scartezzini. A generalised stochastic model for the simulation of occupant presence. *Energy and buildings*, 40(2):83–98, 2008.

[57] Tina Yu. Modeling occupancy behavior for energy efficiency and occupants comfort management in intelligent buildings. In *Machine Learning and Applications (ICMLA), 2010 Ninth International Conference on*, pages 726–731. IEEE, 2010.

[58] Danni Wang, Clifford C Federspiel, and Francis Rubinstein. Modeling occupancy in single person offices. *Energy and buildings*, 37(2):121–126, 2005.

[59] Beat Lehmann, Katharina Wirth, Stephan Carl, Viktor Dorer, Thomas Frank, and Markus Gwerder. Modeling of buildings and building systems. Technical report, in [50], 2009.

[60] *Klimadaten für Bauphysik, Energie- und Gebäudetechnik*. SIA Standard 2028, 2008.

[61] *Standard-Nutzungsbedingungen für die Energie- und Gebäudetechnik*. SIA Standard 2024, 2006.

Curriculum Vitae

David Sturzenegger
born April 21st, 1986 in Zurich, Switzerland.

2010 – 2014	Doctorate at the Automatic Control Laboratory, ETH Zürich, Switzerland
2005 – 2010	Studies in Mechanical Engineering, ETH Zürich, Switzerland (MSc)
1998 – 2004	Kantonsschule Wiedikon, Zürich, Switzerland (High School, Matura)